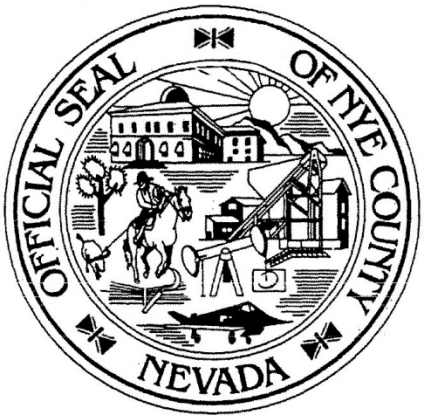

Groundwater Chemistry Analysis
Annual Report for 2008

NWRPO-2012-01

Prepared for
Nye County Nuclear Waste Repository Project Office
Grant No. (DE-FC28-08RW04001)

Prepared by
Arturo Woocay and John C. Walton, University of Texas, El Paso

February 2012

DISCLAIMER

This report was prepared by the Nye County Nuclear Waste Repository Project Office, pursuant to a grant funded by the U.S. Department of Energy, and neither Nye County nor any of its contractors or subcontractors nor the U.S. Department of Energy, nor any person acting on behalf of either, assumes any liabilities with respect to the use of, or for damages resulting from the use of, any information, apparatus, method, or process disclosed in this report. Reference herein to any specific commercial product, process, or service by trade name, trademark, manufacturer, or otherwise, does not necessarily constitute or imply its endorsement, recommendation, or favoring by the U.S. Department of Energy or Nye County. The views and opinions of authors expressed herein do not necessarily state or reflect those of the U.S. Department of Energy.

CONTENTS

TABLES

FIGURES

1.0 INTRODUCTION

This annual report summarizes the results of groundwater chemistry analyses conducted from April 2008 to December 2008 as part of the Nye County Nuclear Waste Repository Project Office (NWRPO) Independent Scientific Investigation Program (ISIP). These activities were funded by cooperative agreement grant DE FC28 08RW04001 with the U.S. Department of Energy (DOE) to support the evaluation of the high-level nuclear waste repository at Yucca Mountain, Nevada.

Multivariate statistical analyses methods (MSMs) were applied to major ion data from groundwater sampling locations in the Yucca Mountain region, NV, to explain the relationships among different groundwater chemical species, suggesting hydrochemical processes and defining hydrochemical facies important to groundwater evolution. Additionally, chloride mass-balance is applied to drill cuttings to determine local infiltration rates and dates; stable water isotope data is interpreted in relation to the global meteoric water line (GMWL); and carbon-14 data, corrected by carbon-13, is presented. These analyses corroborate and/or complement the MSM results and together they all provide further insight into the hydrology of the region. Specifically, evidence is presented of past focused recharge around an ephemeral wash, climate-induced changes surrounding the wash, and some potential interaction of groundwater with a fault line. In addition five more potential groundwater flowpaths are delineated by these methods.

1.1 Data Sources

Groundwater chemistry data were obtained from the NWRPO web site as of April 2008 (NWRPO, 2008) and a Los Alamos National Laboratory report (LANL, 2003); both of these databases have been extensively scrutinized for quality assurance purposes. The LANL (2003) report contains the data used by Kwicklis et al. (2003) and was provided to us by Ed Kwicklis. Data were compiled into a single database covering the Amargosa Desert region, and giving preference to NWRPO (2008) data, due to data from newly developed wells and more recent analyses. All available uncensored water chemistry data from the NWRPO (2008) data base were averaged by well and variable and then complemented by LANL (2003) data from wells not included in the NWRPO data base. The compiled NWRPO and LANL water chemistry data used in this study as input for statistical analyses is presented in Appendix A.

Sampling locations are mostly wells, some of which have multiple screened depths, while the remaining are fresh springs. Multiple sampling locations were developed at well sites that had more than one screen depth at which separate samples could be taken; spatially, they are dealt with by “moving” them one meter north and one meter east. Springs containing high levels of evaporites were excluded from analysis along with samples missing any of the major ion data. Anomalous samples were determined and eliminated from these analyses to avoid distortion of the analyses due to these statistical outliers. Outlier determination is presented in Section 2.3.2 and Section 2.3.5.

Data for boreholes analyzed by chloride mass-balance was obtained from the NWRPO website, and Table 1-1 lists the record index designator (RID) numbers corresponding to each well.

Pertinent information for these boreholes is listed in Table 1-2 and chloride concentrations from borehole drilling extracts are listed in Tables 1-3 through 1-5.

1.2 Contour Generation

All contour plots presented herein were developed with Surfer™ 8 software using the software's existing Natural Neighbor gridding method with 92 by 100 grid lines for x and y directions, respectively. Gridding methods in Surfer are divided into exact and smoothing interpolators, where exact interpolators honor data points exactly when the point coincides with the grid node being interpolated. Natural Neighbor is an exact gridding method, does not extrapolate contours beyond the convex hull of the data locations and does not extrapolate Z grid values beyond the range of data. Natural Neighbor generates good contours from datasets containing dense data in some areas and sparse data in other areas (Sibson, 1981), and therefore was selected for these analyses. Figure 1-1 presents total dissolved solids (TDS) concentrations in milligrams per liter with a thick contour line at the data set's approximate average.

1.3 Static Groundwater Levels in the Region

Static water levels from 1,088 wells (T. Buqo, 2004) were employed to generate the contemporary static groundwater contours presented in Figure 1-2 in meters above mean sea level (amsl). 342 out of the 1,088 wells used to develop the contours are located within the map extent shown. These contours demonstrate a sharp hydraulic gradient under the Funeral Mountains toward Death Valley, and a strong gradient under Yucca Mountain with a southeast direction broadly toward Fortymile Wash. Refined contours next to Yucca Mountain demonstrate a trough surrounding Fortymile Wash indicating groundwater flow toward the wash. In general, hydraulic gradients north of the Amargosa Desert follow a northwest to southeast trend, followed by gradients in the Amargosa Desert that portray a leveling out and then a gradual turn southwest toward Death Valley. Water levels are less than 850 m amsl in most of the western side of the Amargosa Desert, Jackass Flats, and Amargosa Flat and decrease to 660 m at the foothills of the Funeral Mountains. In contrast, topography in the same area changes from 1,050 m amsl in the west and northeast to 700 m in the southeastern end of the desert near Ash Meadows.

In a simple homogeneous and isotropic system, groundwater flows directly from high to low static water levels. In an anisotropic system with spatially variant surface water infiltration, groundwater flow can be significantly more complex and may not go directly downgradient. Further mitigating factors are the numerous geologic faults throughout the region that contribute to the anisotropy of the system that, depending on the particular fault, may retard, accelerate, or divert groundwater flow. Figure 1-3 presents the structural units and tectonic features within the site-scale saturated zone model area after Eddebbarh et al. (2003, fig. 1).

2.0 Multivariate Statistical Methods Applied to Major Ion Data

MSMs are powerful tools used to examine large, complex datasets and they help identify parameters or factors that describe the data and may provide new insight into their behavior (Mellinger, 1987). The MSMs used here broadly fall into one of two categories: dimension reduction and observation classification. Principal component analysis (PCA), factor analysis

(FA) and correspondence analysis (CA) belong to the dimension reduction category, and in general they calculate new descriptive variables from the original variables in an attempt to detect structure or similarities in the original variables Thus, they allow the reduction in the number of variables that describe the system's behavior and the identification of new more descriptive homogeneous subgroups that are easier to identify (Mellinger, 1987). The new variables are usually called axes in PCA, factors in FA, and dimensions in CA, and are basically the solution to an eigenvalue problem, where eigen is German for "own" or "proper" and refers to their individual, representative or characteristic value. All together, the new factors form a factor-space upon which the original dataset and variable-space are projected, and each factor is orthogonal or uncorrelated to the others and accounts for or explains a certain amount of the dataset's variability, where the variability depends on how the eigenvalue problem was constructed. There are several methods of extracting the factor in FA, and the simplest one is by the principal components method (PCFA). Similarly, k-means is one cluster analysis method that belongs to the observation classification category. Cluster analyses differ from classification analyses because the groups into which the observations will be classified are not pre-defined; instead, the goal is to find the optimal grouping that clusters similar observations and produces dissimilar clusters. In k-means cluster analysis (KMCA) this optimal grouping would be the natural grouping of the observations based on their behavior.

Applying PCFA to groundwater chemical data allows the determination of dominant hydrochemical processes extracted as common underlying factors (Lawrence and Upchurch, 1982; Suk and Lee, 1999; Helena et al., 2000; Meng and Maynard, 2001; Adams et al., 2001; Locsey and Cox, 2003). Variables strongly correlated (positively or negatively) or loaded with a factor would present a strong process response relationship; those uncorrelated would be independent of the process and those that correlate with several factors would present a multiple-process involvement (Dalton and Upchurch, 1978). Opposition among variables (one positively and the other negatively correlated) may indicate mutual exclusion resulting from competitive processes (Dawdy and Feth, 1967). Depending on the factor-loadings, each factor can be interpreted as a hydrochemical process or combination of processes (Suk and Lee, 1999) independent of the other factors but overlapping (Lawrence and Upchurch, 1982). Furthermore, applying a cluster analysis to the factor-scores generated for each observation objectively determines hydrochemical facies of the system (Suk and Lee, 1999). When results are presented on biplots, they allow the simultaneous observation of variable and sample relationships based on the defined hydrochemical processes and facies (Usunoff and Guzman-Guzman, 1989). Contours of PCFA results on a digital elevation model (DEM) allow the delineation of groundwater flowpaths, sources (Kreamer et al., 1996), and interaction with the geologic context (i.e., lithology, topography, heterogeneity, and connectivity) (Locsey and Cox, 2003).

Herein, PCFA is applied to major ion data from groundwater sampling locations in the Amargosa Desert region; KMCA is then sequentially applied to PCFA results; and results are presented overlaid on a DEM and using PCFA biplots. These biplots and contours provide, respectively, diagrams indicating dominant hydrochemical processes, and spatial signatures that show potential flowpaths and interactions with surface and geologic features. The work herein provides further understanding of groundwater flow and evolution in the region, and adds insight to the general groundwater flow system and climate-induced changes in recharge at Fortymile Wash, east of Yucca Mountain.

2.1 Factor Analysis by the Principal Component Method (PCFA)

In factor analysis (FA) methods, the original variables that describe the system are expressed as a linear combination of new descriptive variables with an additional error term accounting for variable uniqueness (Rencher, 2002, p. 409; Grande et al., 1996). These methods attempt to detect the underlying common structure (communality) among the original variables in order to describe the systems behavior. The new variables are the extracted underlying common factors containing the communality of the original variables and form a factor space, defined by the factor-loadings, upon which the original variable space and dataset are projected. Each factor is orthogonal, or uncorrelated, to the others and measures, or explains, in a successively decreasing residual manner, data variability not accounted for by the previous factors. Factors are normalized such that the sum of the squares of the component of each factor-loading is equal to the amount of system variation that factor explains (Grande et al., 1996). The projection of the original dataset onto the factor constructs a reduced matrix with factor-scores for each observation indicating the decomposition of each sample into the derived factors. There are several methods of extracting the system's underlying behavior (loading) and constructing the factors (communality). Different FA methods have been developed because the factors are not unique, and a different method may yield better results for a particular system. This non-uniqueness and system particularity are aspects that make this method controversial. Other aspects that make it controversial are the need to determine how many factors exist and interpreting what they represent. The non-uniqueness of factors has the powerful advantage of allowing the rotation of the factors to better describe the system's behavior, revealing similarities within the analyzed variables and allowing the recognition of the factors as physical, measurable or identifiable parameters. There are several types of rotation depending on the desired separation of factors/variables. The most common rotation is the normalized varimax rotation, which attempts to find the rotation that will maximize variability on the rotated axes while minimizing it everywhere else (Rencher, 2002).

Another powerful advantage of the method is that FA is conducted on the data's correlation matrix, which is scale invariant, and therefore variables with different variances and units (mg/L, meq/L, m, ft, °C, pH, ‰) can be used simultaneously, as long as they are continuous. Also, the amount of variation that a system explains is directly relatable to the number of original variables. An explained variation of 2.5 would imply that that factor weighs as much as two and a half of the original variables. Furthermore, factor-scores have a mean of zero and a standard deviation of one; thus values above zero would be above average, and vice-versa, with the scale indicating standard deviations away from the mean.

The principal component (PC) method is one technique of extracting the factor and consists of neglecting the error term and extracting the factors by solving an eigenvalue problem of the variables' correlation matrix. Each factor is an eigenvector with one component, or load, per original variable, and the amount of variation explained by a factor is an eigenvalue. As with PCA, the PC method uses linear combinations of the variables to form the factor space and the linear combinations permit the PCFA to retain as much as possible of the original data variation and spatial distribution.

2.2 *k*-means Cluster Analysis (KMCA)

A cluster analysis groups similar data into clusters by attempting to minimize the variability within each cluster and maximizing variability between clusters. The goal is to find the optimal natural grouping of the data that is interpretable. Cluster analysis is sometimes referred to as classification, pattern recognition, unsupervised learning, and numerical taxonomy (Rencher, 2002, p. 451)

The *k*-means method is a nonhierarchical supervised partitioning cluster analysis (Rencher, 2002, p. 482), where the number of clusters (*k*) is predetermined or supervised and initial seed-observations are selected to maximize initial Euclidean distances between clusters. A vector specifies the mean of a cluster, or centroid, with each component being the average in the cluster of a variable in the analysis. The algorithm uses the initial seed observation as the mean for each cluster and then evaluates each of the remaining observations for inclusion into a cluster, thus partitioning them. As each observation is included, the mean of each cluster is recalculated and previously clustered observations are reevaluated for appropriate clustering. Observations and *k* number of means are reevaluated at each step until no further improvement can be achieved and all observations have been clustered.

2.3 Methodology

All statistical analyses were performed using Statistica™ 8 (StatSoft Inc., 1984–2008). Data, in milligrams per liter and pH units, were input into the software without any transformation: PCFA is conducted on the data's correlation matrix, which is scale invariant, and thus prior normalization-standardization is redundant (Locsey and Cox, 2003). Performing log transformation of the variables would yield more normally distributed input variables, but is not used here because it slightly reduces the variables' correlations.

2.3.1 Outlier detection

MSM tend to be sensitive to outliers of a statistical nature; a good example would be a sample from a brackish spring, which would be geochemically correct but would skew the distribution and standard deviation of the system being analyzed. These statistical outliers need to be identified and excluded from system analyses. Here, a KMCA (Section 2.3.2) applied to available variables, and a PCFA (Section 2.3.5) applied only to the variables selected for further analysis, were used to determine outliers.

2.3.2 Determining Outliers by KMCA

Silica, pH, and F^- data from the complete database were first normalized (mean subtracted) and standardized (divided by the standard deviation) variable-wise based on existing data, and then missing data was substituted with the mean of the dataset (zero). The resulting system is then subjected to a KMCA where the "maximize initial distances" option is selected for the "initial cluster centers", and the numbers of clusters to be generated is set to a large number. Since the dataset contains 220 sampling locations, the number of clusters is set to 44, roughly corresponding to five sampling locations per cluster. As the nature of the clusters is determined by the nature of the dataset, using a KMCA to group the data into a large number of clusters will

classify the samples into actual groups of data with several members, and groups of one member which will be the sought outliers. Simple inspection of the results output yields fifteen clusters formed by a single outlier member; these outliers are listed in Table 2-1.

Figure 2-1 presents the results of this analysis, and although several clusters are observed to present values that exceed five standard deviations of the variables, clusters presenting uncommon variable combinations cannot be observed. This method can be made as strict or as lenient, as required or desired, by using, respectively, a larger or smaller number of clusters, thus forcing separation or agglomeration of samples. For the purposes of describing the variables, this procedure is strict enough (see Appendix B).

2.3.3 Database Summary

Appendix A summarizes the groundwater chemistry data used for this report. Appendix B presents scatter plots of major ions, pH, silica and F^-, highlighting the outliers determined in the previous section. Appendix C presents a basic statistical summary for each of the variables, excluding the outliers determined in the previous section. Note that only silica and pH exhibit clear normal distributions. For pH this is expected as it is a log transformation of H^+ activity, but for silica this may indicate problems with obtaining reliable silica measurements due to its dependence on temperature. Table 2-2 presents a correlation matrix, indicating the number of samples used for each variable pair and the correlation's p-value (records highlighted in bold and red indicate p-values beyond 0.01). Clearly pH, silica and F^- are not correlated to each other. Silica is the least correlated with the major ions with greater correlation with K^+ but only 0.28. Fluoride presents greater correlation with Na^+ and slightly with Cl^- and Alk which is also expected as Na^+, Cl^- and F^- tend to increase their concentration due to water evaporation. Finally, pH correlates best with Ca^{2+} but only 0.49. Note that all the major ions show high cross-correlations with each other even when correlations may be relatively small: Na^+ to Alk, 0.73; Alk to Mg^{2+}, 0.73; and Mg^{2+} to Na^+, only 0.31. Table 2-2 is not easy to interpret due to the large number of variables analyzed.

2.3.4 Variable Selection

There are several ways to determine which variables to analyze; one of them is to inspect the correlation matrix of the variables (Table 2-2). Another method is to perform a PCFA on the system composed of major ions, pH, silica and F^-, with pair-wise deletion and inspecting the results. Using pair-wise deletion here allows the analysis of a correlation matrix constructed from available variable pairs, but no factor-scores can be generated for samples with missing data, and thus biplots cannot be properly generated. Table 2-3 presents a listing of the first eight factors and their respective amount of variance explained, Figure 2-2 presents a scree plot of all factors, and together they indicate that the first three extracted factors have eigenvalues above one and are capable of explaining 77% of the system's variation. The fourth factor explains 8.3% of the systems variation with an eigenvalue of 0.83 (worth slightly less than an original variable), but when added to the previous factors 85.5% of the total system variation is explained. Therefore four factors would be appropriate to reduce the dimensionality of this system.

Further inspection of the first four rotated factors presented in Table 2-4 demonstrates that silica is highly aligned with Factor 3, silica is only loaded on Factor 3, and Factor 3 is mostly loaded

with silica - note again the relationship with K^+. Similarly pH is found to be highly aligned with the fourth factor, with some loading with Ca^{2+}. These results indicate that both silica and pH can be omitted as their variability does not significantly match that of the other variables analyzed and, therefore, a dimension reduction analysis will not reduce these variables. Factor 2 presents high F^-, Cl^- and Na^+ loadings on the same factor. Furthermore, as there are significantly less available fluoride (F^-) samples than major ions samples, F^- was eliminated from further analyses to increase the power of the analyses. As a final check on this analysis, the residual correlations, which represent the difference between the correlation matrix of the original variables and the correlation matrix that the extracted factor could reproduce, are inspected for large discrepancies. Table 2-5 presents the residual correlations for the four rotated factors, and only slight discrepancies are found. An added benefit of this method is the efficiency with which Table 2-4 summarizes the information presented in Table 2-2.

2.3.5 Determining Outliers by Unrotated PCFA

Since pH, silica and F^- were excluded from further MSM analysis, a new outlier determination based on the major ion data was required, as this may include previously excluded samples. Following the same procedure as in Section 2.3.2 (excluding pH, silica and F^-), 18 outliers were determined, and these are listed in Table 2-6.

A PCFA is then performed on the major ions and unrotated factor results are inspected. An outlier determination is performed as follows:

1) Determine the number of significant factors to extract using case-wise deletion. From Figure 2-3 it is observed that the first two unrotated factors encompass most of the systems variation.

2) Construct factors-score scatter plots, either two-dimensional or three-dimensional, of the observation for the significant factors.

3) Identify observations that plot several standard deviations away from the mean (zero) of a factor, or plot separate from the bulk of remaining observations.

Performing a PCFA of the major ions and inspecting the unrotated factor results determines the 11 outliers listed in Table 2-7, which are a subset of those presented in Table 2-6. Scatter plots of the first three unrotated factor scores are presented in Figure 2-4, along with observed outliers. In this manner, from the original 220, 209 observations are deemed appropriate for the PCFA presented here.

2.3.6 Principal Component Factor Analysis (PCFA)

A PCFA of the major ion data was performed on the database of 209 sampling locations (after exclusion of outliers determined in Section 2.3.5) to reduce the number of variables and find relationships among the major ions. Figure 2-5 presents a scree plot of all the eigenvalues of this system and Table 2-8 presents the first four eigenvalues. The first two axes are found to be the more significant in the system as they explain, respectively, 65.8 and 15.2% of the system's variation, and the first four axes account for 96% of the system's variation. The first four factors were determined to adequately describe this system. As part of the PCFA of the major ion

system, a normalized varimax rotation of the factors and scores was performed to find the rotation that will maximize variability on the factors and minimize it everywhere else. Rotated factor-loadings for the major ion chemistry and rotated factor-scores for each of the sampling-locations (observations or cases) were generated. Table 2-9 presents the first four rotated factor-loadings for the major ions.

2.3.7 *k*-Means Cluster Analysis (KMCA)

Factor scores for the sampling locations, having a mean of zero and a standard deviation of one, were used to form nine distinct groups. Since each axis represents a different amount of explained system variation, and in KMCA Euclidean distances are the square root of the sum of the squared factor scores, a weighting scheme was first applied to group the cases according to factor significance. Without the weighting, a large factor explaining much of the system's variation would be as significant as a small factor explaining little system variation. The weighting scheme consists of multiplying each factor score of the cases by the amount of variation each factor explained, thus weighting into the scores the factor loadings. Weighted factor scores were then evaluated by KMCA into nine separate clusters, with "initial cluster centers" option selected to "maximize initial distances". The variables evaluated were factor scores, and the cases were the weighed factor scores for each sampling location (observation). Both empirically and from previous analysis, it was decided to use nine groups for the all the KMCA; and although the number of groups used can be considered subjective, they are justified after careful inspection of the biplot and spatial plots presented in this report.

2.3.8 Biplots

Biplots are simultaneous bivariate (loadings and scores) scatter plots that provide a visual picture of the relationships between and among different variables and observations. The FA biplots presented herein have two scales: one for factor scores of sampling-locations (i.e., bottom and left) and the other for factor loadings of ions (i.e., top and right). Sampling locations are shown as symbols, and ions are shown as vectors with their end located at the loading values for that variable. For illustration purposes, the scale for variables (ions) is arbitrarily selected since only their direction is of relevance to the scores, but for consistency the same scale is used for all ions, furthermore a unit circle in added to provide a greater sense of proportion. Each ion vector indicates the direction of increasing ion content in the samples, and their projection onto the factor axis is their factor loading, which is approximately their correlation or contribution to that factor.

Rotated factor-loadings for major ions and factor-scores for sampling locations, grouped into hydrochemical facies, are presented on the six biplots in Figure 2-6. All biplots of factor combinations are presented for completeness. Figure 2-6(a) explains the most amount of system variation (62%) because it uses the two largest factors (32 and 30%, respectively), and therefore, this is the more descriptive biplot.

2.3.9 Hydrochemical Facies, Spatial Plots and Piper Diagram

The biplots provide diagrams customized to the dominant hydrochemical processes (i.e., the factors), showing the hydrochemical facies and demonstrating the chemical composition of the

processes and facies of the system. Contour plots of each of the resulting factors were overlaid on a DEM of the region to reveal groundwater signatures and potential flowpaths. Figure 2-7 presents contour plots of the first four rotated factor-scores overlaid on the DEM of the region along with marked hydrochemical groups and five potential flowpaths or hydrochemical signatures to be discussed later. The spatial plots of factor-score contours delineate areas influenced by a hydrochemical process and indicate the direction of evolution of that process (perpendicular to the contour), and they allow the exposition of hydrochemical signatures indicating groundwater flowpaths and their interaction with the geologic context. Thus, each factor with a certain chemical composition implies a dominating hydrochemical process, and a clustered group implies a hydrochemical facies with similar genesis, evolution, and/or composition (Thyne et al., 2004) indicated by the underlying factors. Figure 2-8 presents a major ion data Piper diagram with the nine KMCA formed groups for the PCFA and Figure 2-9 shows their spatial distribution. Table 2-10 presents the nine groups determined from the KMCA of the PCFA results along with the mean concentration of major ions demonstrating the different average ions compositions between the groups.

2.4 Results

In Table 2-9 high loadings, presented in bold, indicate a high degree of correlation. Factor 1 now explains 32% of the variance and is dominated by Mg^{2+} and Ca^{2+} ions, whereas Factor 2 explains 30% of the variance and is primarily composed of Cl^-, Na^+, and SO_4^{2-} ions. The remaining two rotated factors explain nearly half as much system variance as the first two: Factor 3, dominated by Alk and Na^+ ions, explains 19% of the variance, while Factor 4, mainly composed of K^+ ion, explains 16%. Loading and alignment of ions and factors can be observed in Figure 2-10 (Figure 2-6[a] reproduced in full size) and Table 2-9. Alignment with a factor is indicated by a lack of loading with other factors. Ions with a high loading and alignment with a factor simplify interpretation of the factors. Further inspection of Figure 2-10 and Table 2-9 demonstrates that SO_4^{2-} presents factor complexity as it does not align with one single factor and instead is present in all four rotated factors, with a greater prevalence in the first two rotated factors; therefore, SO_4^{2-} appears at an angle in Figure 2-10). It is also to be noted that Na^+ presents some factor-complexity as it loads significantly with Factor 2 and Factor 3 and only slightly with Factor 4; in a biplot of Factor 2 vs. Factor 3 Figure 2-6(d), Na^+ appears at an angle to both these factors. These biplots show ion correlation and alignment to factors, along with objective clustering of samples, and thus provide more insight than Piper diagrams (Güler et al., 2002; Dalton and Upchurch, 1978). The Piper diagram similarity is achieved because major ions were used in the PCFA, but there is little limitation to the number or type of variables that can be used (Dalton and Upchurch, 1978), except for the number of available samples (i.e., too few compared to the number of variables).

A contour plot of a factor would be equivalent to a contour plot of a hydrochemical process delineating its areas of influence (Lawrence and Upchurch, 1982) and indicating the direction of evolution of that process (perpendicular to the contour). The first two factor-scores overlain on a DEM are reproduced from Figure 2-7 in full size on Figure 2-11 and Figure 2-12, respectively, along with five inferred potential flowpaths which will be discussed later.

3.0 Chloride Mass-Balance

3.1 The Chloride Mass-Balance Method

Chloride (Cl^-) is an ideal natural tracer for water movement through soil because it is nonvolatile, hydrologically mobile, and chemically inert. Atmospheric dry deposition and concentrations in precipitation are the typical sources of chloride, and chloride soil concentrations increase above precipitation levels due to water evapotranspiration and lack of vegetation uptake. The aforementioned qualities allow chloride mass-balance methods to estimate soil water ages (Stone, 1992) and paleorecharge rates (Stone 1992; Macfarlane et al., 2000). Furthermore, chloride concentrations can be related to the degree water evaporates, prior to its dropping below the root zone, by a chloride mass-balance:

$$\left(V_{\text{precip}} \times C_{\text{precip}}\right) = \left(V_{\text{gw}} \times C_{\text{gw}}\right) \text{ or } \frac{C_{\text{precip}}}{C_{\text{gw}}} = \frac{V_{\text{gw}}}{V_{\text{precip}}} \qquad \textbf{Equation 1}$$

where *V* is volume, *C* is concentration, and the subscripts refer to precipitation (precip) and groundwater (gw). The contemporary estimates of regional chloride concentration in precipitation is 0.35 mg/L (Fabryka-Martin et al., 2000) which means that groundwater containing chloride at a concentration of 35 mg/L represents approximately 1 percent of the initial precipitation, with the other 99 percent is lost to evaporation and transpiration. Chloride concentration contours, in milligrams per liter, generated from 209 sampling locations in the Amargosa Desert region and overlaid on the DEM of the region are presented in Figure 3-1. There is no available information relating chloride concentration variations with respect to climate in the Yucca Mountain area (Liu et al., 2003).

Profiles of chloride concentrations provide a qualitative estimate of downward water moisture fluxes over long periods. These assumptions are: (l) one-dimensional, vertical, downward, piston-type flow; (2) precipitation/deposition as the only source of chloride; (3) mean annual precipitation and chloride concentration of precipitation constant through time; and (4) steady-state chloride flux equal to the chloride concentration in rainfall (Scanlon, 1991; and Bazuhair and Wood, 1996).

3.2 Methodology

For all four boreholes, infiltration dates before present and pore velocities were calculated using a range of annual chloride deposition rates obtained from literature. Two chloride deposition rates (loadings) obtained from literature are used to provide approximate upper and lower calculation limits: a lower chloride loading rate (LL) of 60 mg/m^2/year (Fabryka-Martin et al., 2000), corresponding to contemporary values; and an upper loading rate (UL) of 107 mg/m^2/year (Liu et al., 2003), corresponding to an attempt to correct for either past greater chloride deposition or a past higher precipitation with chloride concentration remaining constant. Considering a 170-mm average precipitation per year, the aforementioned chloride loadings correspond to 0.35 and 0.62 mg/L (Cl^- mg per liter of precipitation), respectively. These upper and lower values are assumed constant throughout time in these calculations, instead of attempting to compensate for fluctuations in chloride deposition and/or precipitation through time. Therefore, two age-rate curves are presented with the lower loading (LL) corresponding to the best estimate. Soil extracts were obtained from borehole cuttings previously collected by the

Nye County Early Warning Drilling Program from boreholes drilled using air as the primary drilling fluid (to preserve sample integrity).

Samples were gathered in an attempt to characterize the upper and lower drill cuttings and are therefore not evenly spaced. Drill cutting samples were separated into two subsamples; the first was oven dried to determine the sample's water percent content by weight, and the second one was used to obtain soil extracts. An extraction dilution of 1:1 (1 liter of DI water per kg of soil) was used with a correction for the sample's original water content. Soil extracts were then sent to ACZ Laboratories Inc. to be analyzed for chloride concentrations following ASTM standards. In instances when the chloride concentration was low (<18 mg/L), the Method Detection Limit (MDL) (same as Minimum Reporting Limit) reported by the laboratory was 1 mg/L.

Using Mathematica™ 5.1, chloride extract concentrations reported at specific depths were linearly interpolated through each borehole's sampling depth based on the number of available samples and their depth distribution. Boreholes NC-EWDP-22S, NC-EWDP-23P, NC-EWDP-24P, and NC-EWDP-29P had respectively, 93, 12, 12, and 11 available samples. Plots of these interpolations are presented in Figure 3-2 (a) through (d). Age-rates for both chloride loadings through depth at 1 meter intervals are calculated with Mathematica™ as follows:

$$\frac{Cl_{Concentration}\left[\frac{kg_{Cl}}{kg_{Soil}}\right]\times\rho_{Soil}\left[\frac{kg_{Soil}}{m^3}\right]}{Cl_{Loading}\left[\frac{kg_{Cl}}{m^2\cdot year}\right]}=Agerate\left[years/meter\right] \qquad \textbf{Equation 2}$$

Integrating these age-rates using Mathematica™ from the surface down to available data depths yields the infiltrations dates before-present shown in Figure 3-3 through Figure 3-6. The inverse of Equation 2 produces pore velocities from which first-order line fits through linear segments in the curves are calculated with $r^2>0.95$. In the calculations presented here, an average soil bulk density of 2,000 kg/m^3 is assumed based on average soil bulk densities of samples collected from boreholes NC-EWDP-24P and NC-EWDP-29P (NWRPO, 2005). This soil bulk density corresponds to alluvium composed of a combination of silt, clay, clayey sand, well-graded sand, and gravel, and is assumed representative of all boreholes.

It should be noted that in the past, depending on atmospheric circulation, humidity and climate at that time, the amounts of precipitation and chloride deposition could have been substantially different from contemporary values, and thus the results presented here require amendment to compensate for these differences. Larger precipitation in the past with present day chloride concentration would produce results indicating faster pore velocities that presented here. In addition, topography inducing runon and runoff of surface water also influences chloride mass-balance. Boreholes located in areas of little or gradual slope would indicate faster infiltration rates than those in areas of greater slope. This holds in spite of the fact that age dates will be underestimated for steeper areas with runoff and overestimated for flatter areas with runon of surface water during storms. These results indicate the variability of infiltration rates under the effects of runoff and runon at the surface. Furthermore, correcting for water content in the drilling samples may further change results. Consequently, the figures presented here provide

only a qualitative and relative significance, offering reasonable upper and lower bounds for infiltration dates and pore velocities and demonstrating their changes over time, attributed to past climate change.

3.3 Results

Figure 3-1 demonstrates that chloride concentrations and the implied degree of evaporation are lowest (i.e., 10 to 20 times the concentration of precipitation [Meijer, 2002]) along the Fortymile Wash to Amargosa River pathway and highest (i.e., more than 100 times the concentration) on either side of the pathway in the Amargosa Desert. As shown in Figure 3-2 each borehole's chloride profile exhibits a concentration bulge at the upper-most part of the profile (i.e., at relatively shallow depths) which is typically observed in arid regions and is attributed to large amounts of evapotranspiration at the surface. Furthermore, three out of four boreholes demonstrate some discontinuity, or noise, at the end of the profile, which is accredited to fluctuations in the water table that disturb the chloride profile record. Table 3-1 presents a summary of the results obtained from the analysis herein. In the following subsections results are discussed in detail.

3.3.1 NC-EWDP-22S

Figure 3-3 presents borehole NC-EWDP-22S drill cuttings' depth-age profiles. Borehole 22S is the closest to Fortymile Wash in what would appear to be a runoff area with a low slope of 1% and it displays the fastest pore velocities of the boreholes analyzed in this work. For this borehole, 93 extract sample data points were available for interpolation and thus provide great confidence in the results. A linear fit for the lower chloride-loading curve from the surface to a depth of 6 meters indicates, with $r^2>0.99$, an average pore velocity of 0.75 mm/year (1.3 mm/year for the UL), taking 8,500 years (4,800 years with the UL) to reach that depth. A pore velocity transition then occurs between 6 and 11 meters below land surface (BLS) corresponding to 8,500 and 26,000 years ago, with the LL. A linear fit for the LL curve from a depth of 26 to 140 meters (before 11,000 years ago) indicates, with $r^2>0.98$, an average pore velocity of 12 mm/year (21.5 mm/year for the UL). The highest pore velocities found in this borehole correspond to the depth segment between 23 and 31 meters with values of 30 mm/year (53.5 mm/year for the UL). Complete profile calculations present ages between 20,400 and 11,400 years down to a depth of 140 meters, for chloride LL and UL, respectively. The final recorded value for this borehole presents a spike in value 27% higher than the general average and is attributed to fluctuation in the water table.

3.3.2 NC-EWDP-23P

Figure 3-4 presents borehole NC-EWDP-23P drill cuttings' depth-age profiles. For borehole 23P, east of Fortymile Wash, 12 extract sample data points were available for analysis. This borehole is located in an area with a topographic slope of 0.9%, slightly lower than that found at 22S. A linear fit for the LL curve from the surface to a depth of 9 meters indicates, with $r^2>0.98$, an average pore velocity of 0.3 mm/year (0.53 mm/year for the UL), taking 26,000 years to reach that depth. A pore velocity transition then occurs between 9 and 14 meters BLS corresponding to 26,000 and 29,000 years ago. A linear fit for the LL curve from a depth of 14 to 100 meters, corresponding to 29,000 to 40,000 years before present, indicates, with $r^2>0.99$, an average pore

velocity of 7.9 mm/year (14 mm/year for the UL). Again, a jump in values (six times larger than the records immediately preceding and following it) is observed in the next to last record at 119 meters. Due to linear interpolation with adjacent records at 103 and 121 meters, this jump is very noticeable. Calculations present ages between 55,000 and 31,000 years from the surface to the total depth of 121 meters, for chloride LL and UL, respectively.

3.3.3 NC-EWDP-24P

Figure 3-5 presents borehole NC-EWDP-24P drill cuttings' depth-age profiles. For borehole 24P, 12 extract sample data points were available for analysis and its location presents a slope of 1.2% based on local topography. A linear fit for the LL curve from the surface to a depth of 12 meters indicates, with r^2>0.98, an average pore velocity of 0.3 mm/year for the last 35,000 years. A pore velocity transition then occurs between 12 and 18 meters BLS. A linear fit for the LL curve from a depth of 18 to 120 meters, corresponding to 36,000 to 50,000 years before present, indicates, with r^2>0.94, an average pore velocity of 6.2 mm/year (11 mm/year for the UL). This borehole does not show any noise in the last record. Calculations present ages between 50,000 and 28,000 years from the surface down to near the water table at 120 meters, for chloride LL and UL, respectively.

3.3.4 NC-EWDP-29P

Figure 3-6 presents borehole NC-EWDP-29P drill cuttings' depth-age profiles. The location of borehole 29P is at a land surface slope of 1.1%, slightly lower than that at 24P, based on local topography. Eleven extract sample data points were available for analysis for this borehole and an interesting trend is observed in values near the water table. A linear fit for the lower chloride-loading curve from the surface to a depth of 11 meters indicates, with r^2>0.98, an average pore velocity of 0.3 mm/year for the last 29,000 years. A pore velocity transition then occurs between 11 and 17 meters BLS. A linear fit for the LL curve from a depth of 17 to 71 meters, corresponding to 31,000 to 40,000 years before present, indicates, with r^2>0.99, an average pore velocity of 5.8 mm/year (10 mm/year for the UL). Calculations yield ages between 57,000 and 32,000 years from the surface to near the water table at approximately 106 meters BLS, for chloride LL and UL, respectively.

4.0 Stable Water Isotopes

4.1 Stable Oxygen-18 (^{18}O) and Deuterium (^{2}H)

Stable oxygen-18 (^{18}O) and deuterium (^{2}H) isotopes are other useful tracers in groundwater and serve as identifiers of potential flowpaths in mixing and source water studies as they are thought to behave conservatively. Concentrations of ^{18}O and ^{2}H isotopes are measured as delta deviations (δ) from the reference standard (Vienna Standard Mean Ocean Water (VSMOW) in permil (per thousand ‰) units). Soil and groundwater isotope composition partially reflects the isotopic composition of precipitation, which is correlated with mean annual temperature and may thus provide paleoclimate information (Liu et al. 1995). When plotted against each other, $\delta^{18}O$ and $\delta^{2}H$ in precipitation usually fall along a single line due to the process of fractionation that occurs at the moment of condensation; this line is referred to as the global meteoric water line (GMWL) (Clark and Fritz, 1997; and Craig, 1961) and is given by the following equation (Craig, 1961):

$$\delta^2 H = 8(\delta^{18}O) + 10‰$$ **Equation 3**

The location of precipitation along the GMWL depends primarily upon the temperature during precipitation.Lighter waters are associated with colder temperatures and fall in the lower left portion of the line, and heavier waters are associated with warmer temperatures and fall in the upper right portion. Initial isotopic precipitation composition is also influenced by relative humidity. Precipitation that occurs in an environment with humidity below approximately 85% (Clark and Fritz, 1997) will plot above the GMWL due to evaporation during its fall, and is said to have an excess of δ^2H, although still depleted compared to VSMOW. In contrast, precipitation that occurs in an environment with humidity above approximately 85% presents values below the GMWL. Precipitated water that accumulates at the earth's surface and then evaporates (i.e., in a lake or along a river) will deviate from its initial composition. Accumulated water values will deviate along a line with a slope lower than the GMWL (8 in Equation 3) towards a less depleted δ^{18}O. The deviation is proportional to the extent of evaporation, and the slope of the deviation depends on the relative humidity of the environment. Deviation slopes of 4.5, 5.2, and 6.8 correspond approximately to relative humidity values of 50, 75, and 95 percent, respectively (Clark and Fritz, 1997).

4.2 Methodology

Contour plots of δ^{18}O groundwater data in permil from 156 sampling locations in the region are presented on a DEM in Figure 4-1, and contour plots of δ^2H groundwater data in permil from 153 sampling-locations in the region are presented on a DEM in Figure 4-2. Figure 4-3 presents paired δ^{18}O vs. δ^2H data in permil from 153 paired sampling-locations compared to the GMWL. Figure 4-4 presents paired δ^{18}O vs. δ^2H data that follow the traces of Fortymile Wash and the Amargosa River until both groundwaters mix.

4.3 Results

In Figure 4-1, values of δ^{18}O at the upper part of Fortymile Wash correspond to the warmer climate of the range, but still colder than present day; furthermore, values found adjacent to the wash correspond to the coldest climate presented in the database. Contour plots of δ^2H, in Figure 4-2, are similar to those of δ^{18}O and also present a distinct pathway following Fortymile Wash. Figure 4-3 presents a plot of regional δ^2H versus δ^{18}O values that fall close to and below the GMWL, with δ^2H values between –117 and –86 ‰, and an average of -103 ‰ and a slope of 6.1. In contrast, isotopic δ^2H values of contemporary precipitation present a wider range due to seasonal variations, with an approximate average of –101 ‰, and fall on the GMWL (Liu et al. 1995), as opposed to below it. In Figure 4-3, the range of the δ^2H and δ^{18}O data corresponds to a relatively cold-climate precipitation, with temperatures in the range of 5 °C to 8 °C (Clark and Fritz, 1997). Data points lie mostly below the GMWL, suggesting some evaporation prior to infiltration, with δ^2H values between -117 ‰ and -86 ‰ and an average of -103 ‰ and a slope of 6.1.

Figure 4-4 shows δ^2H versus $\delta^{18}O$ groundwater values beneath Fortymile Wash, the Amargosa River (i.e., the Oasis Valley and Amargosa Desert southwest), and the junction of the two, plotted against the GMWL; data from each of these areas correspond to one of the marked sections on the figure. The royal blue arrow indicates the approximate downslope direction of the wash; it can be noted that the values of δ^2H and $\delta^{18}O$ beneath the wash (i.e., the blue triangles up) are plotted approximately parallel to the GMWL with a slope of 7.8. The δ^2H and $\delta^{18}O$ values (i.e., the orange triangles down) beneath the Amargosa River from the Oasis Valley until it merges with the fan of Fortymile Wash range from –113 to –102 ‰, and show a slope of 5.4 (i.e., the orange arrow, which indicates the approximate downslope direction of the Amargosa River). If the groundwater age range differed in the order of days and not thousands of years, the slope of the orange arrow would match the evaporation of a river in an atmosphere with relative humidity slightly above 75 percent. On Figure 4-4, the data in the mixing section (i.e., with green crosses) correspond to sampling-locations in the fan of Fortymile Wash, the junction of the Amargosa River with the fan, and slightly beyond the fan of Fortymile Wash near Ash Meadows. These data are associated with groundwater mixing beneath the river and wash; a clear difference can be noted from the unmixed groundwater beneath the wash: δ^2H versus $\delta^{18}O$ values are plotted further below the GMWL and in a more depleted δ^2H range (i.e., -97.5 and -105.5 ‰).

5.0 Radiogenic and Stable Carbon Isotopes

5.1 Radioactive Carbon-14 (^{14}C)

Radioactive carbon-14 (^{14}C) isotopes can provide further understanding of the hydrological behavior of a system when they are used for groundwater dating. With a half-life of 5,730 years, ^{14}C is measured in percent modern carbon (pmc) where ‘‘modern carbon’’ is a standard developed in 1950, before widespread nuclear testing, with an activity of 226 Bq/kg carbon (Clark and Fritz, 1997). The interpretation of ^{14}C data to obtain groundwater age dates is complicated due to this mixing of young (i.e., atmospheric) and old (i.e., carbonate mineral) sources of carbon. Here, distributions of ^{14}C data are considered to establish a general order of development and an attempt is done to estimate corrected groundwater age dates.

5.2 Methodology

In the Amargosa Desert region, the generally thick vadose zone and slow percolation rates permit the vadose zone water to interact with the atmosphere, older carbonate rocks, and more recently formed carbonates (e.g., caliche) for extended periods before reaching the water table. To correct for mineral sources of carbon, it is assumed that all carbon is of atmospheric origin and a correction factor based on estimates of the fraction of carbon from mineral carbonates is applied (Clark and Fritz, 1997). A correction factor (q) is applied to determine the corrected ^{14}C age dates as follows:

$$t = -8267 * \ln \frac{^{14}C_{pmc}}{q * 100} \qquad \textbf{Equation 4}$$

where *t* is time in yr BP and ^{14}C pmc is percent modern carbon. The correction is intended to compensate for the dissolution of older carbonates in the vadose zone water and groundwater.

None of the methods developed to determine *q* apply well to the consolidated dataset. For example, a common method is to base *q* on alkalinity, with the assumption that the Alk is caused by the carbonate weathering. However, an analysis of the NWRPO data suggests that the weathering of silicate minerals, not the dissolution of carbonates, causes the alkalinity. The method used here to obtain an approximation of *q* consists of applying carbon-13 ($\delta^{13}C$) data as follows (Clark and Fritz, 1997):

$$q = \frac{\delta^{13}C_{DIC} - \delta^{13}C_{carb}}{\delta^{13}C_{rech} - \delta^{13}C_{carb}} \qquad \textbf{Equation 5}$$

where $\delta^{13}C_{DIC}$ is the dissolved inorganic carbon (DIC) $\delta^{13}C$ value, $\delta^{13}C_{carb}$ is the carbonate rock value, and $\delta^{13}C_{rech}$ is the value of old recharge. Limitations to this method arise from assumptions, particularly $\delta^{13}C_{rech}$; it is assumed that carbonate rocks have zero permil (‰) of $\delta^{13}C$, and $\delta^{13}C_{rech}$ is estimated to be –15 ‰ from weighed DIC-species-dependent fractionations corresponding to pH values of 6.5 to 9.5 (Clark and Fritz ,1997, fig 5-5). The data present a range of pH values from 6.7 to 9.4, with an average of 7.9, thus the assumptions appear to be applicable to contemporary values. Figure 5-1 represents contours of ^{14}C data in pmc for groundwater from 146 sampling locations in the Amargosa Desert region. Figure 5-2 presents 135 pairs of ^{14}C data corrected by $\delta^{13}C$.

5.3 Results

Figure 5-1 exhibits groundwater ages beneath Fortymile Wash that range from 75 pmc in the upper region to 11 pmc in the lower region near the Amargosa Desert. Furthermore, groundwater beneath Fortymile Wash has higher ^{14}C values, implying that they are younger than groundwater beneath the adjacent highlands, which then cannot be the source of groundwater beneath the wash. Moreover, ^{14}C data demonstrate a similar spatial pattern around Fortymile Wash as the MSM results. Figure 5-2 shows contours of corrected ^{14}C age dates based on ^{14}C and $\delta^{13}C$ data for groundwater from 98 sampling locations. Groundwater ages beneath Fortymile Wash range from 8,000 yr BP in the upper region to 14,000 yr BP in the lower region near the Amargosa Desert. This range corresponds to the end of the Pleistocene and early Holocene epochs, marking the end of Wisconsin glaciation and the start of the current warmer interglacial period (Benson et al., 2002). Figure 5-2 also shows that groundwater beneath the wash is younger than that of adjacent highlands.

6.0 CONCLUSIONS

Chloride mass-balance results indicate that pore velocities among boreholes differ at most by a factor of approximately 2.5. Borehole NC-EWDP-22S, near Fortymile Wash with little slope at the surface, shows the shortest length of time for infiltration to reach the water table, whereas boreholes farther from the wash demonstrate lower velocities. In each borehole, pore velocities present two distinct slopes corresponding to different infiltration regimes. The first one, near the surface (<12 meters), presents the slowest infiltration rate and indicates that infiltration rates over the recent past (approximately 10,000 years) have been negligible at those locations. The second pore velocity corresponds to a past wetter period (late Pleistocene to early Holocene) with pore velocities approximately twenty times faster than near the surface. Boreholes located in areas of little or gradual slope present faster infiltration rates than those in areas of greater slope. Borehole NC-EWDP-22S, near Fortymile wash with little slope at the surface, presents the least length of time for infiltration to reach the water table. This holds in spite of the fact that, assuming this is related to net runoff and runon of water; age dates will be underestimated for steeper areas with runoff and overestimated for flatter areas with runon of surface water during storms. These results indicate how much infiltration rates can differ under the effects of runoff and runon at the surface.

Groundwater chloride concentrations and the implied degree of evaporation indicate that the most dilute groundwater is present beneath Fortymile Wash rather than beneath the mountain ridges, suggesting that infiltration of surface runoff is one of the dominant forms of groundwater recharge in the region. The only feasible explanation for the younger and fresher groundwater beneath Fortymile Wash (with negligible infiltration for the last 10,000 years) is that the younger groundwater arises primarily from infiltration and recharge of surface runoff that accumulates in localized areas, such as the wash.

The first four PCFA factors explain 96% of the system's variation, with the first unrotated factor encompassing more than 65% of the variation and depicting TDS (Figure 1-1). The factor-loading distributions of the second unrotated factor are also important. They pair Mg^{2+} with Ca^{2+}, generally associated with the underlying carbonate aquifer, and Na^{+} with Cl^{-}, generally associated with evolution of water due to evapotranspiration. They also demonstrate an opposition between these pairs, thus implying that groundwater mainly presents either a carbonate influence or an evaporation evolution. Further insight is determined from the rotated PCFA results, particularly those explaining a large amount of system variation. Rotated Factor 1, dominated by Mg^{2+} and Ca^{2+} ions, is associated with dissolution of carbonates. In Figure 2-11 high values of Factor 1 are found at Crater Flat, Amargosa Flat, and Ash Meadows, which are downgradient of outcrops of the underlying carbonate aquifer, and in some instances, Factor 1 is interpreted as an indication of the degree of influence of, or mixing with, the carbonate aquifer. Rotated Factor 2, dominated by Cl^{-} and Na^{+}, is interpreted as a measure of the degree of evolution through evaporation, and in Figure 2-12, contour plots of Factor 2 are very similar to those of Cl^{-} concentrations (Figure 3-1). . In addition, rotated Factor 3, dominated by Alk and Na^{+}, is most likely related to weathering of silicate minerals with generation of alkalinity and the concomitant release of Na^{+}; and finally, rotated Factor 4, dominated by K^{+}, may indicate that silicate weathering is important in the region.

Factors-score contours and hydrochemical facies together indicate the six potential groundwater flowpaths or signatures presented in Figure 6-1; the most distinct of these flowpaths (dark blue arrow) follows Fortymile Wash until it merges with and then follows the Amargosa River. Two common trends are observed from contours of Factor 1 (Figure 2-11), Factor 2 (Figure 2-12), and Factor 3 (Figure 2-7[c]). The first trend is the presence of distortions in the contours along the Highway 95 fault that indicate some mixing between deep and shallow groundwater along the fault or groundwater diversion by the fault. Further evidence is demonstrated by contours of groundwater TDS, Cl^-, $\delta^{18}O$, and δ^2H that demonstrate similar distortion or ''noise'' corresponding with the location of the Highway 95 fault.

The second trend is a large trough of more dilute water below and following the Fortymile Wash path and then turning southeast where the wash joins the Amargosa River. This trough surrounding the pathway of the Fortymile Wash is a groundwater signature that indicates a hydrochemical evolution originating at the wash and progressing away from it; this is in contrast to the inverted trough presented by the static groundwater elevation contours that indicate a flow toward the wash. Based on contours of piezometric head that indicate potentiometric flatness in the Amargosa Desert, groundwater would be unlikely to follow so precisely the surface contours of this arid region. The signature under Fortymile Wash is present in contour plots of ^{14}C, $\delta^{18}O$, δ^2H, TDS (Figure 1-1 analogous to unrotated Factor 1 – not presented), and Cl^- (analogous to rotated Factor 2) that indicate that, relative to groundwater on either side, the less isotopically depleted groundwater (warmer origin) with lower TDS and Cl^- concentrations is found under the wash. The fact that TDS and chloride are lowest in the groundwater along the wash weighs in favor of less rock/water interaction and low evaporation prior to infiltration, both of which are most consistent with a pattern of infiltration and recharge of surface runoff subsequent to runoff-generating storms. Isotopic values under Fortymile Wash plotting below the GMWL also suggest low evaporation before infiltration. The distinct signature under Fortymile Wash could result from groundwater flow beneath the wash and/or some infiltration and recharge of water along the wash; however, the trend is very distinct, narrow, and follows the surface drainage more than the groundwater flow direction, thus indicating a signature more consistent with focused infiltration. Carbon-14 data around Fortymile Wash indicate that groundwater directly underneath the wash is younger that those under highlands adjacent to the wash, and therefore these cannot be the source of groundwater under the wash. The trend of increasing groundwater age and isotopic depletion with increasing distance from the canyon, and the relatively low TDS and Cl^- concentrations beneath Fortymile Wash, suggest that the average reach of recharge and runoff events diminished over time as the climate became warmer and drier. Considered together, these facts suggest that groundwater under Fortymile Wash is not derived primarily from migration of adjacent groundwater, as indicated by coarse contoured water levels, but instead from past-focused infiltration that diminished due to a changing climate, which then produced the contemporary water levels. The broad well spacing within the wash combined with high hydraulic conductivity of the alluvium material beneath the wash masks the potentiometric signal of recharge that is so clearly marked in the water chemistry.

The five other signatures or possible groundwater pathways derived from the MSM results are each presented with an arrow (green, cyan, red, black and pink) in Figure 6-1. Groundwater originating in the Oasis Valley appears to follow the Amargosa River (red arrow) demonstrating a gradual increase in Ca^{2+}, Mg^{2+}, and Cl^- along the pathway of the Amargosa River coming out

of the Oasis Valley until just south of Crater Flat. This pathway is supported by the potentiometric surface that also indicates this sequence. However, the low sample density in this portion of the region and factor-score contours somewhat dominated by NC-EWDP-12PA and 12PB values complicate the definition of a plume or flowpath analogous to along Fortymile Wash. Based on distinct chemical signatures, groundwater flowpaths coming off the Yucca Mountain west (green arrow) and east (cyan arrow) faces are shown as diverging. Groundwater coming off the east face of Yucca Mountain is shown as being diverted to the south as it approaches Fortymile Wash, based upon the fact that it is older and that recharge has historically been greater in the wash than on the adjacent highlands. A groundwater pathway is shown (black arrow) flowing south-east down Crater Flat, between Bear Mountain and Yucca Mountain with a high Ca^{2+} and Mg^{2+} signature. Last, a connection formed by the Amargosa Desert east facies is seen between sampling-locations in Amargosa Flat, Ash Meadows, southeast Amargosa Desert, and Death Valley that follows the direction of potentiometric water gradients from Specter Range toward Death Valley. The Amargosa Desert east facies, with the second highest values of Mg^{2+} and third highest of Ca^{2+}, indicate possible mixing with or upwelling from the underlying carbonate aquifer. The stable water isotope mixing zone presented in Figure 4-4 also suggest such possible mixing. Comparing these six flowpaths with those presented by Kwicklis et al. (2003) (Figure 1-5) a good agreement is found without the use of PHREEQC inverse models or numeric modeling.

The geochemical data presented herein suggests that groundwater beneath Fortymile Wash follows the surface of the wash until it appears to merge and mix with groundwater beneath the Amargosa River. The δ^2H and $\delta^{18}O$ signatures are similar to ^{14}C and PCFA signatures and are evidence of changes to the groundwater system as the climate became warmer and dryer during the past 14,000 years. The stable isotope values beneath the wash fall parallel to the GMWL, with successive depletion of δ^2H and $\delta^{18}O$ values suggesting not an evaporation curve but evidence of climate change from cold to warm, although still colder than the present.

If the hypothesis that current groundwater chemistry along the major washes primarily represents past focused infiltration of surface runoff rather than groundwater migration is correct, then it also follows that groundwater movement since the end of the last ice age has been too slow to erase the old signature. Thus, saturated zone transport from Yucca Mountain may be much slower than currently estimated in regional groundwater flow models (Eddebbarh et al., 2003; Winterle et al., 2003; Kelkar et al., 2003; and Liu et al., 2003).

7.0 References

Adams, S., R. Titus, K. Pietersen, G. Tredoux, and C. Harris. 2001. Hydrochemical characteristics of aquifers near Sutherland in the western Karoo, South Africa. *Journal of Hydrology* 241, no. 1–2: 91–103.

Bazuhair, A.S. and W.W. Wood. 1996. Chloride mass-mass balance for estimating ground water recharge in arid areas: examples from western Saudi Arabia. *Journal of Hydrology* 186, no. 1-4: 153-159.

Benson, L., M. Kashgarian, R. Rye, S. Lund, F. Paillet, J. Smoot, C. Kester, S. Mensing, D. Meko, and S. Lindstro¨m. 2002. Holocene multidecadal and multicentennial droughts affecting northern California and Nevada. *Quaternary Science Reviews* 21, no. 4–6: 455-733.

Buqo, T. 2004. Personal communication by email. buqo@aol.com, with attachment "Master Regional Water Levels 2004.xls". August 27. Pahrump, California.

Clark, I., and P. Fritz. 1997. *Environmental Isotopes in Hydrogeology*. Boca Raton, Florida: Lewis Publishers.

Craig, H. 1961. Isotopic variations in meteoric water. *Science* 133, no. 3465: 1702–1703.

Dalton, M.G., and S.B. Upchurch. 1978. Interpretation of hydrochemical facies by factor analysis. *Ground Water* 16, no. 4: 228–233.

Dawdy, D.R., and J.H. Feth. 1967. Application of factor analysis in studies of chemistry and ground water quality: Mojave River Valley, California. *Water Resources Research* 3, no. 2: 505–510.

Eddebbarh, A.A., G.A. Zyvoloskki, B.A. Robinson, E.M. Kwicklis, P.W. Reimus, B.W. Arnold, T. Corbet, S.P. Kuzio, and C. Faunt. 2003. The saturated zone at Yucca Mountain: An overview of the characterization and assessment of the saturated zone as a barrier to potential radionuclide migration. *Journal of Contaminant Hydrology* 62–63, April-May: 477–493.

Fabryka-Martin, J.T., Meijer, A., Marshall, B., Neymark, L., Paces, J., Whelan, J., Yang, A., 2000. "Analysis of Geochemical Data for the Unsaturated Zone" *OCRWM M&O*, Las Vegas, Nevada. ANL-NBS-HS-000017.

Grande, J.A., A. Gonza´lez, R. Beltra´n, and D. Sa´nchez-Rodas. 1996. Application of factor analysis in the aquifer system of Ayamonte-Hueva (Spain). *Ground Water* 34, no. 1: 155-161.

Güler, C., G. Thyne, J.E. McCray, and A.K. Turner. 2002. Evaluation of graphical and multivariate statistical methods for classification of water chemistry data. *Hydrogeology Journal* 10, no. 4: 455–474.

Helena, B., R. Pardo, M. Vega, E. Barrado, J.M. Fernandez, and L. Fernandez. 2000. Temporal evolution of ground water composition in an alluvial aquifer (Pisuerga River, Spain) by principal component analysis. *Water Research* 34, no. 3: 807–816.

Kelkar, S., P. Tseng, T. Miller, R. Pawar, A. Meijer, B. Robinson, G. Zyvoloski, E. Kwicklis, A.A. Eddebbarh, and B. Arnold. 2003. Site/subsite scale saturated-zone flowtransport models for Yucca Mountain. International High- Level Radioactive Waste Management Conference, Las Vegas, Nevada. La Grange Park, Illinois: American Nuclear Society.

Kreamer, D.K., V.F. Hodge, I. Rabinowitz, K.H. Johannesson, and K.J. Stetzenbach. 1996. Trace element geochemistry in water from selected springs in Death Valley National Park, California. *Ground Water* 34, no. 1: 95–103.

Kwicklis, E.M., A. Meijer, and J.T. Fabryka-Martin. 2003. Geochemical inverse models of ground water mixing and chemical evolution in the Yucca Mountain area. International High-Level Radioactive Waste Management Conference, Las Vegas, Nevada. La Grange Park, Illinois: American Nuclear Society.

Lawrence, F.W., and S.B. Upchurch. 1982. Identification of recharge areas using geochemical factor analysis. *Ground Water* 20, no. 6: 680–687.

Liu, B., F. Phillips, S. Hoines, A.R. Campbell, and P. Sharma. 1995. Water movement in desert soil traced by hydrogen and oxygen isotopes, chloride, and chlorine-36, southern Arizona. *Journal of Hydrology* 168, no. 1: 91–110.

Liu, J., E.L. Sonnenthal, G.S. Bodvarson. 2003. Calibration of Yucca Mountain unsaturated zone flow and transport model using porewater chloride data. *Journal of Contaminant Hydrology* 62-63: 213-235.

Locsey, K.L., and M.E. Cox. 2003. Statistical and hydrochemical methods to compare basalt- and basement rockhosted ground waters: Atherton Tablelands, north-eastern Australia. *Environmental Geology* 43, no. 6: 698 713.

Los Alamos National Laboratory (LANL). 2003. Regional ground water hydrochemical data in the Yucca Mountain area used as direct input to ANL-NBS-HS-000021, Revision 01. LA0309RR831233.001. Las Vegas, Nevada: CRWMS M70.

Macfarlane, P.A., J.F. Clark, M.L. Davisson, G.B. Hudson, and D.O. Whittemore. 2000. Late-quaternary recharge determined from chloride in shallow ground water in the central Great Plains. *Quaternary Research* 53, no. 2: 131–276.

Meijer, A. 2002. Conceptual model of the controls on natural water chemistry at Yucca Mountain, Nevada. *Applied Geochemistry* 17, no. 6: 793–805.

Mellinger, M. 1987. Multivariate data analysis: Its methods. *Chemometrics and Intelligent Laboratory Systems* 2, no. 1– 3: 29–36.

Meng, S.X., and J.B. Maynard. 2001. Use of statistical analysis to formulate conceptual models of geochemical behavior: Water chemical data from the Botucata Aquifer in Sao Paulo state, Brazil. *Journal of Hydrology* 250, no. 1–4: 78–97.

Nuclear Waste Repository Project Office (NWRPO). 2008. Geochemistry data files. Nye County, Nevada website. http:// www.nyecouty.com.

Rencher, A.C. 2002. *Methods of Multivariate Analysis*, 2nd ed. New York: Wiley-Interscience. StatSoft Inc. 1984–2007.

Scanlon, B.R. 1991. Evaluation of moisture flux from chloride data in desert soils. *Journal of Hydrology*, 128, no. 1-4: 137-156.

Sibson, R. 1981. "A brief description of natural neighbor interpolation (Chapter 2)". in V. Barnett. *Interpreting Multivariate Data*. Chichester: John Wiley. pp. 21–36

Statistica Computer Program Manual for Windows. Tulsa, Oklahoma: StatSoft. Kernel release 5.5. www.statsoft.com.

Stone, W.J. 1992. Paleohydrologic implications of some deep soilwater chloride profiles, Murray Basin, South Australia. *Journal of Hydrology* 132, no. 1–4: 201–223.

Suk, H., and K.-K. Lee. 1999. Characterization of a ground water hydrochemical system through multivariate analysis: Clustering into ground water zones. *Ground Water* 37, no. 3: 358–366.

Thyne, G., C. Gu¨ler, and E. Poeter. 2004. Sequential analysis of hydrochemical data for watershed characterization. *Ground Water* 42, no. 5: 711–723.

Usunoff, E.J., and A. Guzman-Guzman. 1989. Multivariate analysis in hydrochemistry: An example of the use of factor and correspondence analysis. *Ground Water* 27, no. 1: 27–34.

Winterle, J.R., A. Claisse, and H.D. Arlt. 2003. An independent site-scale ground water flow model for Yucca Mountain. International High-Level Radioactive Waste Management Conference, Las Vegas, Nevada. La Grange Park, Illinois: American Nuclear Society.

Table 1-1

Record Index Designator (RID) Numbers for Summary Lithological Logs and Well Completion Diagrams Data Collected by the Nuclear Waste Repository Project Office for Selected Boreholes.

Borehole Name	RID Numbers
NC-EWDP-22S	5472, 5364
NC-EWDP-24P	6707, 6096
NC-EWDP-16P	6705, 5714
NC-EWDP-29P	6710, 6093
NC-EWDP-23P	5473, 5267

Table 1-2
Summary of Information for Boreholes Analyzed by Chloride Mass-Balance.

Borehole	Latitude (North)	Longitude (West)	Elevation (AMSL)	Depth to Water	Drilling Depth	Number of Extracts	Drilling Composition
NE-EWDP-22S	36° 42' 15.132"	116° 25' 06.636"	868.45 meters	144 meters	142 meters	93	0 to 109.7 meters: well-graded sand with silt and gravel (SW-SM) 109.7 to 338.3 meters: silty sand with gravel (SM)
NE-EWDP-24P	36° 42' 16.775"	116° 26' 52.756"	850.45 meters	124 meters	120 meters	12	0 to 18.3 meters interbedded well-graded sand with silt, clay and gravel (SW-SM/SC) and silty, clayey sand with gravel (SM/SC) 18.3 to 74.7 meters: well-graded sand with silt, clay and gravel (SW-SM/SC) 74.7 to 121.9 meters: silty, clayey sand with gravel (SM/SC)
NE-EWDP-16P	36° 43' 29.089"	116° 29' 22.219"	880.60 meters	152 meters	35 meters	8	0 to 50.6 meters: silty, clayey sand with gravel (SM/SC) 50.6 to 120.4 meters: ash-flow tuff (pre-ammonia tanks tuff)
NE-EWDP-29P	36° 40' 57.297"	116° 26' 52.884"	830.41 meters	106 meters	96 meters	11	0 to 38.1 meters: well-graded sand with silt, clay and gravel (SW-SM/SC) 38.1 to 80.8 meters: interbedded silty, clayey sand with gravel (SM/SC) and well-graded sand with silt, clay and gravel (SW-SM/SC)
NE-EWDP-23P	36° 41' 05.137"	116° 23' 50.412"	868.58 meters	130 meters	120 meters	12	0 to 137.2 meters: well-graded sand with silt and gravel (SW-SM)

Table 1-3
Chloride Concentrations In Drilling Extract Of Borehole NC-EWDP-22S Reported By ACZ (RID 6800).

Depth From (ft)	Depth To (ft)	Cl (mg/L)
2.5	5	49
7.5	10	40
12.5	15	43
17.5	20	27
22.5	25	19
27.5	30	10
32.5	35	7
37.5	40	5
42.5	45	3
47.5	50	3
52.5	55	3
57.5	60	2
62.5	65	1
67.5	70	2
72.5	75	1
77.5	80	1
82.5	85	1
87.5	90	1
92.5	95	1
97.5	100	1
102.5	105	1
107.5	110	2
112.5	115	1
117.5	120	1
122.5	125	1
127.5	130	1
132.5	135	1
137.5	140	2
142.5	145	2
147.5	150	1
152.5	155	2
157.5	160	2
162.5	165	2
167.5	170	2
172.5	175	2
177.5	180	2
182.5	185	3
187.5	190	2
192.5	195	1
197.5	200	1
202.5	205	2
207.5	210	2
212.5	215	2
217.5	220	2
222.5	225	2
227.5	230	2
232.5	235	1
237.5	240	5
242.5	245	3
247.5	250	3
252.5	255	2
257.5	260	2
262.5	265	2
267.5	270	2
272.5	275	5
277.5	280	1
282.5	285	2
287.5	290	3
292.5	295	4
297.5	300	2
302.5	305	2
307.5	310	1
312.5	315	2
317.5	320	2
322.5	325	4
327.5	330	3
332.5	335	2
337.5	340	2
342.5	345	4
347.5	350	3
352.5	355	2
357.5	360	4
362.5	365	3
367.5	370	2
372.5	375	6
377.5	380	2
382.5	385	2
387.5	390	4
392.5	395	4
397.5	400	3
402.5	405	3*
407.5	410	3
412.5	415	4
417.5	420	3
422.5	425	4
427.5	430	5
432.5	435	4
437.5	440	4
442.5	445	4
447.5	450	3
452.5	455	2
457.5	460	3
462.5	465	29

Table 1-4
Chloride Concentrations In Drilling Extract Of Borehole NC-EWDP-24P Reported By ACZ (RID 6800).

Depth From (ft)	Depth To (ft)	Cl (mg/L)
2.5	5	41
7.5	10	122
12.5	15	149
42.5	45	4
92.5	95	4
142.5	145	6
192.5	195	9
237.5	240	4
292.5	295	1
342.5	345	2
387.5	390	4
392.5	395	2

Table 1-5
Chloride Concentrations In Drilling Extract Of Borehole NC-EWDP-29P Reported By ACZ (RID 6800).

Depth From (ft)	Depth To (ft)	Cl (mg/L)
2.5	5	32
7.5	10	86
12.5	15	133
42.5	45	5
87.5	90	5
132.5	135	5
177.5	180	6
222.5	225	3
267.5	270	18
307.5	310	30
312.5	315	100

Table 2-1
KMCA determined outliers.

	Cluster	Sample Name	Sample#
1	9	ER-OV-03a2 (11/9/97)	10
2	18	ER-18-2 (3/21/2000)	20
3	25	UE-18t (9/23/88)	27
4	44	H-3	51
5	28	UZ#16	56
6	30	p#1(c)	63
7	27	UE-25 J-11	67
8	14	McCracken Domestic	117
9	34	17S/50E-19aab	171
10	38	Cherry Patch Well, 17S/52E-08cdb	189
11	42	UE-16f (7/12/93)	194
12	12	NC-EWDP-01DX-1	NC01
13	33	NC-EWDP-01DX-2	NC02
14	13	NC-EWDP-07S	NC10
15	6	Bond Gold Mining Well -13	NC59

Table 2-2
Correlation matrix of system's variables, with pair-wise deletion and excluding KMCA determined outliers.

Variable	Mg^{2+}	Ca^{2+}	SO_4^{2-}	Cl^-	Na^+	Alk	K^+	pH	SiO_2	F^-
Mg^{2+}	1.0000 N=205 p= ---	**.8161** **N=205** **p=0.00**	**.6562** **N=205** **p=0.00**	**.3487** **N=205** **p=.000**	**.3119** **N=205** **p=.000**	**.7271** **N=205** **p=0.00**	**.5143** **N=205** **p=.000**	**-.3100** **N=205** **p=.000**	**-.2504** **N=199** **p=.000**	-.1409 N=146 p=.090
Ca^{2+}	**.8161** **N=205** **p=0.00**	1.0000 N=205 p= ---	**.7899** **N=205** **p=0.00**	**.5788** **N=205** **p=0.00**	**.3630** **N=205** **p=.000**	**.6375** **N=205** **p=0.00**	**.6308** **N=205** **p=0.00**	**-.4869** **N=205** **p=.000**	-.0628 N=199 p=.378	-.1868 N=146 p=.024
SO_4^{2-}	**.6562** **N=205** **p=0.00**	**.7899** **N=205** **p=0.00**	1.0000 N=205 p= ---	**.7933** **N=205** **p=0.00**	**.7484** **N=205** **p=0.00**	**.6637** **N=205** **p=0.00**	**.6540** **N=205** **p=0.00**	**-.2650** **N=205** **p=.000**	-.0873 N=199 p=.220	.0720 N=146 p=.388
Cl^-	**.3487** **N=205** **p=.000**	**.5788** **N=205** **p=0.00**	**.7933** **N=205** **p=0.00**	1.0000 N=205 p= ---	**.7729** **N=205** **p=0.00**	**.4836** **N=205** **p=.000**	**.5023** **N=205** **p=.000**	**-.2247** **N=205** **p=.001**	.0715 N=199 p=.315	**.2466** **N=146** **p=.003**
Na^+	**.3119** **N=205** **p=.000**	**.3630** **N=205** **p=.000**	**.7484** **N=205** **p=0.00**	**.7729** **N=205** **p=0.00**	1.0000 N=205 p= ---	**.7271** **N=205** **p=0.00**	**.4687** **N=205** **p=.000**	.0196 N=205 p=.781	-.0466 N=199 p=.513	**.4674** **N=146** **p=.000**
Alk	**.7271** **N=205** **p=0.00**	**.6375** **N=205** **p=0.00**	**.6637** **N=205** **p=0.00**	**.4836** **N=205** **p=.000**	**.7271** **N=205** **p=0.00**	1.0000 N=205 p= ---	**.5746** **N=205** **p=0.00**	-.1597 N=205 p=.022	-.1288 N=199 p=.070	**.2177** **N=146** **p=.008**
K^+	**.5143** **N=205** **p=.000**	**.6308** **N=205** **p=0.00**	**.6540** **N=205** **p=0.00**	**.5023** **N=205** **p=.000**	**.4687** **N=205** **p=.000**	**.5746** **N=205** **p=0.00**	1.0000 N=205 p= ---	**-.2812** **N=205** **p=.000**	**.2585** **N=199** **p=.000**	.0123 N=146 p=.883
pH	**-.3100** **N=205** **p=.000**	**-.4869** **N=205** **p=.000**	**-.2650** **N=205** **p=.000**	**-.2247** **N=205** **p=.001**	.0196 N=205 p=.781	-.1597 N=205 p=.022	**-.2812** **N=205** **p=.000**	1.0000 N=205 p= ---	.0399 N=199 p=.576	.1034 N=146 p=.214
SiO_2	**-.2504** **N=199** **p=.000**	-.0628 N=199 p=.378	-.0873 N=199 p=.220	.0715 N=199 p=.315	-.0466 N=199 p=.513	-.1288 N=199 p=.070	**.2585** **N=199** **p=.000**	.0399 N=199 p=.576	1.0000 N=199 p= ---	-.0406 N=142 p=.631
F^-	-.1409 N=146 p=.090	-.1868 N=146 p=.024	.0720 N=146 p=.388	**.2466** **N=146** **p=.003**	**.4674** **N=146** **p=.000**	**.2177** **N=146** **p=.008**	.0123 N=146 p=.883	.1034 N=146 p=.214	-.0406 N=142 p=.631	1.0000 N=146 p= ---

Marked correlations are significant at $p < 0.01$

Table 2-3
First eight eigenvalues for PCFA of system's variables.

Factor #	Eigenvalue	% Total	Cumulative	Cumulative
1	4.80	48.00	4.80	48.00
2	1.70	16.96	6.50	64.96
3	1.23	12.26	7.72	77.22
4	0.83	8.27	8.55	85.50
5	0.62	6.23	9.17	91.73
6	0.32	3.19	9.49	94.92
7	0.28	2.78	9.77	97.70
8	0.12	1.18	9.89	98.88

Table 2-4
Loading for first four rotated PCFA factors of system's variables.

Variable	Factor 1	Factor 2	Factor 3	Factor 4
Mg^{2+}	**0.855**	-0.208	-0.280	0.132
Ca^{2+}	**0.866**	-0.133	-0.012	0.374
SO_4^{2-}	**0.876**	0.269	0.029	0.156
Cl^-	**0.630**	**0.534**	0.205	0.209
Na^+	**0.634**	**0.706**	0.038	-0.137
Alk	**0.837**	0.255	-0.145	-0.069
K^+	**0.744**	0.053	0.417	0.145
pH	-0.187	0.047	0.021	**-0.959**
SiO_2	-0.071	-0.040	**0.952**	-0.033
F^-	-0.099	**0.886**	-0.078	-0.049
Expl.Var	4.352	1.775	1.231	1.193
Prp.Totl	43.5%	17.7%	12.3%	11.9%
Accumulated	43.5%	61.3%	73.6%	85.5%
Marked loadings are > 0.5				

Table 2-5
Residual correlations for PCFA of system's variables.

Variable	Mg^{2+}	Ca^{2+}	SO_4^{2-}	Cl^-	Na^+	Alk	K^+	pH	SiO_2	F^-
Mg^{2+}	0.13	0.00	-0.05	-0.05	-0.05	0.03	-0.01	-0.01	0.07	**0.11**
Ca^{2+}	0.00	0.09	0.01	0.03	-0.04	-0.03	-0.06	0.04	0.02	0.03
SO_4^{2-}	-0.05	0.01	0.13	0.06	0.02	**-0.12**	-0.05	0.03	-0.04	-0.07
Cl^-	-0.05	0.03	0.06	0.23	0.02	**-0.14**	**-0.11**	0.06	-0.05	**-0.14**
Na^+	-0.05	-0.04	0.02	0.02	0.08	0.01	-0.04	-0.03	-0.01	-0.10
Alk	0.03	-0.03	**-0.12**	**-0.14**	0.01	0.21	0.01	-0.08	0.08	0.06
K^+	-0.01	-0.06	-0.05	**-0.11**	-0.04	0.01	0.25	-0.01	-0.08	0.08
pH	-0.01	0.04	0.03	0.06	-0.03	-0.08	-0.01	0.04	-0.02	0.00
SiO_2	0.07	0.02	-0.04	-0.05	-0.01	0.08	-0.08	-0.02	0.09	0.06
F^-	**0.11**	0.03	-0.07	**-0.14**	-0.10	0.06	0.08	0.00	0.06	0.20
Marked residuals are > 0.1										

Table 2-6
KMCA determined major-ion outliers.

	Sample Name	Sample#
1	ER-OV-03a2 (11/9/97)	10
2	US Ecology MW-600	16
3	ER-18-2 (3/21/2000)	20
4	UE-18t (9/23/88)	27
5	p#1(c)	63
6	UE-25 J-11	67
7	McCracken Domestic	117
8	16S/49E-12ddd	158
9	17S/50E-19aab	171
10	18S/50E-7aa	176
11	Cherry Patch Well, 17S/52E-08cdb	189
12	UE-17a (6/9/93)	191
13	UE-16f (7/12/93)	194
14	Pluto 5	197
15	NC-EWDP-01DX-1	NC01
16	NC-EWDP-01DX-2	NC02
17	NC-EWDP-07SC Z4	NC14
18	Bond Gold Mining Well -13	NC59

Table 2-7
PCFA determined major-ion outliers.

	Sample Name	Sample#
1	ER-OV-03a2 (11/9/97)	10
2	ER-18-2 (3/21/2000)	20
3	p#1(c)	63
4	UE-25 J-11	67
5	McCracken Domestic	117
6	17S/50E-19aab	171
7	Cherry Patch Well, 17S/52E-08cdb	189
8	UE-16f (7/12/93)	194
9	NC-EWDP-01DX-1	NC01
10	NC-EWDP-01DX-2	NC02
11	Bond Gold Mining Well -13	NC59

Table 2-8
First four eigenvalues for PCFA of major ion system.

Value	Eigenvalue	% Total	Cumulative	Cumulative
1	4.60	65.76	4.60	65.76
2	1.06	15.20	5.67	80.96
3	0.58	8.28	6.25	89.25
4	0.47	6.72	6.72	95.96

Table 2-9
First four rotated PFCA factors for the major ion system.

Variable	Factor 1	Factor 2	Factor 3	Factor 4
Mg^{2+}	**0.909**	0.056	0.317	0.148
Ca^{2+}	**0.853**	0.352	0.053	0.310
SO_4^{2-}	**0.552**	**0.677**	0.239	0.299
Cl^-	0.200	**0.920**	0.146	0.188
Na^+	0.015	**0.719**	**0.668**	0.154
Alk	0.493	0.224	**0.795**	0.220
K^+	0.299	0.257	0.194	**0.897**
Expl.Var	2.234	2.066	1.298	1.120
Prp.Totl	31.9%	29.5%	18.5%	16.0%
Accumulated	31.9%	61.4%	80.0%	96.0%
Marked loadings are > 0.5				

Table 2-10
Average major ion composition for the PCFA KMCA for nine groups.

Cluster	N	Ca (mg/L)	Mg (mg/L)	Na (mg/L)	K (mg/L)	Cl (mg/L)	SO4 (mg/L)	Alk (mg/L)
1	23	3.2	0.3	101.2	2.9	8.9	29.8	190.0
2	94	16.6	1.9	49.9	5.1	8.4	28.7	113.4
3	10	16.2	2.4	132.4	6.5	50.7	84.3	179.0
4	22	19.8	3.0	90.1	6.3	22.9	84.2	139.1
5	13	55.1	10.9	153.0	11.7	68.7	191.7	226.4
6	21	46.2	15.6	112.6	13.4	29.7	141.3	247.2
7	12	28.2	13.9	84.0	7.0	15.2	63.7	226.7
8	11	61.2	32.2	74.7	7.4	17.7	127.0	273.8
9	3	27.8	9.4	125.3	24.4	16.1	101.9	268.9
All Samples	209	24.0	6.2	80.8	6.8	18.9	67.0	165.3

Table 3-1
Summary of chloride mass-balance results for boreholes NC-EWDP- 22S, NC-EWDP-23P, NC-EWDP-24P and NC-EWDP 29P.

	22S		**23P**		**24P**		**29P**	
Topography Slope	1.0%		0.9%		1.2%		1.1%	
CHLORIDE LOADING ($60\ mg/m^2/y$ =LL; $107\ mg/m^2/y$ = UL)	LL	UL	LL	UL	LL	UL	LL	UL
FIST PORE VELOCITY REGIME								
Surface to Depth (meters)	6		9		12		11	
Corresponding Age (thousands of years)	8.5	4.8	26	14.6	35	19.6	29	16.3
Average Pore Velocity (millimeters/year)	0.75	1.34	0.3	0.53	0.3	0.53	0.3	0.53
PORE VELOCITY TRANSITION END (thousands of years)	11	6.2	29	16.3	36	20.2	31	17.4
SECOND PORE VELOCITY REGIME								
Depth Range (meters)	26-140		14-100		18-120		17-71	
Average Pore Velocity (millimeters/year)	12	21.5	7.9	14.1	6.2	11.1	5.8	10.3
Complete Profile Age (thousands of years)	20.4	11.4	54.5	30.6	50.4	28.3	56.6	31.7

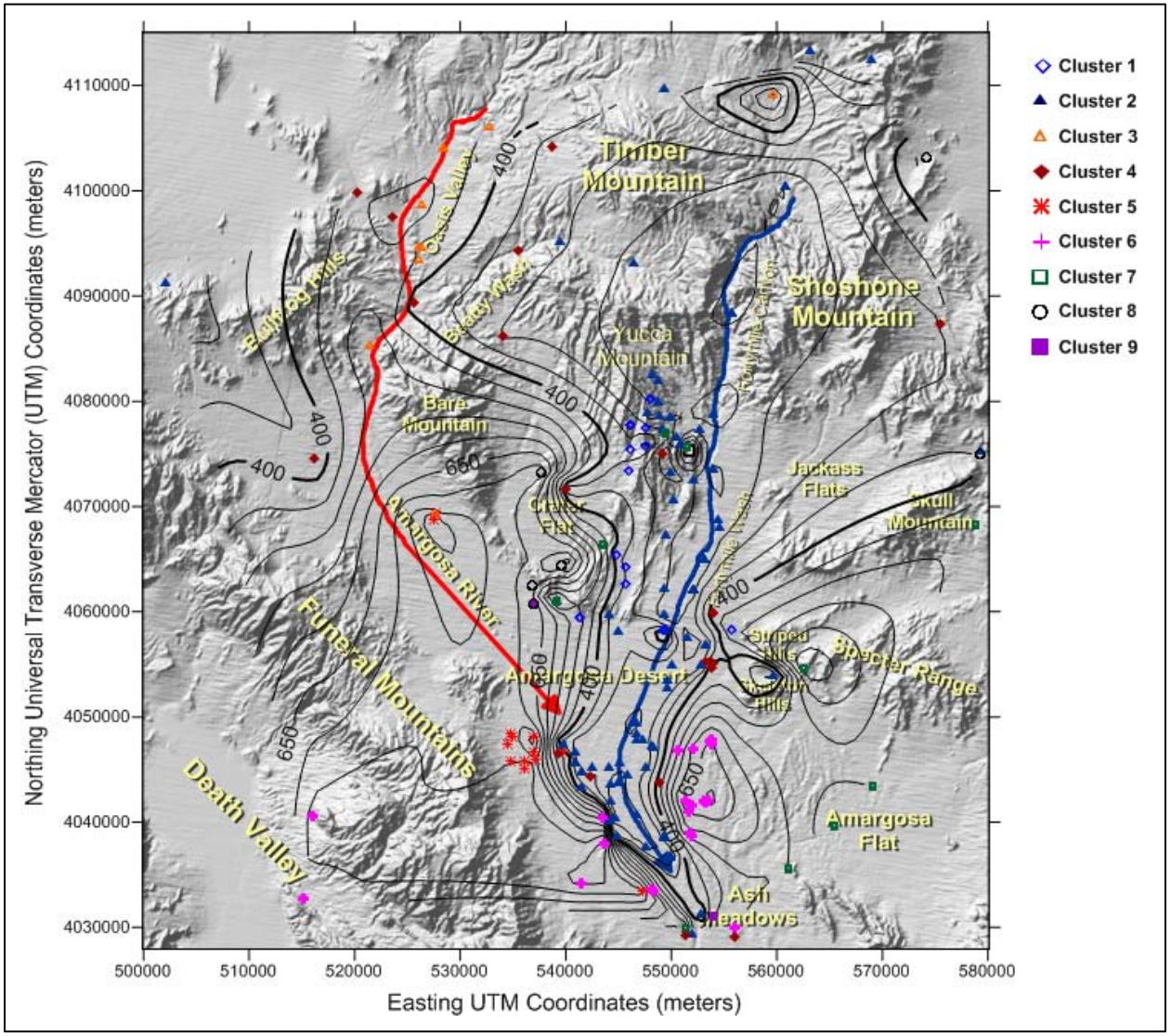

Figure 1-1

TDS concentrations in milligrams per liter with a thick contour at the data set's approximate average with sampling-locations grouped into nine hydrochemical facies.

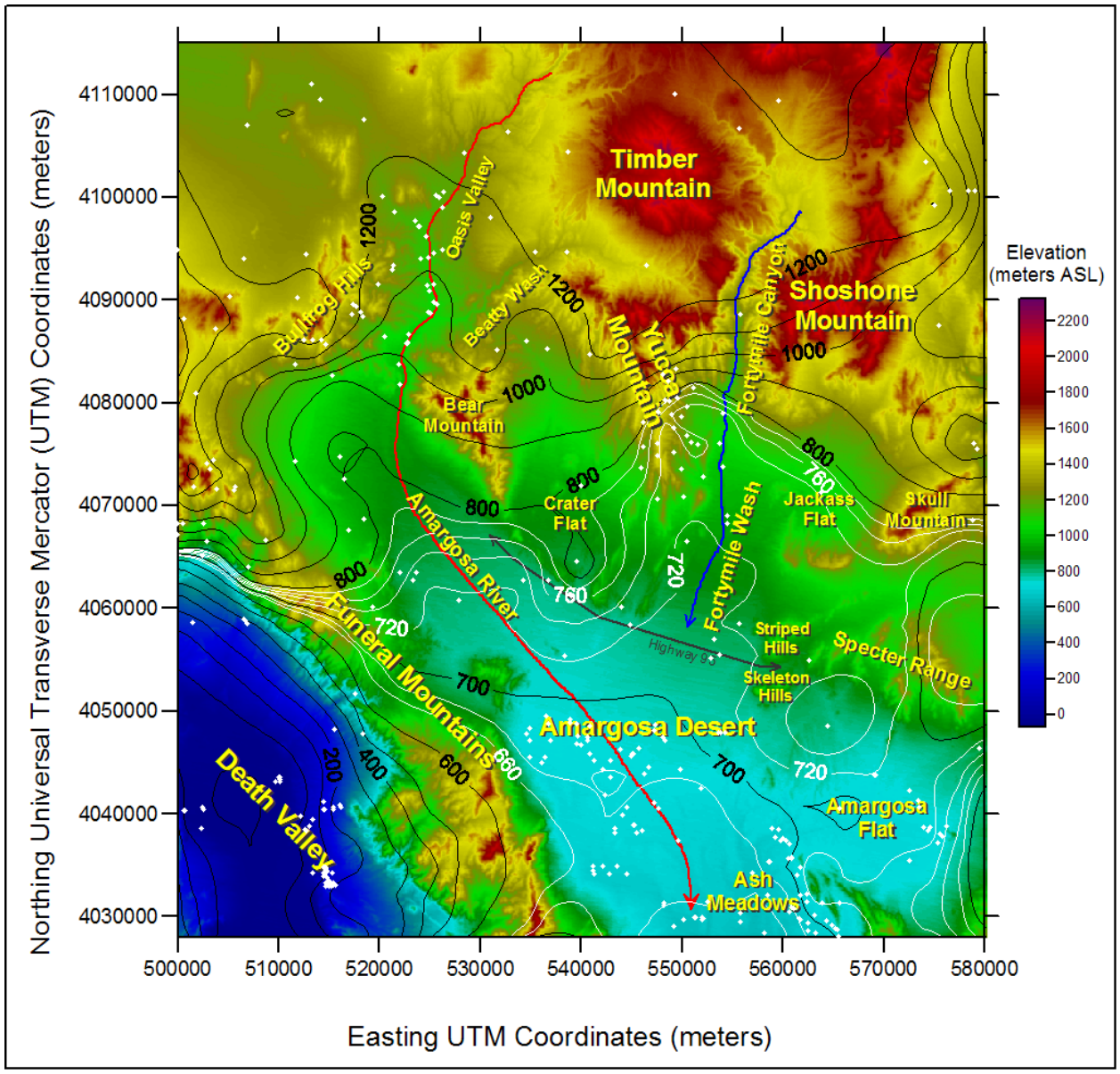

Figure 1-2

Static groundwater elevation contours overlaid on a DEM of the Amargosa Desert region. Contours based on 1,088 wells (only 342 wells located within map extent). For illustration purposes, contour intervals are reduced from 100 to 20 m, between the 800 and 660 m levels, and presented in white. Data from T. Buqo, (2004).

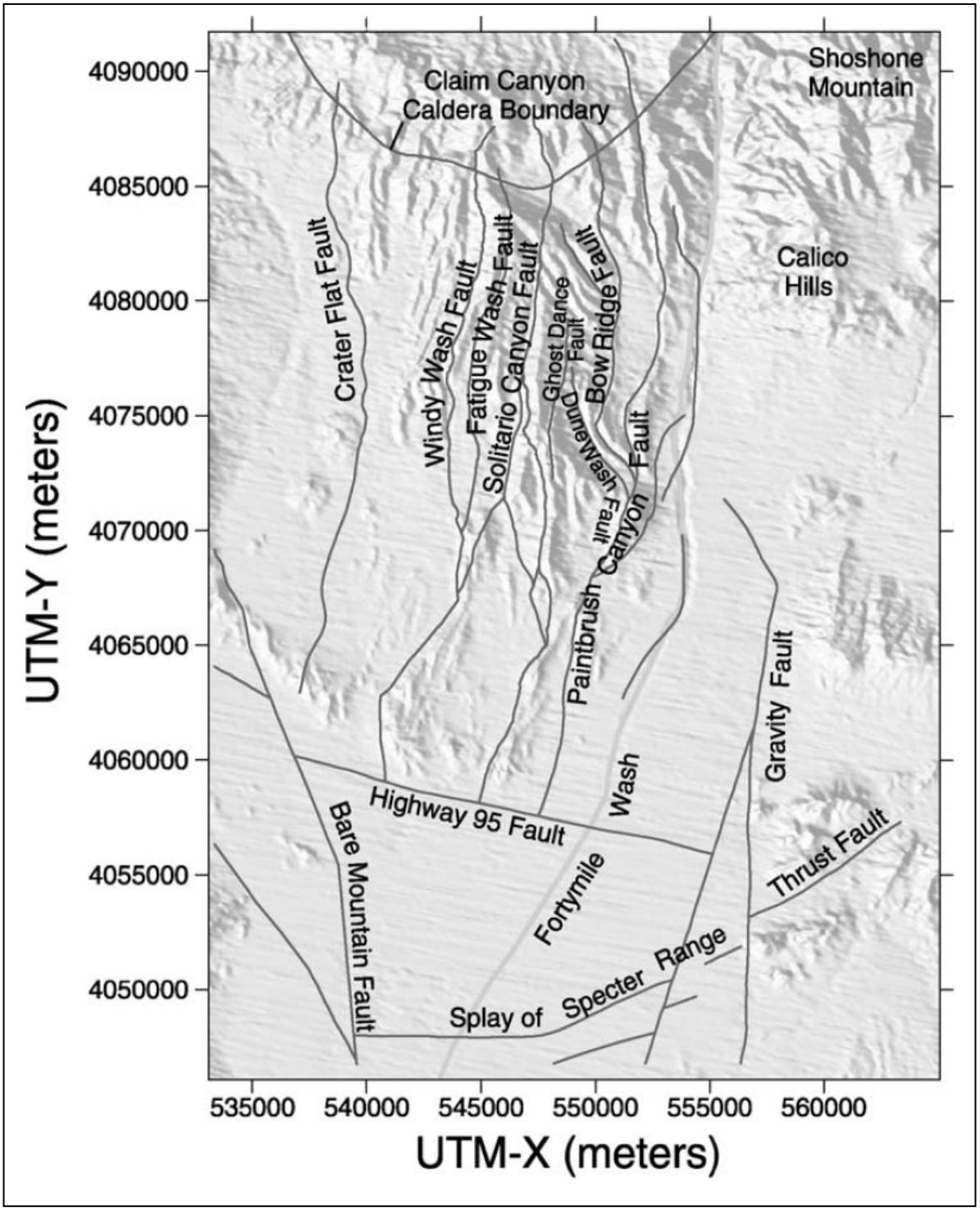

Figure 1-3

Structural units and tectonic features within the site-scale saturated zone model area. After Eddebbarh et al. (2003, fig. 1).

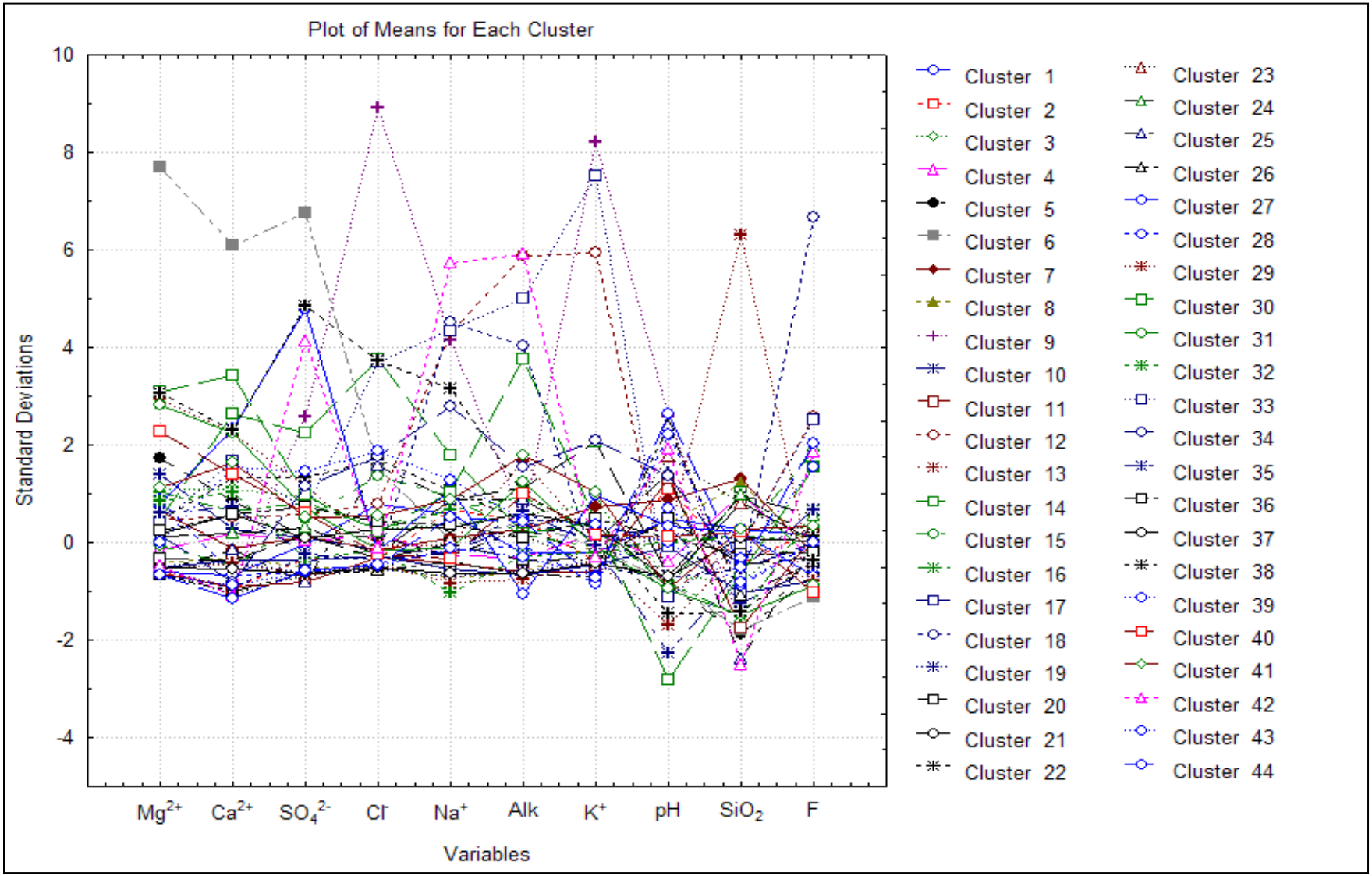

Figure 2-1

Forty-four cluster variable means plot. KMCA is applied on normalized and standardized variables, with mean substitution for missing data. Outliers are detected as clusters formed by one member or with large standard deviations.

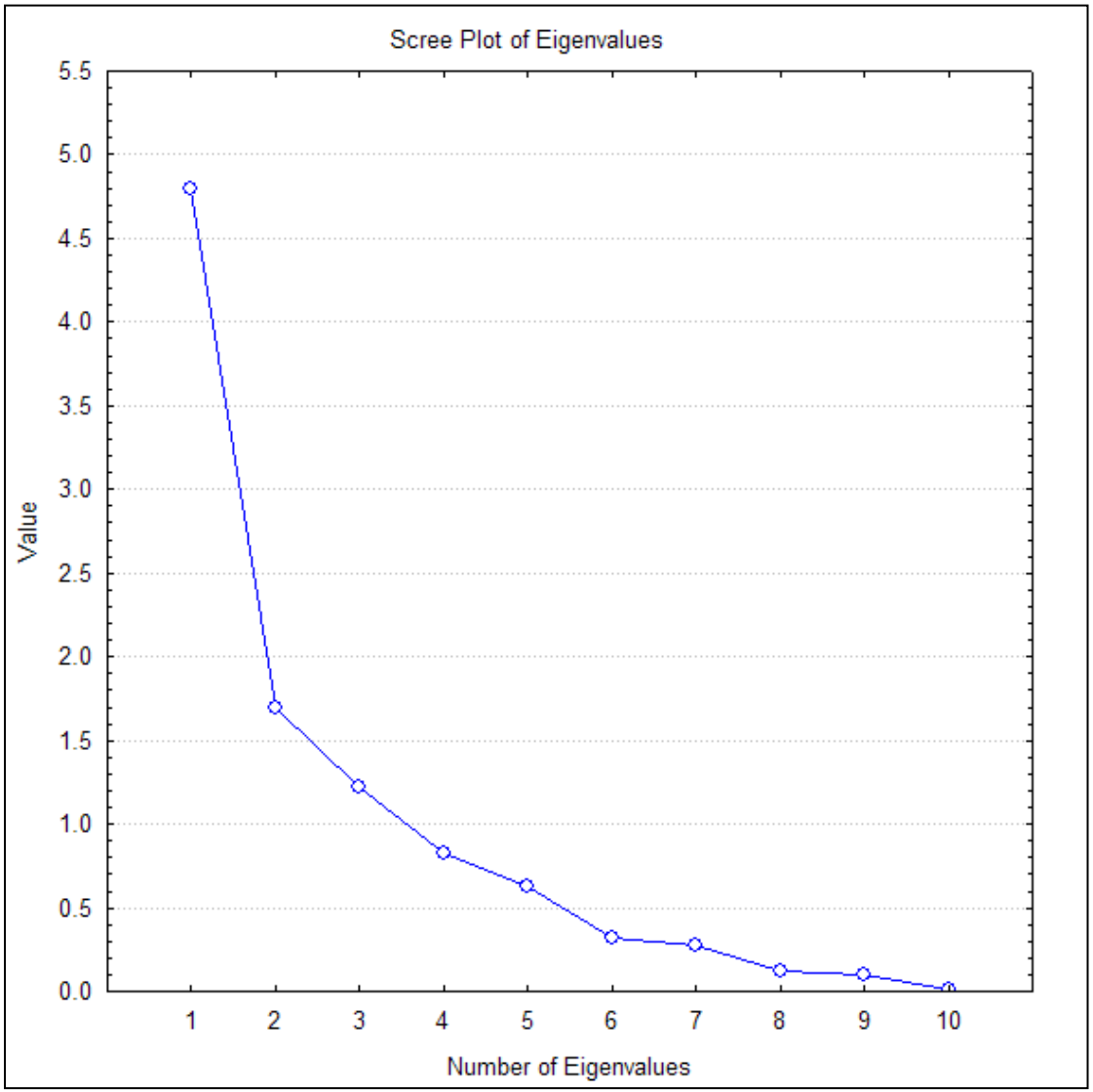

Figure 2-2

Scree plot of all eigenvalues for PCFA of system's variables. The first four factors are determined to be significant.

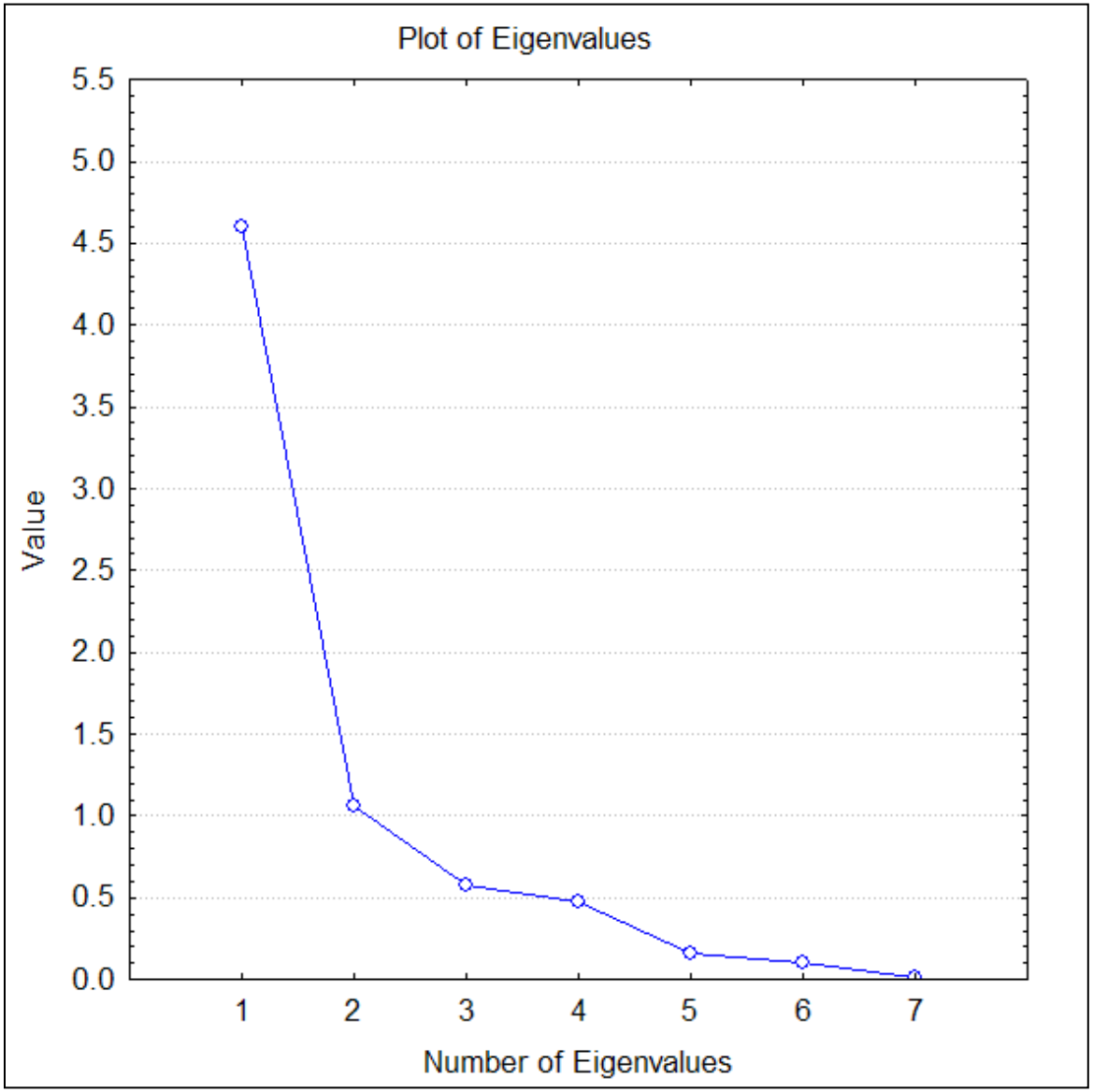

Figure 2-3

Scree plot of all eigenvalues for PCFA of major ion data. The first two factors are determined to be significant.

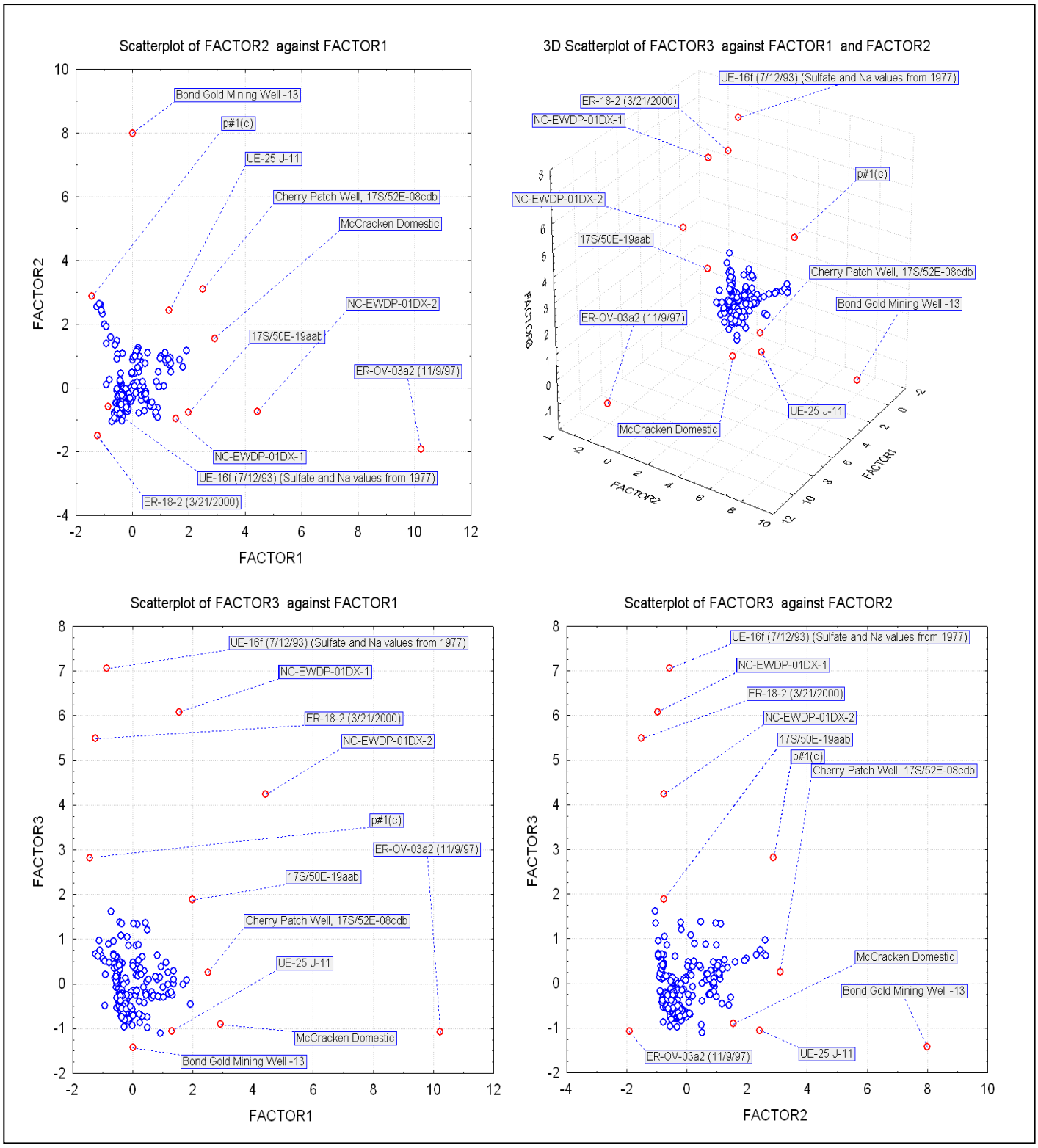

Figure 2-4

Outliers of major ions determined by PCFA.

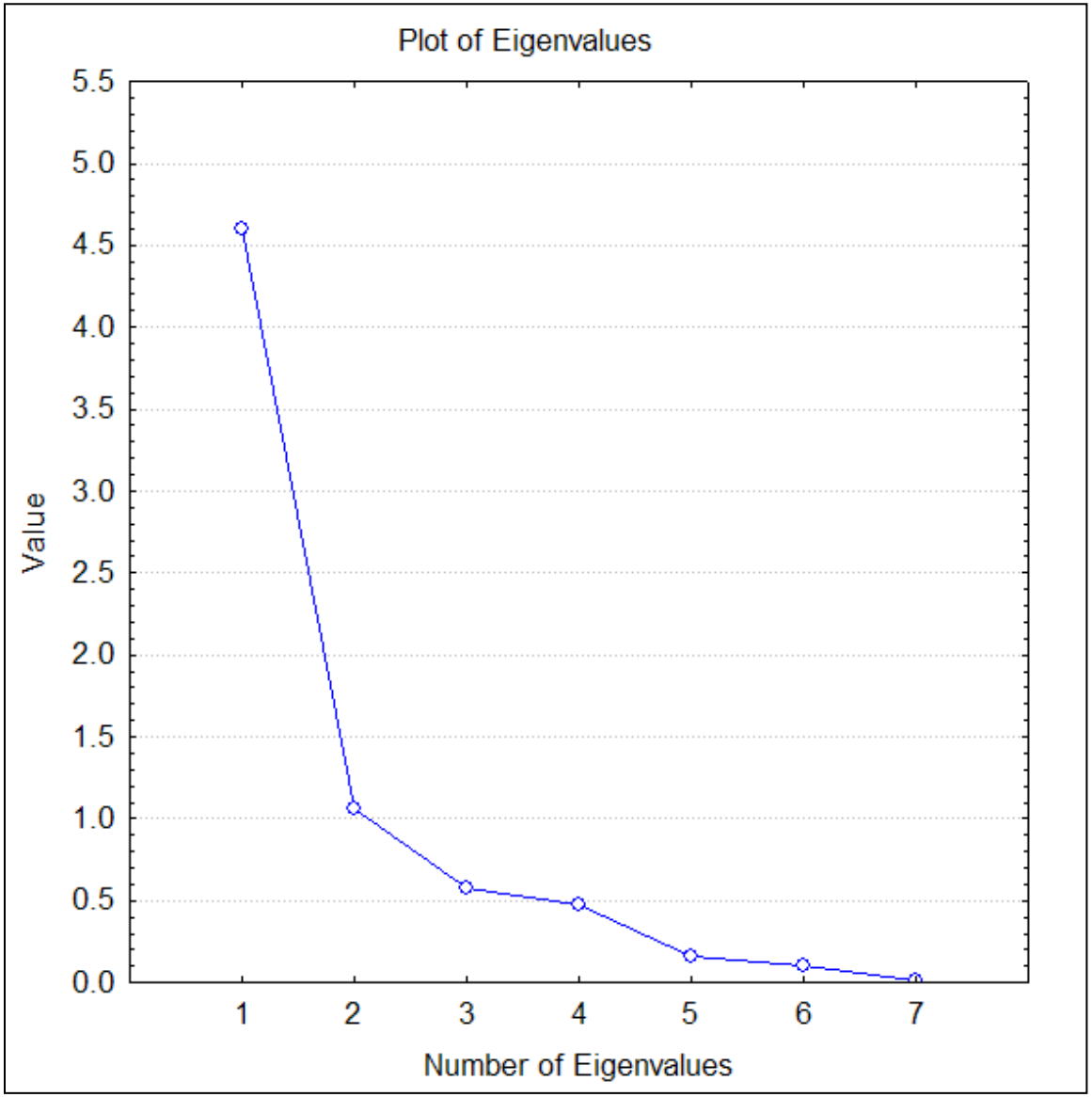

Figure 2-5
Scree plot of all eigenvalues for PCFA of major ion system excluding outliers. The first two factors are determined to be significant, but the first four are of interest.

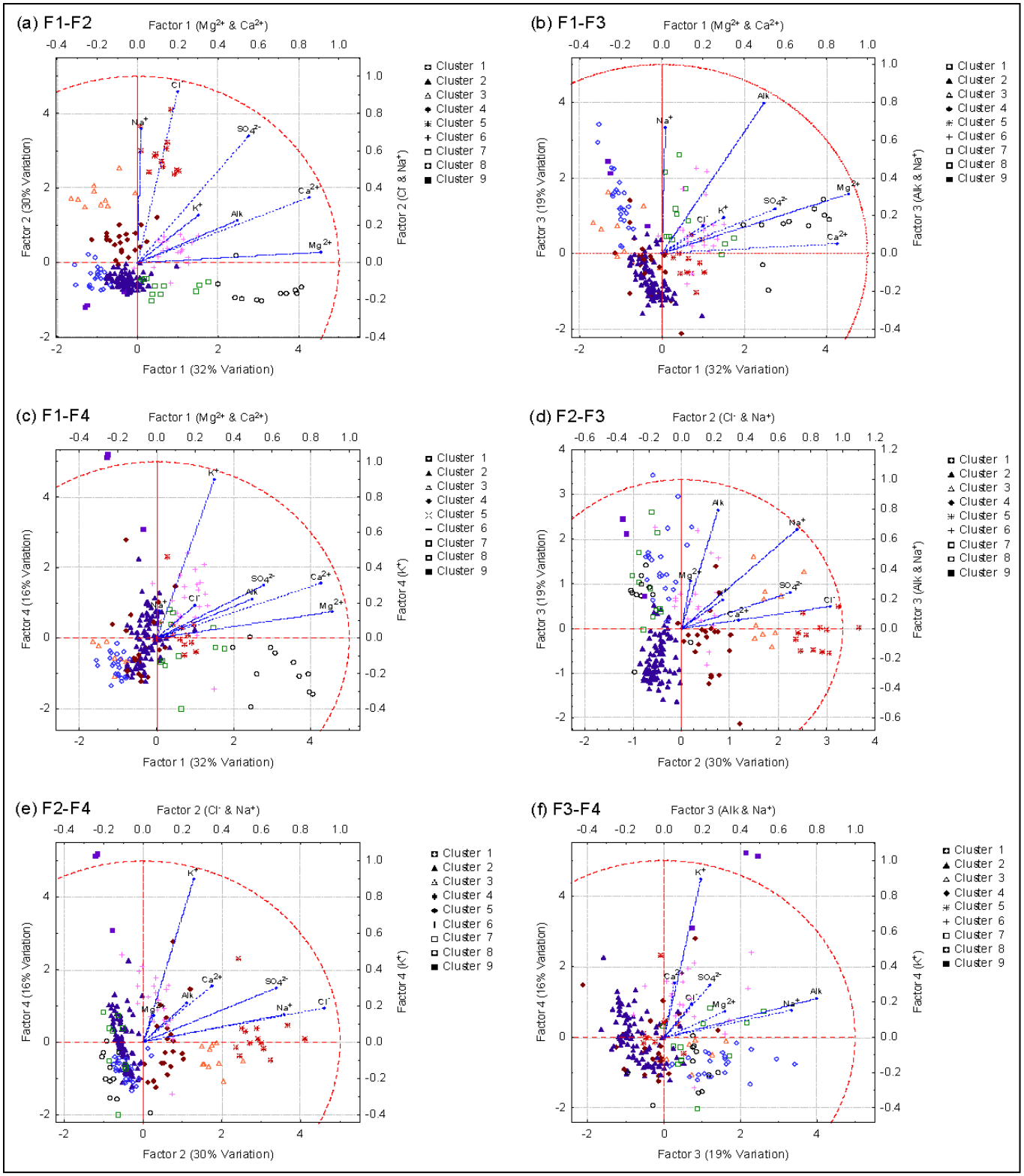

Figure 2-6
PCFA biplots with sampling-locations grouped into nine hydrochemical facies.

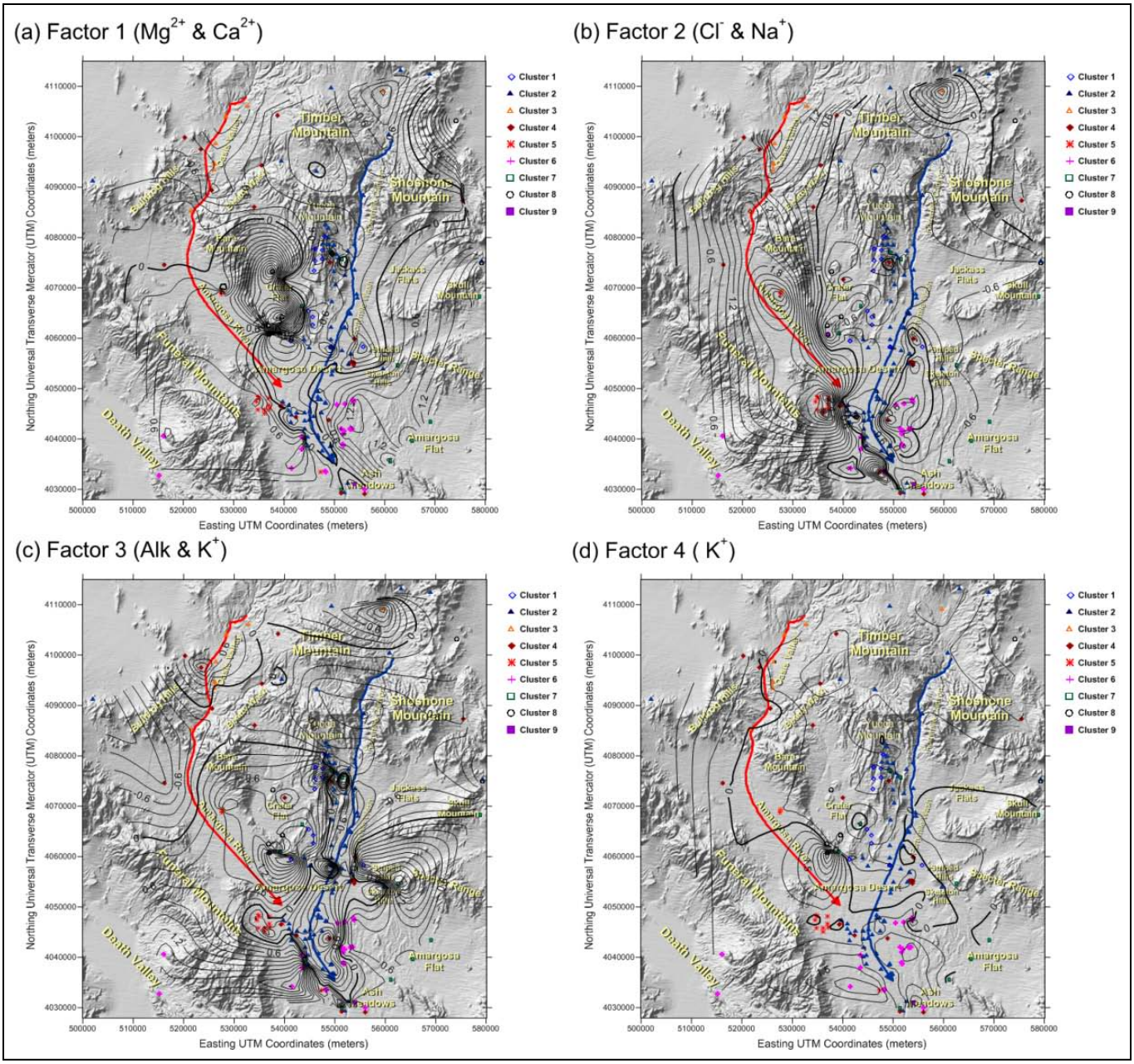

Figure 2-7

First four rotated factor-score contours overlain on a DEM with sampling-locations grouped into nine hydrochemical facies. Factor-scores have a mean of zero (thick contour).

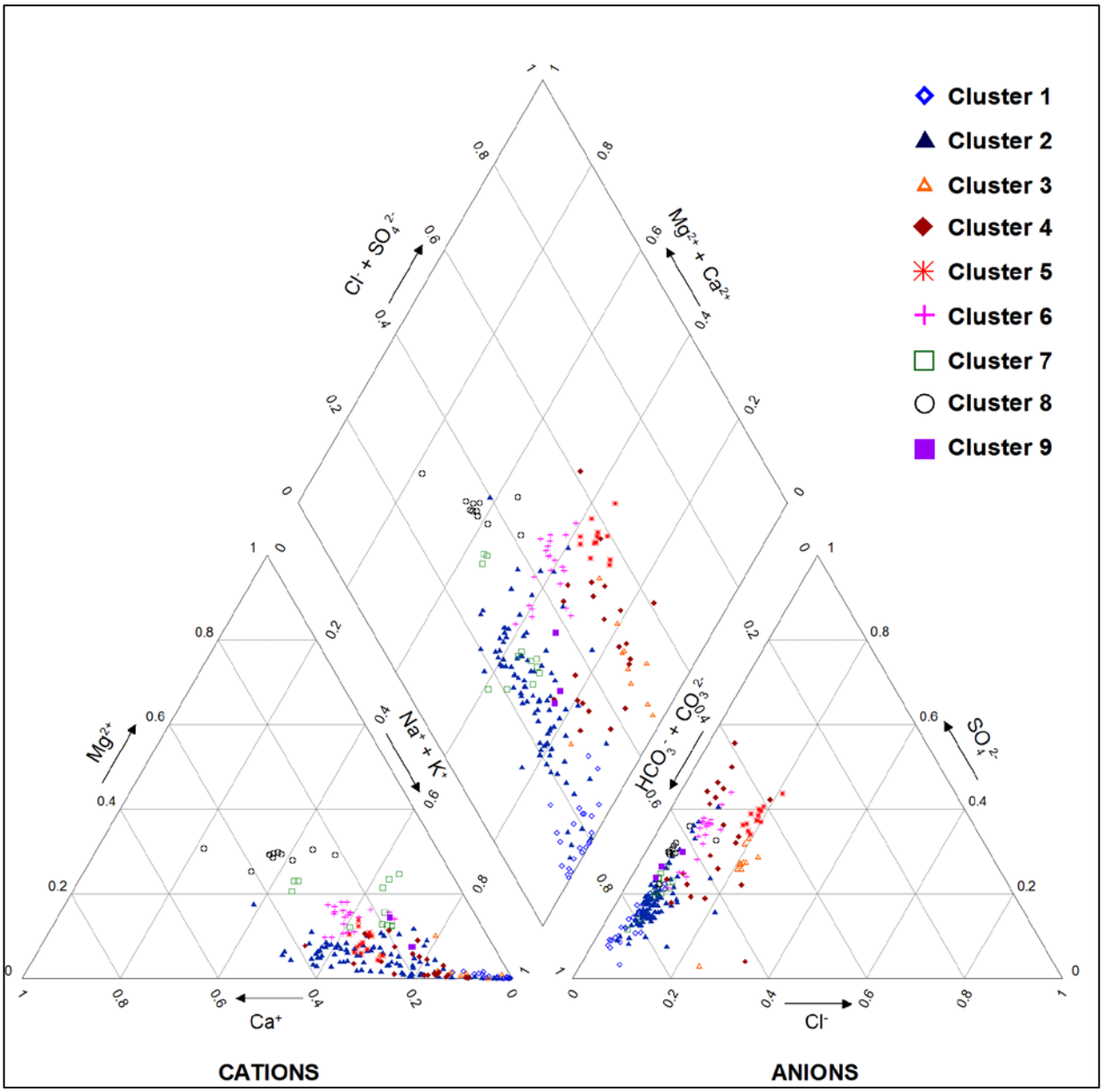

Figure 2-8

Piper diagram for PCFA-KMCA into nine groups.

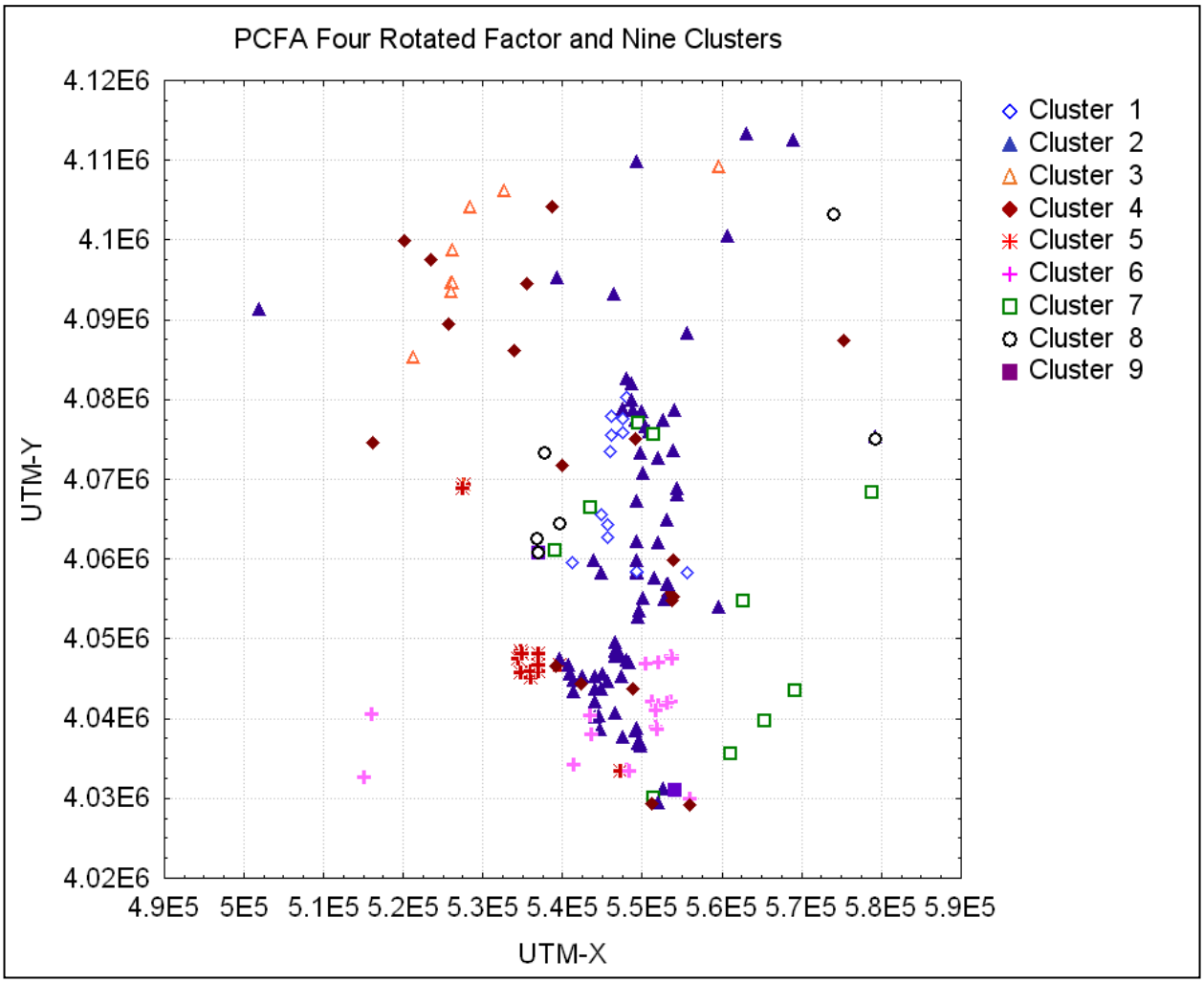

Figure 2-9

Spatial distribution of sampling-locations KMCA into nine groups based on PCFA first four factors.

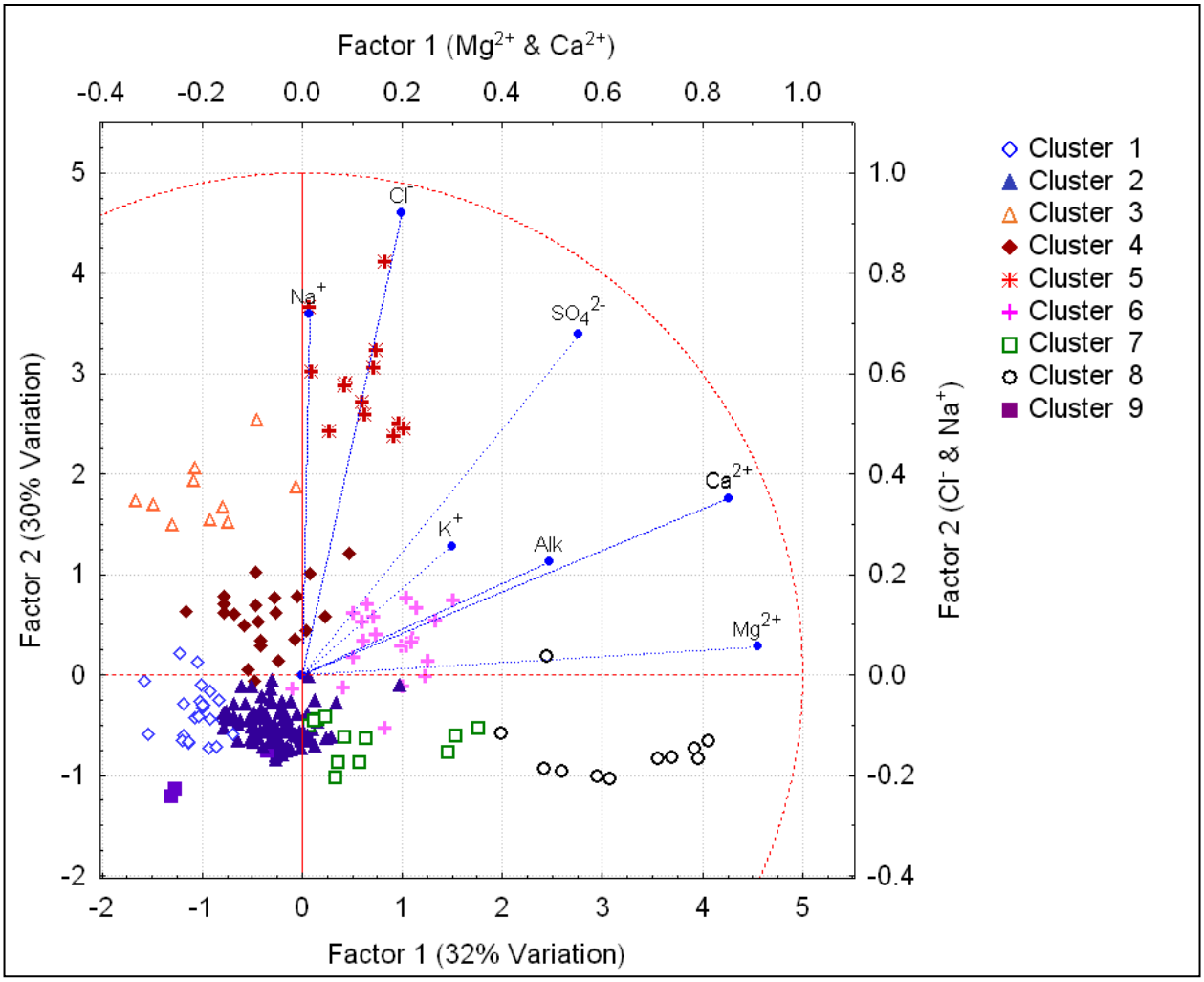

Figure 2-10

PCFA biplot of the first two factors with sampling-locations grouped into nine hydrochemical facies. A unit circle is included to provide further axis proportion.

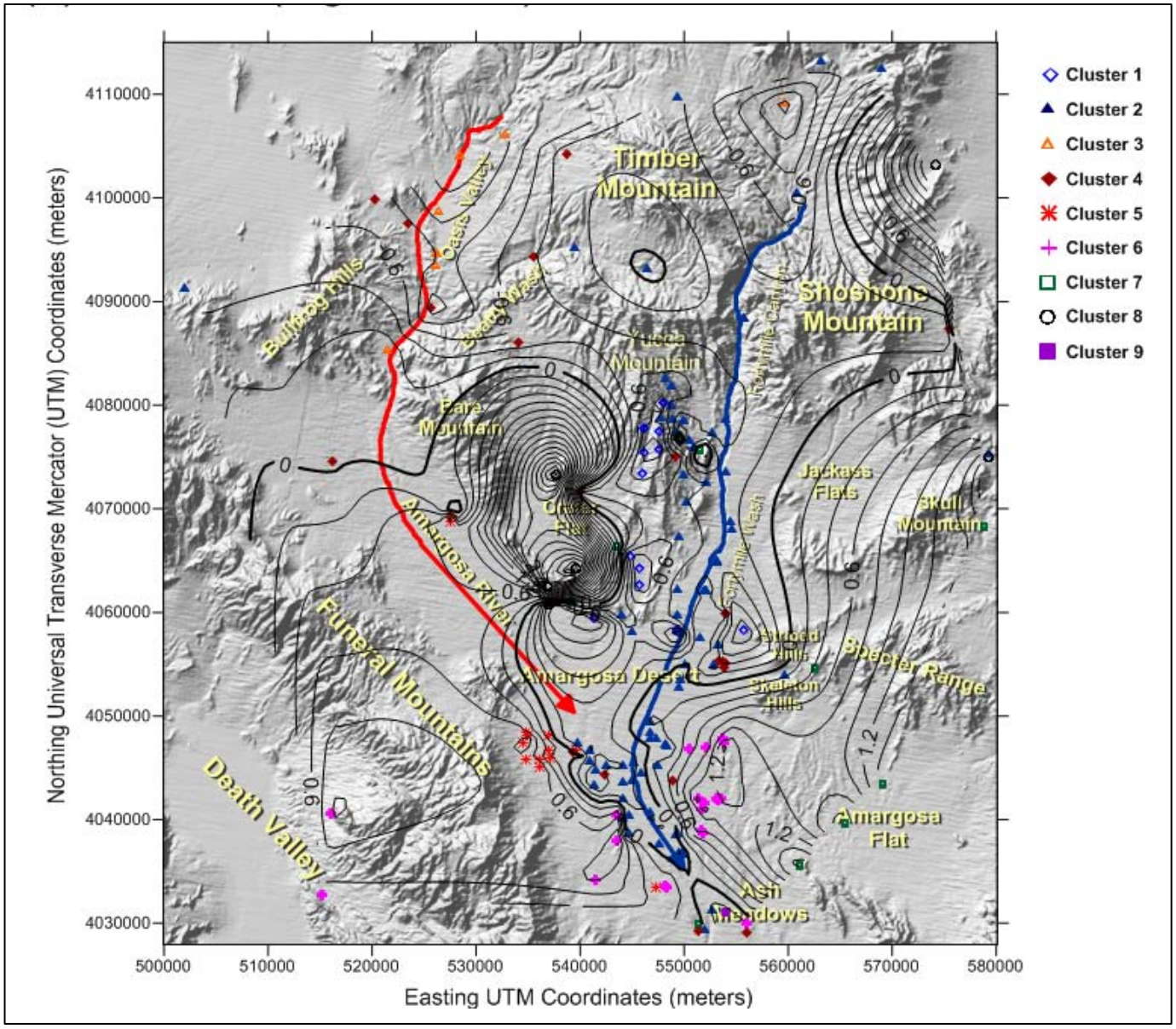

Figure 2-11

PCFA Factor 1 score contours with nine hydrochemical facies.

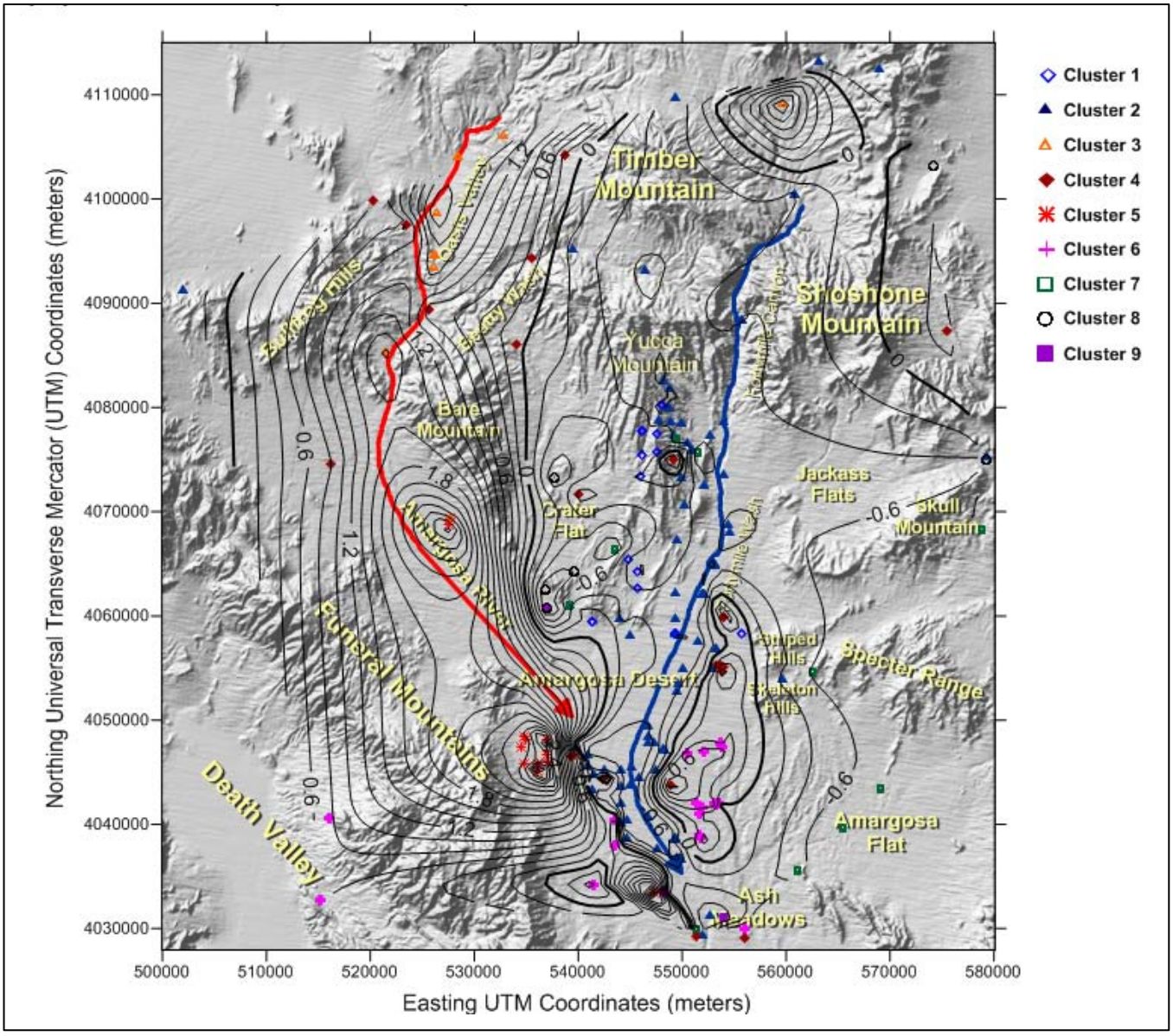

Figure 2-12

PCFA Factor 2 score contours with nine hydrochemical facies.

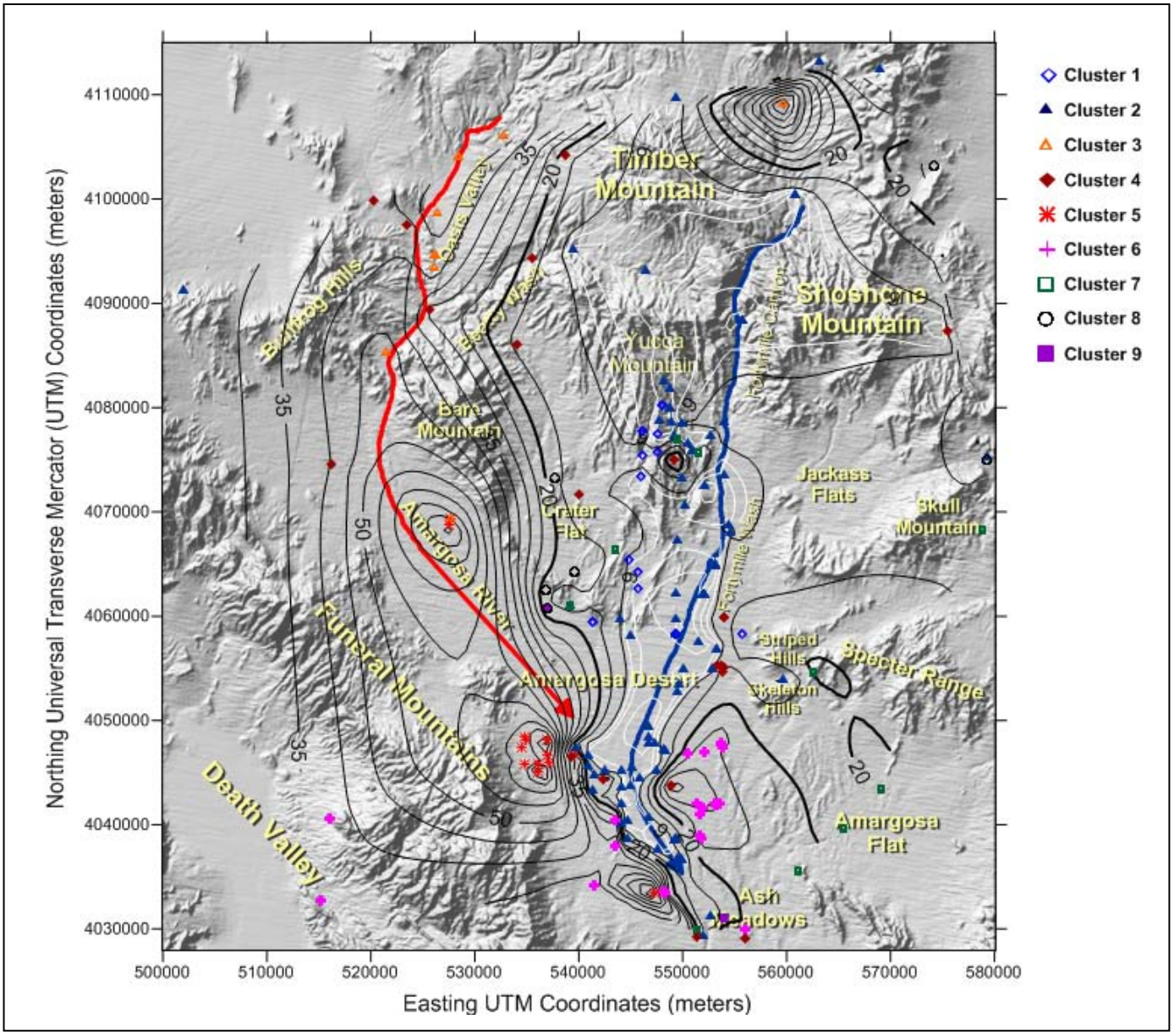

Figure 3-1

Cl^- concentration contours (mg/L) with nine hydrochemical facies.

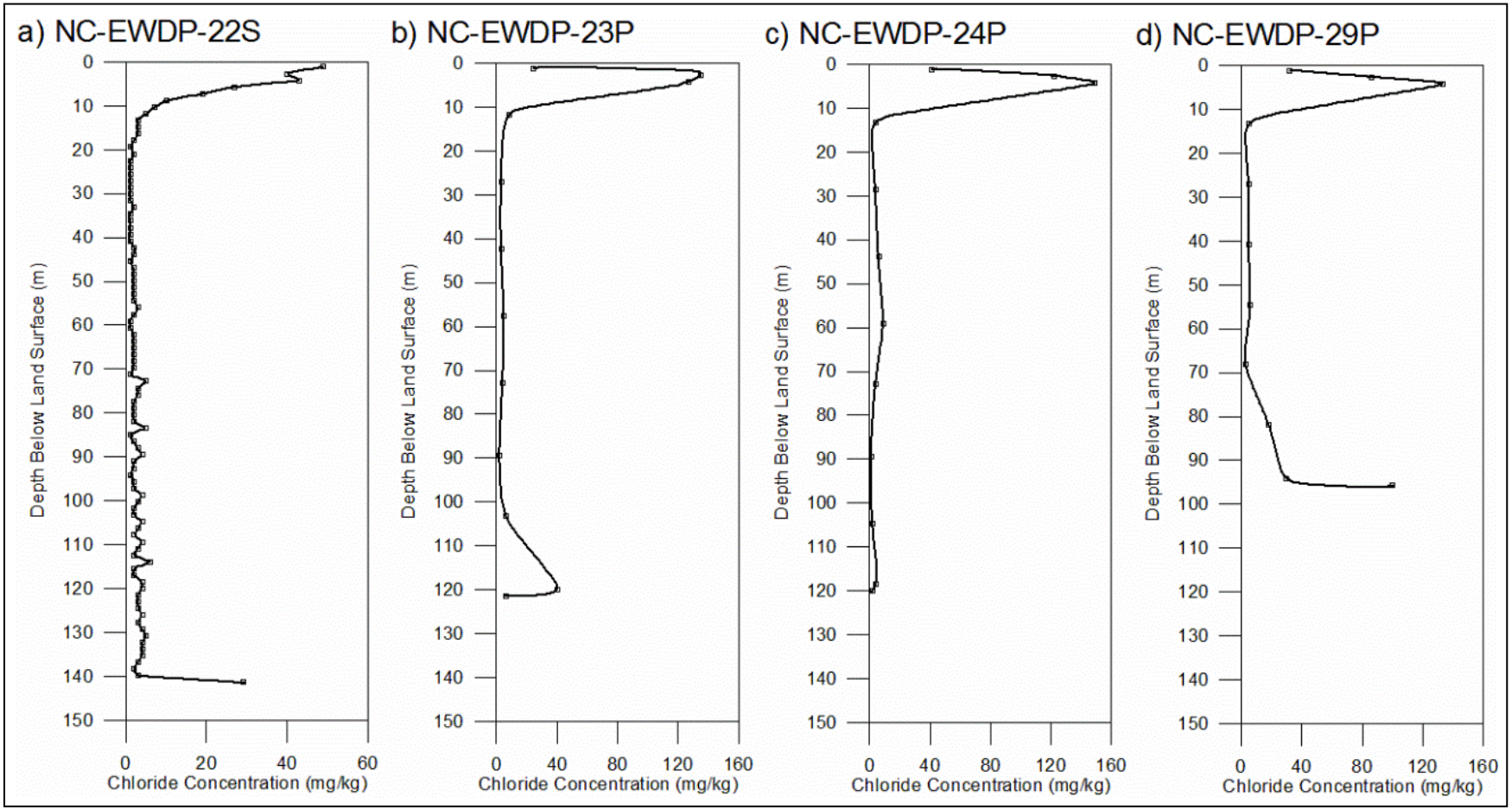

Figure 3-2

Interpolations of drill cutting chloride extracts from boreholes: (a) NC-EWDP-22S; (b) NC-EWDP-23P; (c) NC-EWDP-24P; and (d) NC-EWDP-29P.

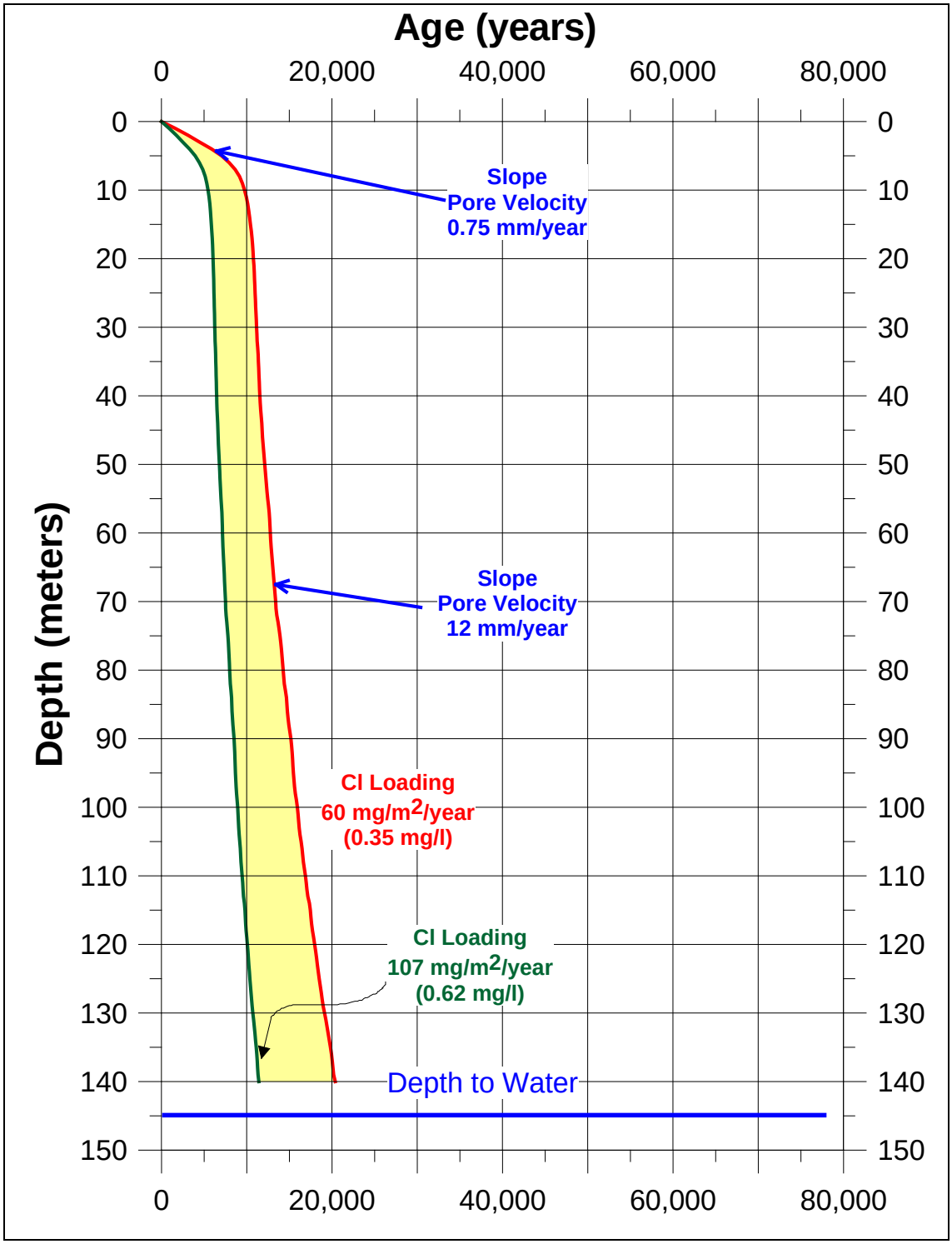

Figure 3-3
Depth-age profiles from borehole 22S drill cuttings' chloride mass-balance analysis.

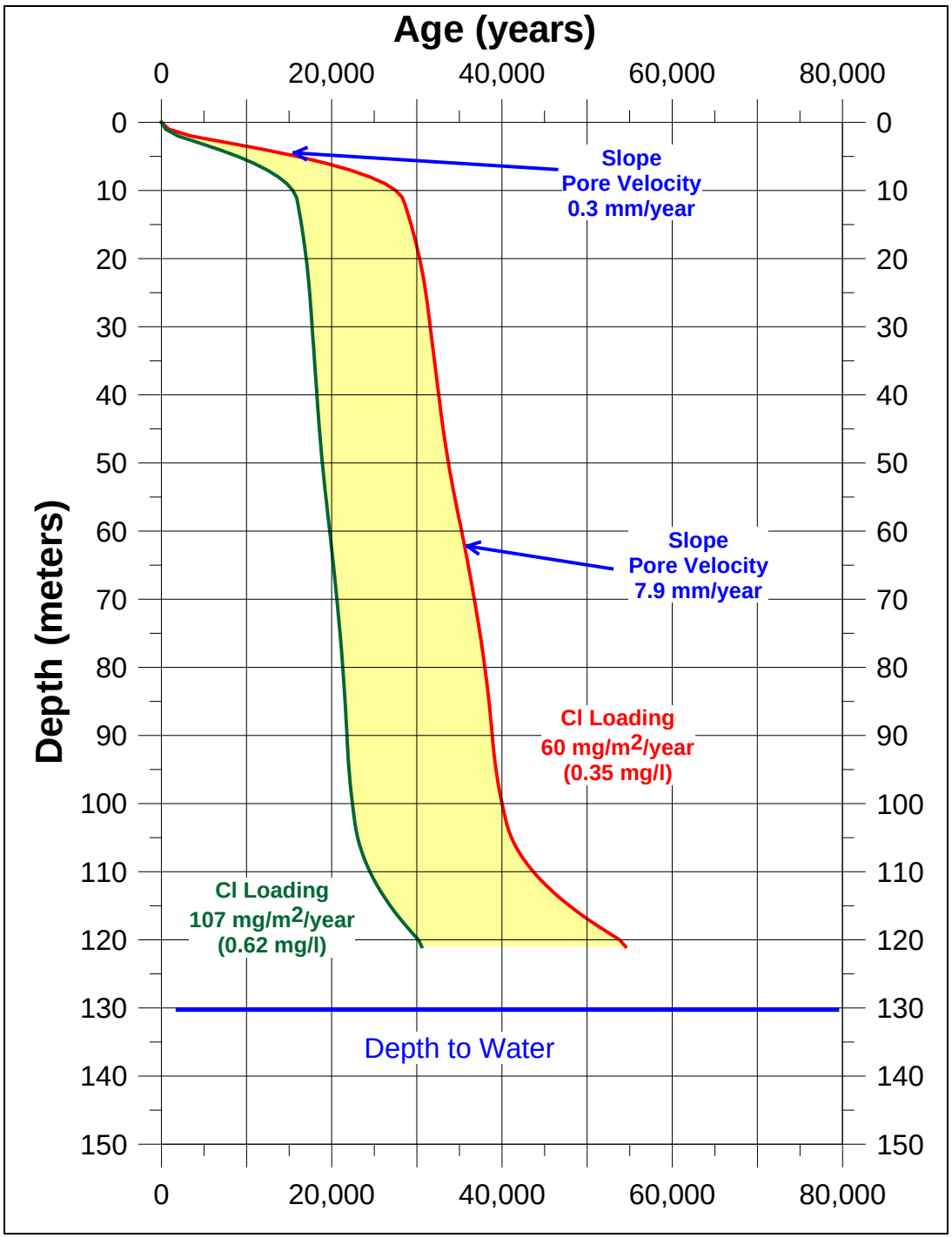

Figure 3-4
Depth-age profiles from borehole 23P drill cuttings' chloride mass-balance analysis.

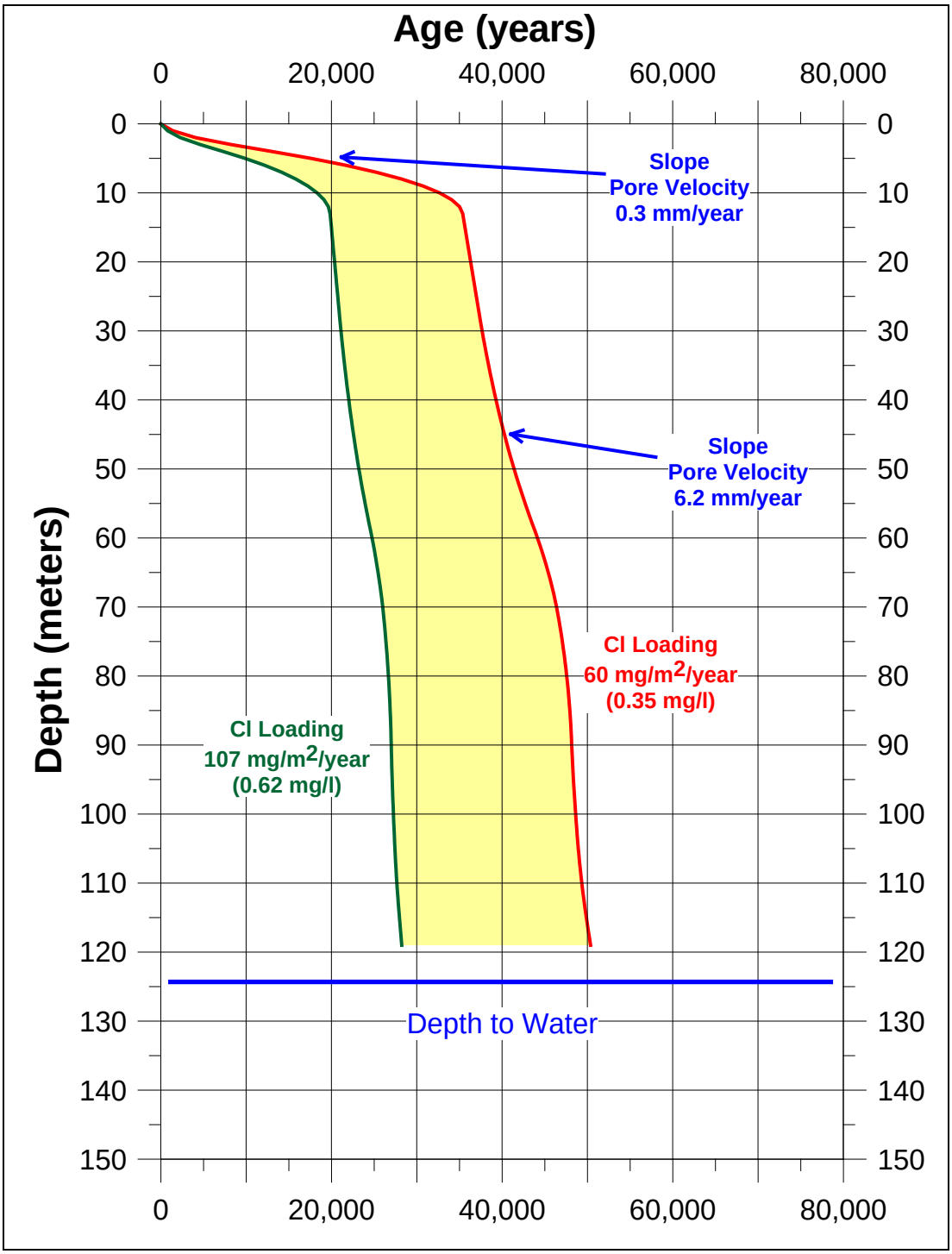

Figure 3-5
Depth-age profiles from borehole 24P drill cuttings' chloride mass-balance analysis.

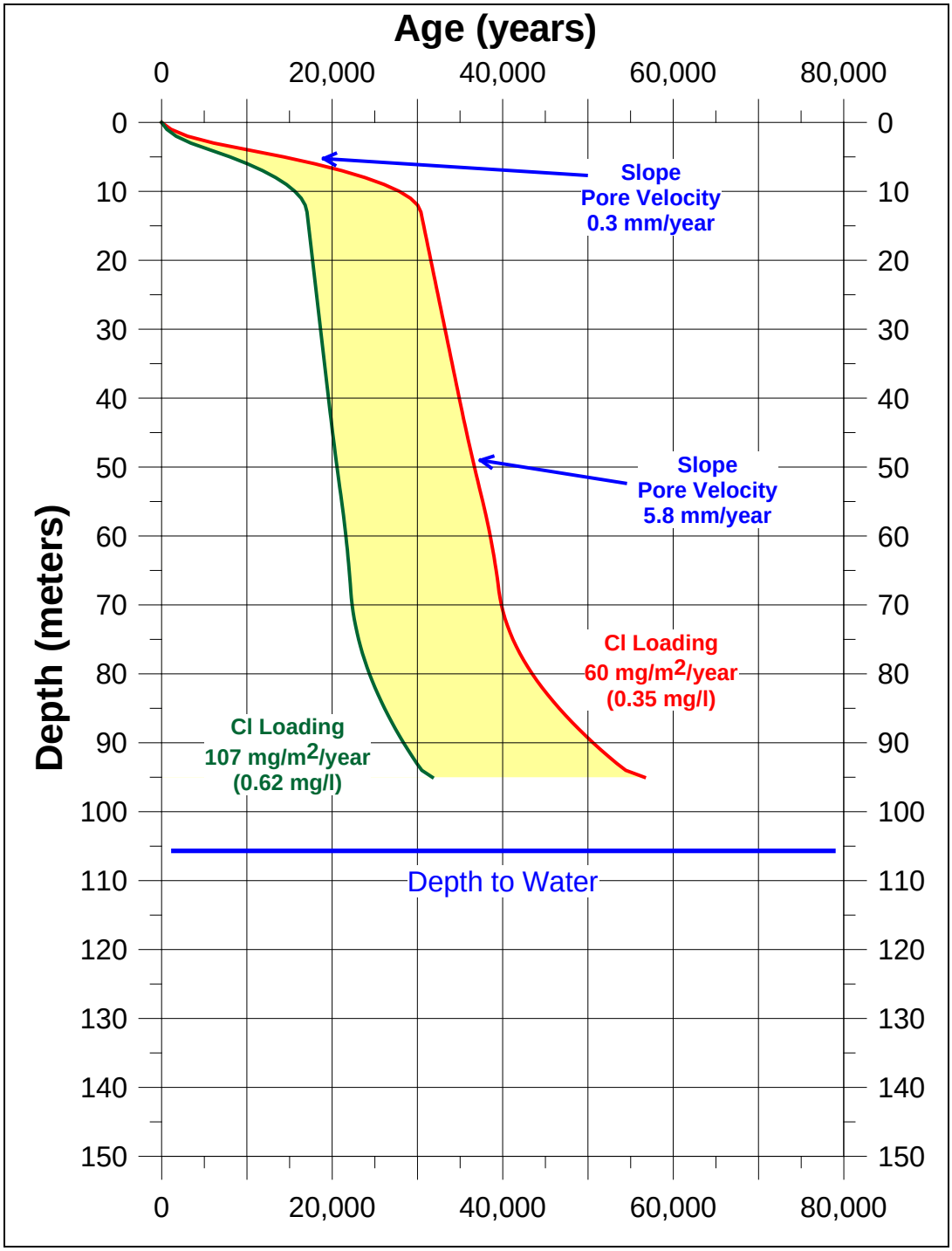

Figure 3-6
Depth-age profiles from borehole 29P drill cuttings' chloride mass-balance analysis.

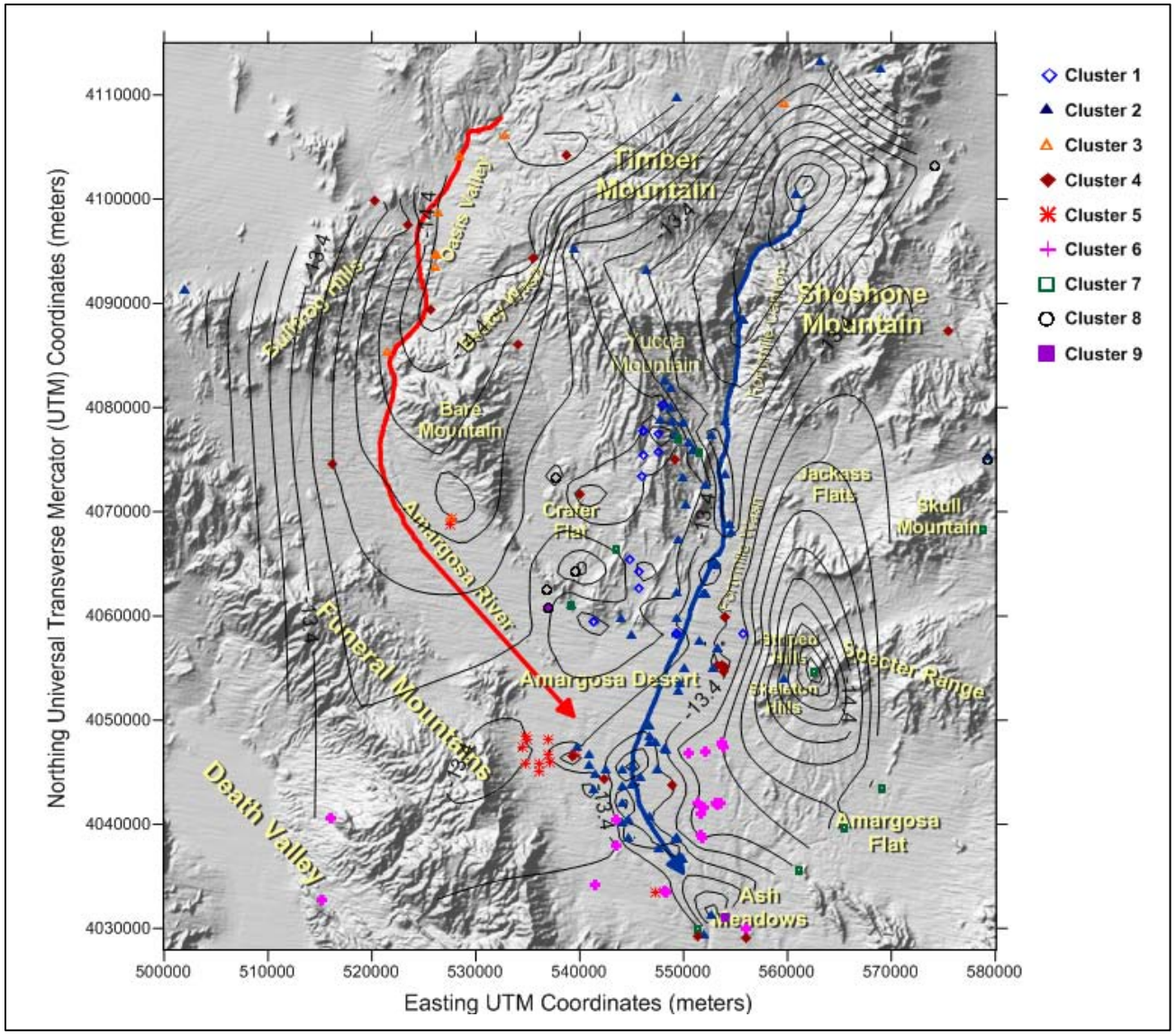

Figure 4-1
Groundwater oxygen-18 concentration contours in permil overlaid on DEM with samples grouped by PCFA-KMCA nine clusters.

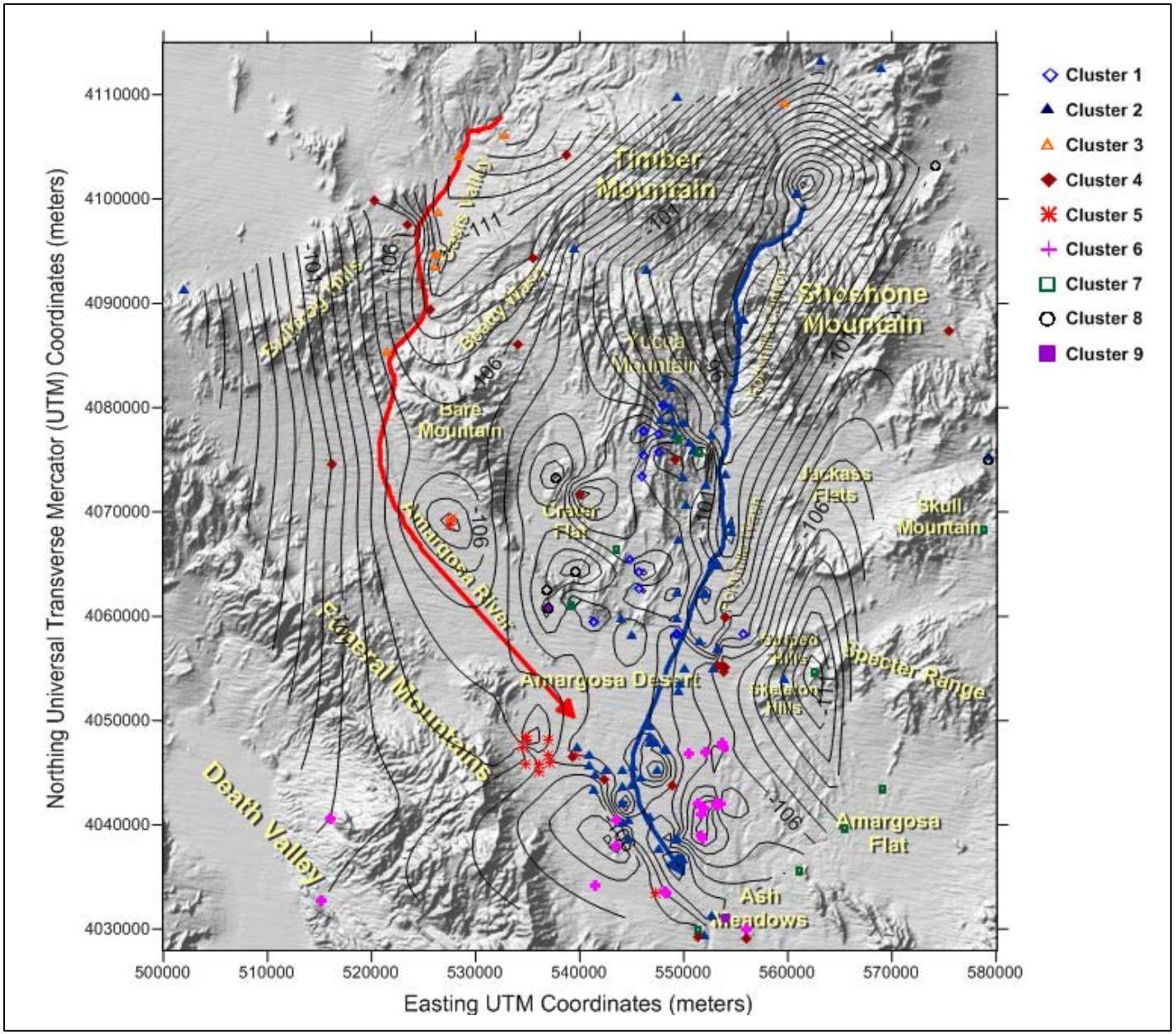

Figure 4-2

Groundwater hydrogen-2 concentration contours in permil overlaid on DEM with samples grouped by PCFA-KMCA nine clusters.

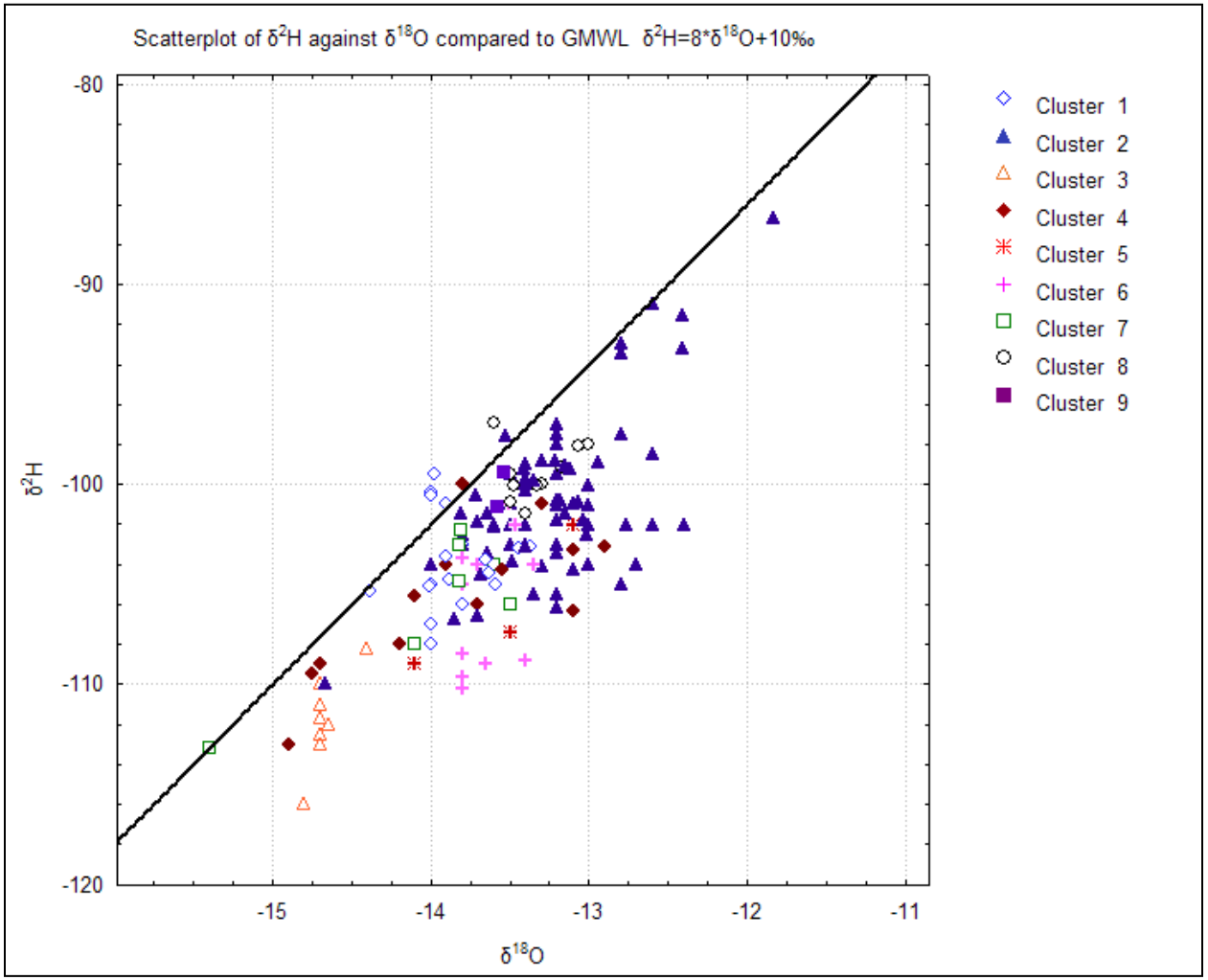

Figure 4-3

Groundwater stable isotope data by sample groups compared to the Global Meteoric Water Line with PCFA-KMCA nine clusters.

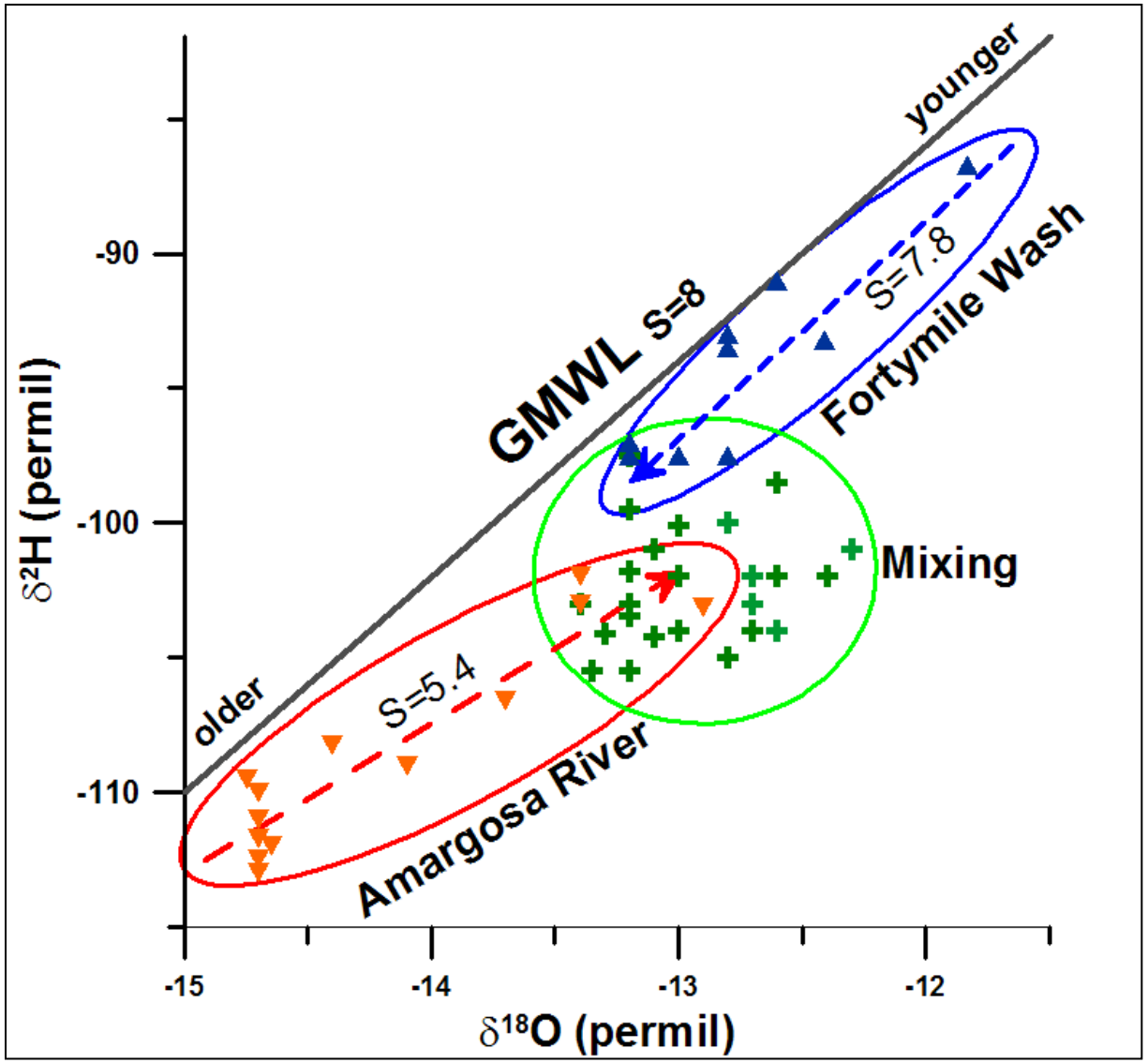

Figure 4-4
Groundwater stable isotope data following the traces of the wash, the river and their mixing, compared to the Global Meteoric Water Line.

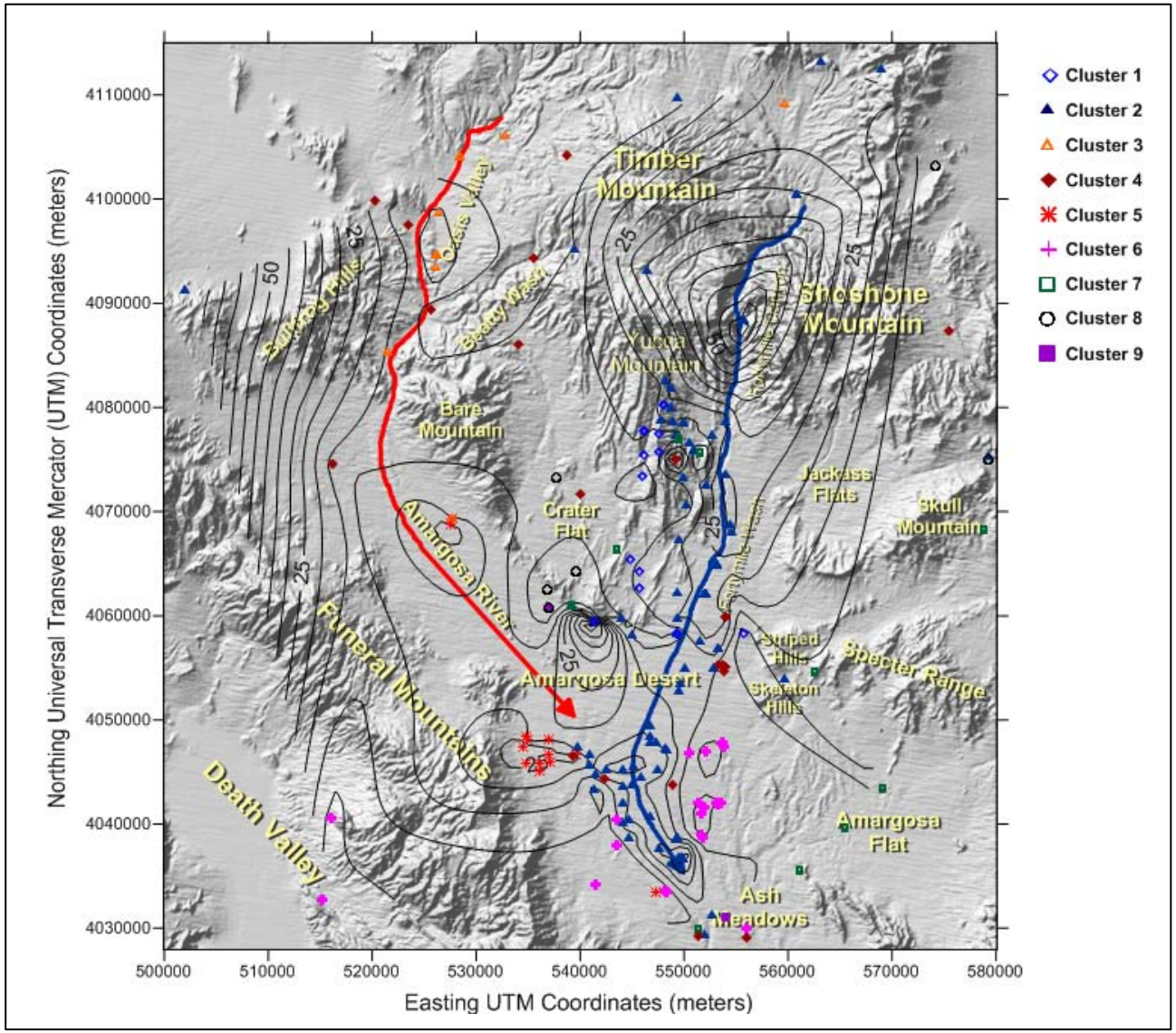

Figure 5-1
Groundwater carbon-14 data contours in pmc overlaid on DEM with samples grouped by PCFA-KMCA nine clusters.

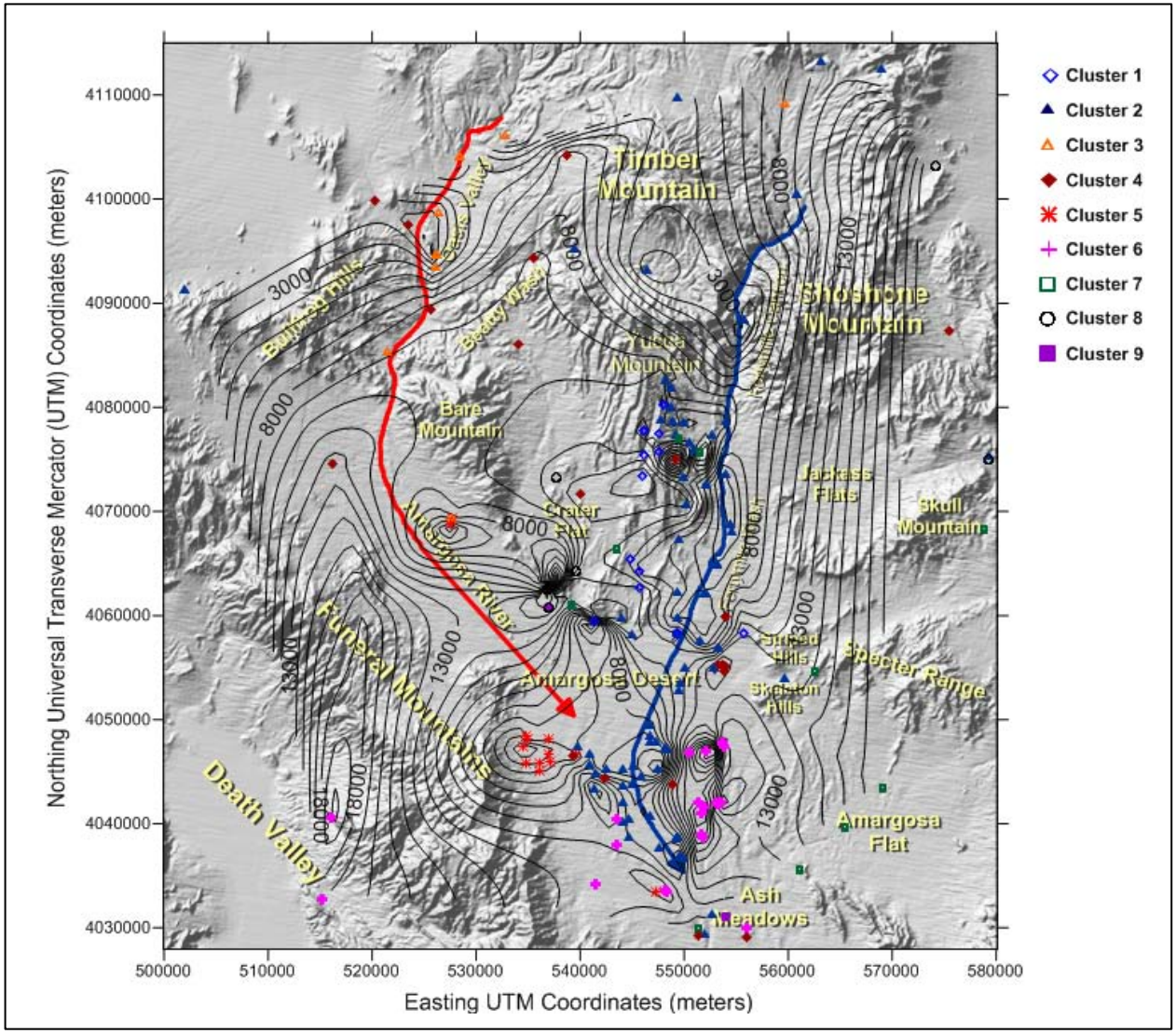

Figure 5-2
Groundwater carbon-14 data carbon-13 corrected age contours overlain on a DEM with samples grouped by PCFA-KMCA nine clusters.

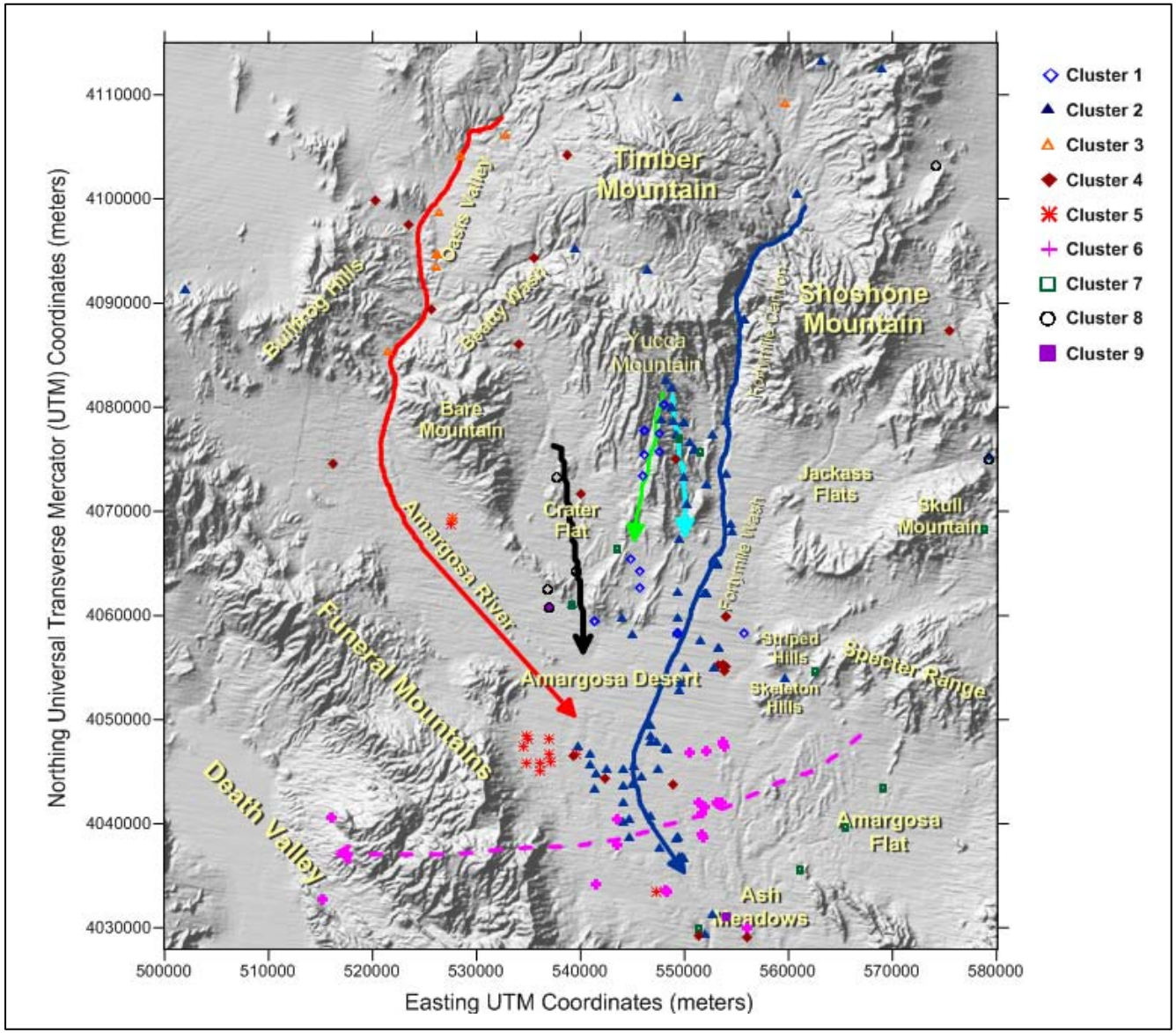

Figure 6-1
Six flowpaths inferred from PCFA-KMCA hydrochemical facies and processes.

APPENDIX A

Well Name	Well#	PCFA Cluster	pH	Ca (mg/L)	Mg (mg/L)	Na (mg/L)	K (mg/L)	Cl (mg/L)	SO4 (mg/L)	Total Alkalinity as CaCO3 (mg/L)	F (mg/L)	SiO2 (mg/L)	dD (permil)	d18O (permil)	d13C (permil)	14C (pmc)
Test Well 1 (USGS HTH #1)	26	2	8.7	1.2	0.01	51.3	0.5	3.2	8.7	85.3		19.5		-14.7	-10.2	30.1
ER-30-1 (upper)	28	2	9.4	3.5	0.05	62.0	1.8	6.2	12.0	108.6	1.7	29.0	-93.2	-12.4	-6.3	
ER-30-1 (lower)	29	2	9.2	2.1	0.07	65.0	1.0	6.5	9.9	105.7	1.4	25.0	-86.7	-11.8	-6.0	
H-6(Tct)	39	1	8.3	1.4	0.02	88.0	1.3	7.2	25.0	178.0	3.9	47.0	-105.0	-14.0	-7.3	10.0
H-6(Tcb)	40	1	8.3	4.7	0.07	88.0	1.4	7.4	32.0	191.9	4.7	49.0	-107.0	-14.0	-7.1	12.4
WT-7	41	1	8.7	2.6	0.18	97.0	2.1	13.0	7.2	206.7		20.0			-9.0	
USW WT-24 (4/24/98 sample)	44	2	7.9	0.3	0.03	59.0	1.6	6.7	15.0	97.6	0.9	53.0	-101.1	-13.2	-10.6	27.3
UZ-14(sh)	45	1	8.4	0.3	0.10	78.6	2.0	6.9	13.7	108.3	6.3		-100.4	-14.0	-14.1	24.6
UZ-14(dp)	46	1	8.4	0.2	0.10	80.0	2.4	8.4	14.5	112.4	6.7		-100.6	-14.0	-14.4	21.1
H-5	49	2	7.9	2.0	0.01	60.0	2.1	6.1	16.0	103.7	1.4	48.0	-102.0	-13.6	-10.3	19.8
USW SD-6	50	1	8.4	0.4	0.01	90.6	1.5	6.8	26.7	153.2	4.7	45.6	-105.3	-14.4	-9.4	
H-3	51	1	9.2	0.8	0.02	120.0	1.1	9.5	31.0	224.7	5.5	43.0	-101.0	-13.9	-4.9	10.5
NC-EWDP-03S-Z2	NC05	1	8.5	1.1	0.22	148.0	4.5	16.4	45.7	262.2	2.6	64.1	-103.6	-13.9	-10.1	61.4
NC-EWDP-19D	NC30	1	8.5	2.0	0.10	148.5	3.6	6.8	28.1	279.0	3.0	40.4	-105.0	-13.6	-4.6	8.4
NC-EWDP-19IM1 Z1	NC31	1	8.7	4.7	0.56	90.3	3.4	6.8	23.2	214.6	2.0	71.0				
NC-EWDP-19IM1 Z2	NC32	1	8.5	5.4	0.49	77.0	4.0	8.5	19.0	194.4	1.9	70.0				
NC-EWDP-19IM1 Z3	NC33	1	8.7	1.3	0.10	99.0	4.0	6.8	22.0	192.7	1.9	69.0				
NC-EWDP-19IM1 Z4	NC34	1	9.1	0.6	0.25	100.0	3.5	6.1	15.0	191.1	2.2	67.0				
NC-EWDP-19IM1 Z5	NC35	1	8.9	0.6	0.06	97.8	2.9	5.4	20.2	202.1	2.2	65.6	-108.0	-14.0	-6.0	5.9
NC-EWDP-19IM2 Z1	NC36	1	8.8	0.3	0.04	97.4	2.6	5.1	16.8	195.9	2.2	66.1	-105.1	-14.0	-6.1	5.9
UE-18r(7/11/91,8/11/92 and 12/9/99)	19	2	8.2	18.5	0.68	73.3	2.7	6.8	19.7	175.0	2.7	48.6	-110.0	-14.7	-1.7	7.7
Coffer's Ranch Windmill Well (samples from 1994thru1997)	22	2	8.3	16.2	0.19	70.6	0.9	7.5	30.2	150.9	3.4	40.2	-103.9	-13.5	-3.9	9.6

Well Name	Well#	PCFA Cluster	pH	Ca (mg/L)	Mg (mg/L)	Na (mg/L)	K (mg/L)	Cl (mg/L)	SO4 (mg/L)	Total Alkalinity as CaCO3 (mg/L)	F (mg/L)	SiO2 (mg/L)	dD (permil)	d18O (permil)	d13C (permil)	14C (pmc)
UE-18t (9/23/88)	27	3	8.6	22.2	1.00	141.0	8.2	64.4	10.8	271.5		7.0				
WT#15	33	2	7.5	12.0	1.70	62.0	4.6	12.0	16.0	136.1		52.0	-97.5	-13.2	-11.8	21.6
H-6(bh)	38	1	8.1	4.1	0.09	86.0	1.3	7.6	29.0	149.3	4.7	48.0	-106.0	-13.8	-7.5	16.3
WT-10	42	1	8.4	2.6	0.05	94.5	1.0	7.8	33.5	152.5	3.7	46.5	-103.0	-13.8	-6.1	7.3
G-2	43	2	7.5	7.7	0.47	46.0	5.3	6.5	15.0	99.2	1.0	51.0	-98.8	-13.3	-11.8	20.5
H-1(Tcp)	47	2	7.7	4.5	0.10	51.0	2.4	5.7	18.0	94.3	1.2	47.0	-103.0	-13.4		19.9
H-1(Tcb)	48	2	7.7	6.2	0.10	51.0	1.6	5.8	19.0	100.1	1.0	40.0	-101.0	-13.5	-11.4	23.9
G-4	52	2	7.7	13.0	0.20	57.0	2.1	5.9	19.0	114.0	2.5	45.0	-103.0	-13.8	-9.1	22.0
H-4	55	2	7.4	17.0	0.29	73.0	2.6	6.9	26.0	141.9	4.6	46.0	-104.0	-14.0	-7.4	11.8
c#1	58	2	7.6	11.0	0.34	56.0	2.0	7.4	23.0	123.8	2.1	56.0	-102.0	-13.5	-7.1	15.0
c#3	59	2	7.7	11.0	0.40	55.0	1.9	7.2	22.0	112.4	2.0	53.0	-103.0	-13.5	-7.5	15.7
c#3(95-97)	60	2	7.7	11.0	0.30	57.0	1.9	6.5	19.0	115.6		58.0	-99.7	-13.4		
c#2	61	2	7.7	12.0	0.40	54.0	2.1	7.1	22.0	114.0	2.1	54.0	-100.0	-13.4	-7.0	16.6
WT#12	66	2	7.6	15.0	0.30	66.0	2.6	7.8	28.0	137.0	3.1	47.0	-102.5	-13.8	-8.1	11.4
16S/48E-23bdb	124	2	7.3	9.2	1.00	66.0	6.6	8.9	26.9	128.1		73.9				
NC-EWDP-04PB	NC08	2	9.1	5.0	0.17	70.7	1.8	5.6	34.5	117.2	1.7	37.6	-106.7	-13.9	-9.4	17.4
NC-EWDP-10S Deep	NC20	2	7.9	10.8	1.79	51.9	5.5	6.5	18.6	105.8	2.2	56.9	-98.9	-12.9	-6.6	23.5
NC-EWDP-16P	NC28	1	8.6	2.5	0.25	102.5	1.9	8.8	42.6	161.3	2.9	44.2	-99.5	-14.0	-6.9	17.9
NC-EWDP-18P	NC29	2	8.1	10.4	0.19	67.8	2.1	8.4	20.0	121.8	2.5	52.6	-103.5	-13.6	-7.4	19.6
NC-EWDP-19PB Deep	NC39	1	8.3	9.1	0.73	78.4	3.2	5.2	22.5	161.3	1.5	56.3	-103.1	-13.4	-6.3	9.9
NC-EWDP-27P	NC51	1	8.5	4.8	0.95	102.8	3.4	8.8	34.7	175.8	3.2	42.9	-103.8	-13.6	-6.3	12.0
NC-EWDP-28P	NC52	1	8.9	4.0	0.32	97.9	4.0	7.1	38.1	177.3	2.1	71.4	-104.4	-13.6	-11.0	16.0
UE-25 WT#17	NC58	2	7.8	11.3	0.30	55.7	2.5	15.0	10.0	105.8	1.7	36.2	-101.9	-13.7	-8.3	16.2
ER-EC-08 (6/28/2000 and 07/12/2000)	1	3	8.0	10.3	0.85	120.0	5.6	50.7	84.8	145.0	5.3	49.1	-116.0	-14.8	-1.0	8.7
ER-OV-01 (11/08/97)	2	3	8.3	6.2	0.07	139.7	6.8	45.6	82.7	164.3	2.1	70.0	-112.5	-14.7	-2.0	5.0

Well Name	Well#	PCFA Cluster	pH	Ca (mg/L)	Mg (mg/L)	Na (mg/L)	K (mg/L)	Cl (mg/L)	SO4 (mg/L)	Total Alkalinity as CaCO3 (mg/L)	F (mg/L)	SiO2 (mg/L)	dD (permil)	d18O (permil)	d13C (permil)	14C (pmc)
ER-OV-06a (11/7/97)	3	3	8.3	2.1	0.74	144.5	7.5	48.5	80.0	167.3	3.1	52.9	-113.0	-14.7	-2.2	6.0
ER-OV-02 (11/11/97)	5	3	8.2	14.3	0.60	143.0	4.1	51.2	88.1	186.3	2.3	57.4	-112.0	-14.7	-2.6	16.2
Goss Springs North (11S/47E 10bad) (11/13/97)	7	3	8.2	16.4	1.17	107.0	5.0	43.0	76.4	147.7	2.4	53.2	-110.0	-14.7	-2.9	21.8
Er-OV-03a (11/09/97)	8	3	8.1	14.0	1.03	118.0	5.2	42.6	76.0	150.6	2.3	54.7	-111.0	-14.7	-3.0	16.3
Goss Spring (11S/47E-10bcc) (9/7/95)	11	3	7.7	17.5	1.29	116.5	5.1	45.0	78.1	148.4	2.8	50.4	-111.7	-14.7		20.8
ER-OV-04a (11/07/97)	12	4	8.4	8.7	0.11	98.8	7.8	28.2	59.9	136.8	2.8	68.9	-109.5	-14.8	-3.4	8.0
US Ecology MW-600	16	3	7.9	20.0	11.50	167.5	8.8	67.5	153.0	242.8	5.2	62.5	-108.3	-14.4	-8.4	19.3
15S/50E-18ccc	103	4	8.4	16.8	0.50	93.1	3.9	13.1	99.9	128.6	2.1	34.3				
NDOT	104	4	8.0	16.3	0.81	101.3	3.8	14.7	110.0	131.2	1.9	43.7				
15S/50E-18cdc	105	4	8.0	12.0	0.50	93.0	3.9	13.1	100.0	128.8	1.9	34.0				
UE-14b (7/24/91 sample)	195	4	8.4	10.5	0.24	77.5	1.5	7.1	80.8	95.1		43.8				
NC-EWDP-04PA	NC07	2	8.0	14.6	0.37	58.1	3.1	7.4	54.6	89.4	1.2	34.4	-100.8	-13.2	-9.5	18.1
ER-OV-05 (11/07/97)	4	4	7.8	21.5	4.36	103.5	10.0	37.7	55.6	193.2	1.7	82.4	-106.0	-13.7	-3.1	17.3
Springdale Upper Well (10S/47E-32adc) (11/12/97)	6	4	7.7	22.0	4.09	130.0	8.7	37.2	67.7	240.1	2.1	69.9	-104.0	-13.9	-1.7	10.8
ER-EC-05 (7/8/99,5/4/00, and 5/25/2000)	21	4	8.0	20.3	0.57	73.9	1.7	16.2	35.5	145.0	4.7	40.9	-113.0	-14.9	-2.5	6.3
ER-OV-03c (11/10/97)	23	4	8.2	15.1	0.40	79.7	1.3	17.4	43.6	132.5	4.5	42.9	-109.0	-14.7	-3.2	6.8
Water Well 8	25	2	7.3	7.9	1.22	31.1	3.3	7.3	15.0	64.0	0.7	50.0	-103.0	-13.5	-11.6	25.0
a#2sm1	30	2	7.2	10.0	0.20	44.0	1.1	11.0	22.0	87.8	1.0	44.0	-93.5	-12.8	-13.0	62.3
a#2sm2	31	2	7.0	10.0	0.30	44.0	1.3	8.8	21.0	87.8	0.9	44.0	-93.0	-12.8	-13.1	60.0
WT#14	34	2	7.3	10.0	0.80	45.0	5.0	8.2	22.0	97.6		57.0	-97.5	-12.8	-12.8	24.1
ONC#1	57	2	8.7	13.0	1.10	51.0	3.6	7.1	24.0	94.3		27.0				
GexaWell4	68	4	7.9	11.5	0.37	71.0	3.3	13.5	45.5	123.0	3.2	48.0	-105.6	-14.1		
VH-1	69	4	7.6	10.3	1.53	79.0	1.9	10.3	44.3	135.1	2.7	49.7	-108.0	-14.2	-8.5	12.2

Well Name	Well#	PCFA Cluster	pH	Ca (mg/L)	Mg (mg/L)	Na (mg/L)	K (mg/L)	Cl (mg/L)	SO4 (mg/L)	Total Alkalinity as CaCO3 (mg/L)	F (mg/L)	SiO2 (mg/L)	dD (permil)	d18O (permil)	d13C (permil)	14C (pmc)
Airport Well	106	2	8.7	5.6	0.10	69.0	1.5	6.6	45.0	105.5	1.8	38.0	-106.2	-13.2	-10.0	10.5
Funeral Mountain Ranch Irrig.	126	2	8.2	12.0	2.40	80.0	7.0	12.0	43.0	164.0	2.3	87.0	-106.6	-13.7	-5.5	6.5
NC-EWDP-03S-Z3	NC06	1	8.5	8.4	1.01	139.7	5.7	18.9	76.1	246.4	2.4	45.9	-104.8	-13.9	-5.6	6.5
NC-EWDP-05SB	NC09	1	8.2	11.5	1.34	125.7	6.3	19.9	69.4	238.6	1.9	34.1	-103.2	-13.4	-1.3	1.7
NC-EWDP-15P	NC27	2	7.9	11.7	1.59	68.5	3.4	8.1	50.4	126.7	1.8	45.8	-100.6	-13.7	-5.8	8.2
USW WT#1	NC55	4	8.2	5.5	0.10	60.3	2.3	30.5	5.0	81.2	3.2	10.1			-6.6	36.1
US Ecology MW-313	15	5	7.5	54.0	16.00	146.0	13.0	69.0	205.0	275.6	5.0	68.0	-109.0	-14.1	-6.1	17.0
NECWell	17	5	7.6	54.9	14.10	170.1	10.2	79.1	190.2	269.3		70.3			-5.9	28.8
Desert Farms Garlic Plot	101	4	7.8	30.0	2.10	71.0	5.1	13.0	117.0	102.5	0.8	40.0	-106.4	-13.1	-9.1	8.8
15S/50E-19b1	107	4	8.1	20.0	3.90	107.5	6.0	17.5	127.5	137.4	1.4	43.0				
16S/48E-8ba	108	5	7.9	58.5	6.30	180.5	12.9	79.8	202.7	242.7		37.9				
16S/48E-7bba	109	5	7.4	52.9	9.50	140.0	10.2	63.1	179.6	205.7		69.1				
16S/48E-7cbc	110	5	7.7	46.9	16.00	130.1	9.4	62.0	179.6	196.2		64.3	-102.0	-13.1	-6.2	31.4
16S/48E-18bcc	111	5	8.0	54.9	10.90	150.1	11.7	61.0	190.2	222.7		79.9				
16S/48E-17ccc	112	5	7.7	66.1	10.90	169.9	12.1	83.0	235.3	196.2		77.5				
16S/48E-18dad	113	5	7.7	52.9	8.50	149.9	10.6	63.1	187.3	193.6		76.9	-104.0	-13.6	-5.7	
16S/48E-8cda	114	5	7.6	48.1	6.80	160.0	10.2	67.0	179.6	216.7		67.9				
16S/48E-17abb	115	5	7.4	60.1	7.80	157.0	12.1	69.1	178.7	247.7		75.1				
Barrachman Dom/Irr.	116	5	7.5	53.0	12.00	128.0	10.0	62.0	179.0	234.6	1.8	66.0	-107.4	-13.5	-5.8	17.9
16S/48E-15ba	118	5	8.0	60.1	7.80	147.1	9.8	65.6	198.8	216.7		37.3				
Ponderosa Dairy #1	149	2	7.5	30.0	4.50	59.0	11.0	16.0	93.0	118.9	1.2	74.0	-105.5	-13.4	-7.2	14.2
16S/49E-15aaa	160	6	7.7	40.9	7.50	80.0	9.8	23.0	129.7	160.2		46.3	-105.0	-13.8	-3.4	
Anvil Ranch Irrigation	161	4	7.9	47.0	5.80	68.0	13.0	40.0	120.0	113.2	1.1	71.0	-103.3	-13.1	-10.4	11.8
17S/49E-11ba	169	6	8.1	40.1	14.10	97.0	14.1	28.0	160.4	172.1		52.9				
17S/49E-29acc	181	5	7.6	54.1	15.10	160.0	19.9	69.8	186.4	226.2		72.1				

Well Name	Well#	PCFA Cluster	pH	Ca (mg/L)	Mg (mg/L)	Na (mg/L)	K (mg/L)	Cl (mg/L)	SO4 (mg/L)	Total Alkalinity as CaCO3 (mg/L)	F (mg/L)	SiO2 (mg/L)	dD (permil)	d18O (permil)	d13C (permil)	14C (pmc)
NC-EWDP-23P Shallow	NC48	4	8.0	23.4	5.31	91.7	8.5	13.3	130.0	136.1	1.3	43.2	-101.0	-13.3	-8.3	22.8
NC-EWDP-23P Deep	NC49	4	8.2	17.9	1.07	119.0	4.8	10.9	158.0	114.8	0.8	37.7	-104.3	-13.5	-7.7	19.0
Beatty Well no. 1 (Wat&Sanit Distr) (2/11/97 and 4/28/97)	13	3	8.0	39.2	5.46	126.3	8.5	48.4	113.0	166.5	1.4					
Bond Gold Mining #1	14	4	8.3	23.0	6.00	65.0	7.3	40.0	52.0	132.0	0.6	29.0	-100.0	-13.8	-8.8	12.8
Selbach Domestic	121	4	8.0	23.0	8.10	90.0	6.6	36.0	96.0	146.0	1.4	68.0	-103.2	-12.9	-8.1	30.7
16S/48E-23da	125	4	8.2	22.0	2.20	69.0	6.6	26.6	67.2	110.1						
16S/49E-9cda	146	2	7.6	30.5	3.40	51.0	8.6	12.1	64.4	117.6		65.5				
16S/49E-9dcc	147	2	8.2	22.8	2.70	56.1	9.0	9.9	67.2	115.6		72.1	-103.0	-13.4	-7.3	21.9
16S/49E-16ccc	148	2	7.9	30.1	1.90	39.8	4.3	8.2	50.9	108.6		76.9	-97.5	-13.2	-5.2	24.8
17S/49E-9aa	150	2	8.0	24.8	3.60	48.0	9.8	9.9	69.2	107.6		70.3	-105.0	-12.8		18.9
16S/50E-7bcd	156	6	7.6	47.7	17.50	111.5	12.9	29.1	151.8	239.2		28.8	-105.0	-13.8	-3.6	7.0
Nelson Domestic	157	6	7.5	43.0	16.00	110.0	11.5	26.5	154.0	252.6	3.8	25.5	-110.2	-13.8	-2.0	0.9
16S/49E-12ddd	158	6	7.6	45.7	17.00	120.0	4.3	24.1	160.4	236.7		20.4				
Lowe Domestic	159	6	7.7	44.0	11.00	111.0	11.0	30.0	147.0	224.7	1.4	43.0	-103.7	-13.8	-3.0	1.2
16S/49E-36aaa	162	6	7.8	52.1	22.10	120.0	18.0	26.9	168.1	257.8		37.9	-104.0	-13.7	-4.4	10.3
16S/49E-35baa	163	6	7.4	53.3	18.00	113.1	13.3	31.2	170.0	248.3		37.9				
Payton Domestic	164	6	7.6	51.0	19.00	107.0	16.0	41.0	155.0	237.8	3.9	36.0	-109.7	-13.8	-2.7	3.3
16S/49E-36aba	165	6	7.7	44.9	19.90	110.1	16.8	24.1	155.6	240.2		42.7				
16S/49E-35aaa	166	6	7.7	44.1	16.00	120.0	16.0	29.1	147.9	222.7		36.7				
Oettinger Well	167	6	7.5	50.0	16.00	103.0	15.0	29.0	157.0	238.7	3.3	39.0	-108.5	-13.8	-2.6	1.4
Amargosa Motel (b)	168	6	7.6	49.5	18.00	97.5	14.0	27.0	151.0	234.6	3.0	43.5	-109.0	-13.7	-3.0	1.9
18S/50E-6dac	175	6	8.2	23.6	11.90	102.5	13.7	20.6	106.6	188.6		80.5				
18S/50E-7aa	176	4	8.4	25.7	9.50	140.9	19.2	37.6	147.0	214.2		47.5				
16S/48E-36dcc	177	6	7.2	54.9	9.70	100.0	12.9	33.0	110.5	246.2		70.3				

Well Name	Well#	PCFA Cluster	pH	Ca (mg/L)	Mg (mg/L)	Na (mg/L)	K (mg/L)	Cl (mg/L)	SO4 (mg/L)	Total Alkalinity as CaCO3 (mg/L)	F (mg/L)	SiO2 (mg/L)	dD (permil)	d18O (permil)	d13C (permil)	14C (pmc)
18S/49E-11bbb	185	4	7.6	34.1	8.50	99.1	11.7	30.8	90.3	184.2		78.1				
Nevares Spring	201	6	7.4	42.0	20.00	140.0	11.0	37.0	170.0	289.5	3.2	26.0	-101.0	-13.5	-5.5	3.0
Travertine Spring	202	6	7.4	33.0	18.00	140.0	12.0	37.0	150.0	281.3	3.7	30.0	-102.0	-13.5	-3.8	3.3
JF#3	37	2	7.7	18.0	3.10	38.0	8.9	10.0	30.0	98.4	1.6	56.0	-97.0	-13.2	-8.6	30.7
16S/48E-15dda	122	2	8.0	20.0	5.80	70.8	7.4	17.4	37.5	144.1		71.5				
16S/49E-23add	123	2	8.2	16.0	1.70	55.9	6.6	8.9	34.6	104.1		76.3		-13.2	-8.4	27.4
16S/49E-05acc	127	2	8.1	29.0	2.20	35.0	5.1	6.0	26.0	110.7	1.0	62.0	-103.0	-13.2	-7.1	19.3
16S/49E-8abb	128	2	7.5	30.1	2.70	37.0	5.5	7.8	29.8	124.6		54.1	-99.5	-13.2	-6.8	21.4
16S/49E-8acc	129	2	7.9	22.8	2.40	37.0	6.6	6.0	28.8	113.1		58.3				
16S/49E-19daa	132	2	8.2	24.0	1.20	36.1	8.2	6.7	32.7	110.1		75.1	-101.0	-13.1		20.8
DeLee Large Irrigation	133	2	8.0	24.0	1.10	37.0	8.4	6.2	25.0	110.7	1.1	76.5	-104.1	-13.3	-8.4	20.5
Bray Domestic	136	2	8.0	22.0	1.80	35.0	8.8	7.9	25.0	107.4	1.0	74.0	-103.5	-13.2	-10.0	23.5
17S/49E-7bb	139	2	8.3	24.0	1.70	48.0	7.4	9.6	30.7	125.6		79.9	-104.0	-12.7		10.0
17S/49E-8ddb	140	2	8.4	20.8	2.70	36.1	7.4	6.4	26.9	101.1		81.1	-102.0	-13.0		27.8
17S/49E-35ddd	141	2	8.0	15.2	4.60	50.6	8.2	6.7	40.3	129.1		81.1	-102.0	-12.4		13.8
15S/49E-22a1	142	2	8.0	25.0	2.40	41.0	5.2	8.0	33.0	118.9	1.4	52.0				
15S/49E-22dcc	143	2	6.7	27.0	2.00	43.0	4.6	8.5	33.0	122.2	1.0	49.0				
15S/49E-27acc	144	2	7.8	22.0	1.60	48.0	2.9	7.3	36.0	123.8	0.9	19.0				
O'Neill Domestic	145	2	7.9	26.0	2.40	44.0	7.6	7.4	43.0	115.6	0.8	65.0	-101.8	-13.2	-6.7	17.7
17S/49E-15bbd	151	2	8.1	20.8	3.90	31.3	8.2	9.9	34.6	98.6		72.7				40.3
M. Gilgan Well	152	2	8.2	19.0	2.30	41.0	7.5	8.0	28.0	105.8	1.6	77.0	-100.1	-13.0	-9.0	27.9
17S/49E-15bc	153	2	8.2	21.6	1.00	39.1	6.6	10.6	27.9	100.1						
18S/49E-1aba	174	9	8.6	24.0	11.90	94.9	19.2	18.1	99.9	215.7		72.7				
Crane Domestic	178	6	7.2	64.0	18.00	147.0	16.0	41.0	138.0	369.9	3.3	45.0	-108.8	-13.4	-4.3	7.9
27N/4E-27bbb	179	6	7.8	58.1	19.00	134.0	19.2	31.9	106.6	359.3		72.1				

Well Name	Well#	PCFA Cluster	pH	Ca (mg/L)	Mg (mg/L)	Na (mg/L)	K (mg/L)	Cl (mg/L)	SO4 (mg/L)	Total Alkalinity as CaCO3 (mg/L)	F (mg/L)	SiO2 (mg/L)	dD (permil)	d18O (permil)	d13C (permil)	14C (pmc)
IMV on Windjammer	180	6	7.5	45.0	9.85	100.0	11.0	30.5	89.0	248.5	2.8	67.5	-104.0	-13.4	-5.0	6.6
17S/49E-28bcd	182	6	7.6	42.9	10.00	100.0	12.1	24.1	89.3	241.7		70.3				
Mom's Place	184	2	7.8	27.0	6.70	77.0	9.4	14.0	55.0	193.6	2.6	75.0	-105.5	-13.2	-4.9	11.4
TW-5	186	7	7.9	33.0	17.00	130.0	12.0	21.0	99.0	324.0	3.4	19.0	-113.2	-15.4		
Unnamed Well 15S/50E-22-7	187	2	6.7	27.0	2.00	43.0	4.6	8.5	33.0	122.0	0.9	49.0				
Amargosa Tracer Hole #2	188	7	8.0	42.8	18.50	63.8	7.5	21.0	68.7	228.9	1.9	22.0		-13.6	-6.0	4.6
USDOE-MSH-C shallow Well	190	7	8.0	16.0	17.00	81.0	9.4	17.0	58.0	214.1	1.7	34.0	-108.0	-14.1		
Woodcamp Spring	199	2	7.2	23.0	3.30	38.0	14.0	24.0	24.0	100.1	0.2	57.0	-91.6	-12.4	-12.2	78.0
NC-EWDP-09SX Z1	NC15	2	8.2	17.1	6.08	76.4	5.3	14.4	55.4	166.4	1.9	45.6	-101.5	-13.8	-6.2	9.4
NC-EWDP-09SX Z2	NC16	7	8.1	19.1	7.61	75.5	4.2	10.3	58.2	177.7	1.9	53.4	-102.3	-13.8	-5.9	8.8
NC-EWDP-09SX Z3	NC17	7	8.3	17.6	7.34	74.5	4.0	10.0	57.2	176.3	1.9	47.6	-103.0	-13.8	-5.8	8.7
NC-EWDP-09SX Z4	NC18	7	8.2	19.7	7.73	73.6	3.8	10.0	60.8	175.6	1.9	54.8	-104.9	-13.8	-5.1	8.0
NC-EWDP-12PB	NC24	9	7.6	29.6	8.05	137.5	27.1	14.9	107.5	288.1	3.3	71.2	-99.4	-13.5	-3.3	3.6
NC-EWDP-13P	NC26	7	8.3	20.4	17.00	87.8	11.0	14.0	60.0	222.3	1.1	81.5				
Washburn - 1X	NC56	2	8.0	20.8	2.70	36.3	4.8	6.4	26.9	100.1	1.2	57.9	-100.8	-13.2	-6.5	20.1
Poderosa Dairy Well	NC60	2	8.1	18.2	3.35	51.8	10.3	7.6	46.7	118.1	1.6	91.2	-99.0	-13.4	-7.6	14.2
VH-2	70	8	7.1	78.5	29.80	70.8	8.1	16.0	142.5	321.3	1.1	26.3	-99.5	-13.5		
USFWS - Five Springs Well	172	7	7.5	47.0	20.00	67.5	7.9	23.3	82.0	249.4	1.6	21.8	-104.0	-13.6		
UE-17a (6/9/93)	191	8	7.6	41.0	29.90	80.0	3.0	27.7	95.5	164.0	0.9	11.8	-100.0	-13.3	-9.9	4.9
Pluto 1	196	2	8.0	40.5	9.83	36.2	7.7	23.7	46.9	123.0		54.0				
Pluto 5	197	8	7.9	55.0	21.60	26.4	4.3	11.5	54.2	178.8		58.0				
USGS Test Well F (HTH)	198	7	6.9	46.0	16.67	63.0	9.1	12.9	79.3	208.5	3.2	36.4				
NC-EWDP-01S-Z1	NC03	8	8.0	60.2	31.80	69.3	8.9	15.3	130.0	292.2	0.5	58.8	-101.5	-13.4	-4.5	5.2
NC-EWDP-01S-Z2	NC04	8	8.0	57.4	31.62	69.3	9.4	15.9	131.2	285.7	0.5	52.6	-100.0	-13.5	-5.0	5.0

Well Name	Well#	PCFA Cluster	pH	Ca (mg/L)	Mg (mg/L)	Na (mg/L)	K (mg/L)	Cl (mg/L)	SO4 (mg/L)	Total Alkalinity as CaCO3 (mg/L)	F (mg/L)	SiO2 (mg/L)	dD (permil)	d18O (permil)	d13C (permil)	14C (pmc)
NC-EWDP-07S	NC10	8	8.0	74.4	37.40	86.7	8.3	20.4	175.0	354.3	0.8	175.0	-98.0	-13.0	-4.9	8.4
NC-EWDP-07SC Z1	NC11	8	7.6	74.7	37.80	84.6	5.9	16.6	132.0	304.3	0.8	23.1	-100.1	-13.3	-3.9	5.2
NC-EWDP-07SC Z2	NC12	8	7.5	76.3	38.95	86.3	6.1	20.6	136.0	304.3	0.8	20.9	-99.1	-13.2	-3.8	5.1
NC-EWDP-07SC Z3	NC13	8	7.7	69.3	38.20	89.1	7.8	19.6	136.0	309.6	0.8	28.7	-98.1	-13.1	-4.6	5.5
NC-EWDP-07SC Z4	NC14	8	8.3	35.5	29.10	87.9	9.0	16.3	135.0	225.5	0.8	32.6	-96.9	-13.6	-4.7	6.0
NC-EWDP-12PC	NC25	8	8.0	50.6	27.75	71.6	10.0	15.1	130.0	271.9	1.0	60.0	-100.9	-13.5	-4.8	5.3
ER-EC-07 (06/05/2000)	24	2	7.9	21.6	1.75	36.8	3.1	6.0	18.3	122.0	1.5	44.0	-98.0	-13.2	-6.3	36.5
UE-29a#1 HTH (11/6/97)	32	2	7.6	15.0	2.25	36.5	4.1	7.9	16.2	89.3	0.6	57.2	-91.0	-12.6	-10.5	75.7
J-12	36	2	7.1	14.0	2.10	38.0	5.1	7.3	22.0	97.6	2.1	54.0	-97.5	-12.8	-7.9	32.2
b#1(Tcb)	53	2	7.1	18.0	0.72	46.0	2.8	7.5	21.0	109.1	1.6	51.0	-99.5	-13.5	-8.6	18.9
b#1(bh)	54	2	7.3	18.0	0.66	49.5	3.6	10.8	23.0	127.9	1.6	52.5	-100.3	-13.4	-10.6	16.7
UZ#16	56	7	9.0	11.4	16.00	79.2	0.0	10.6	29.1	172.2		36.2			-12.9	
p#1(v)	62	7	6.8	37.0	10.00	92.0	5.6	13.0	38.0	282.1	3.4	49.0	-106.0	-13.5	-4.2	3.5
CIND-R-LITE	89	2	7.8	12.3	6.17	71.7	4.0	9.2	46.0	158.9	2.5	54.3	-102.0	-13.6		
16S/48E-10cba	119	2	8.3	9.2	3.90	60.9	5.5	8.2	32.7	136.1		64.3	-102.0	-13.4	-5.6	15.6
16S/48E-15aaa	120	2	8.1	9.6	3.20	57.9	5.9	7.4	27.9	125.6		67.9	-103.0	-13.4	-7.1	17.1
16S/49E-18dc	130	2	8.1	20.0	2.70	42.1	9.0	7.4	27.9	123.1		58.9	-102.0	-12.6		28.4
16s/48E-24aaa	131	2	8.1	18.0	0.70	54.0	7.0	7.8	29.8	120.6		78.7				
16S/48E-25aa	134	2	8.1	18.8	0.70	43.0	7.4	9.2	27.9	109.1		72.1	-102.0	-13.0		19.3
16S/48E-36aaa	135	2	8.4	16.8	1.90	40.0	6.3	6.7	25.0	109.1		78.7	-98.5	-12.6		
Amargosa Estates #2	137	2	8.1	20.0	2.10	38.0	6.8	6.5	22.0	109.9	1.6	79.0	-104.3	-13.1	-10.6	21.6
17S/48E-1ab	138	2	8.1	18.8	1.50	40.0	7.0	6.4	25.0	110.6		78.7	-104.0	-13.0		18.4
18S/49E-2cbc	183	7	7.8	28.9	11.90	120.0	9.8	19.9	74.0	288.8		58.9				
NC-EWDP-10S Shallow	NC19	2	7.7	13.7	2.57	43.3	5.8	6.6	17.0	93.9	2.2	62.3	-102.0	-12.8	-7.3	23.8
NC-EWDP-10P Shallow	NC21	2	7.9	14.3	2.23	46.5	5.7	8.6	19.0	93.5	2.1	56.7	-99.3	-13.4	-7.1	23.1

Well Name	Well#	PCFA Cluster	pH	Ca (mg/L)	Mg (mg/L)	Na (mg/L)	K (mg/L)	Cl (mg/L)	SO4 (mg/L)	Total Alkalinity as CaCO3 (mg/L)	F (mg/L)	SiO2 (mg/L)	dD (permil)	d18O (permil)	d13C (permil)	14C (pmc)
NC-EWDP-10P Deep	NC22	2	7.7	14.4	2.27	40.8	5.4	7.9	18.8	93.1	2.1	63.6	-99.8	-13.3	-7.0	23.4
NC-EWDP-12PA	NC23	9	7.6	30.0	8.36	143.5	27.0	15.4	98.3	303.0	3.0	72.1	-101.1	-13.6	-3.5	3.5
NC-EWDP-19P	NC37	2	8.0	17.3	1.38	45.1	4.0	7.1	22.3	109.6	1.7	56.7	-101.4	-13.6	-6.4	18.0
NC-EWDP-19PB Shallow	NC38	2	8.3	14.6	1.44	55.5	3.8	6.3	26.9	119.7	1.7	48.6	-101.4	-13.1	-6.2	19.9
NC-EWDP-22PA Shallow	NC40	2	7.6	14.7	2.59	43.4	5.2	6.3	19.7	88.8	2.0	59.2	-101.0	-13.0	-7.0	23.2
NC-EWDP-22PA Deep	NC41	2	7.4	19.5	2.89	37.3	4.9	7.3	16.7	93.5	1.7	59.7	-99.1	-13.2	-6.9	21.0
NC-EWDP-22PB Shallow	NC42	2	8.0	25.1	3.37	38.9	5.5	7.6	18.4	118.1	1.0	59.1	-98.8	-13.2	-6.6	19.9
NC-EWDP-22PB Deep	NC43	2	8.0	23.5	3.21	47.3	5.2	8.3	20.0	112.8	0.9	46.6	-97.6	-13.5	-8.2	21.3
NC-EWDP-22S Z1	NC44	2	7.7	14.9	2.63	39.3	5.3	6.2	17.4	93.5	1.7	57.6	-99.2	-13.1	-6.6	22.0
NC-EWDP-22S Z2	NC45	2	7.9	17.1	2.66	35.0	4.6	8.1	18.7	99.2	1.4	56.6	-102.5	-13.0	-6.8	20.5
NC-EWDP-22S Z3	NC46	2	8.0	20.0	3.09	36.3	5.3	8.5	17.1	100.9	1.1	56.6	-100.9	-13.1	-6.9	18.6
NC-EWDP-22S Z4	NC47	2	8.0	20.6	2.79	43.2	5.4	7.8	19.7	103.3	1.0	51.9	-101.8	-13.0	-7.5	19.6
NC-EWDP-24P	NC50	2	8.2	16.2	1.24	54.7	3.7	6.2	27.3	119.3	1.6	45.6	-104.5	-13.7	-7.8	17.7
NC-EWDP-29P	NC53	2	8.5	14.7	1.19	50.2	4.0	6.0	24.9	105.0	1.8	60.6	-103.1	-13.4	-6.9	20.3
J-13 well	NC54	2	7.7	11.0	1.75	39.5	4.4	7.9	16.5	80.0	2.4		-97.5	-12.8	-7.9	32.2
UE-25 WT#3	NC57	2	8.1	11.5	1.10	52.9	4.0	6.0	30.0	121.4	2.4	62.1	-102.1	-13.6	-8.2	22.3
OUTLIERS																
ER-OV-03a2 (11/9/97)	10		9.2	5.7	1.03	331.0	84.7	262.0	295.0	222.1		20.0			-5.0	21.0
ER-18-2 (3/21/2000)	20		7.6	5.8	0.20	351.7	3.1	13.2	54.0	598.7	12.8	42.8			-0.7	1.6
p#1(c)	63		6.6	100.0	39.00	150.0	12.0	28.0	160.0	569.2	4.7	41.0			-2.3	2.3
UE-25 J-11	67		8.1	76.5	15.00	154.0	17.0	17.5	479.5	67.3	1.2	57.5			-11.0	12.3
McCracken Domestic	117		7.5	83.0	12.00	194.0	12.0	123.0	266.0	199.3	1.7	73.0			-12.5	32.9
17S/50E-19aab	171		8.6	7.6	8.50	252.0	27.4	69.8	175.8	340.8		42.7				
Cherry Patch Well, 17S/52E-08cdb	189		7.3	76.0	38.75	272.5	9.6	122.5	485.0	282.7	1.7	25.5				

Well Name	Well#	PCFA Cluster	pH	Ca (mg/L)	Mg (mg/L)	Na (mg/L)	K (mg/L)	Cl (mg/L)	SO4 (mg/L)	Total Alkalinity as CaCO3 (mg/L)	F (mg/L)	SiO2 (mg/L)	dD (permil)	d18O (permil)	d13C (permil)	14C (pmc)
UE-16f (7/12/93) (Sulfate and Na values from 1977)	194		8.9	1.8	1.87	421.2	5.0	18.8	423.0	793.2	5.2	4.5			-11.7	3.4
NC-EWDP-01DX-1	NC01		7.5	37.1	11.90	339.0	63.4	43.4	127.0	790.6	6.4	51.8	-106.1	-14.2	-2.3	1.7
NC-EWDP-01DX-2	NC02		7.4	62.0	11.05	342.0	78.2	121.5	133.5	701.2	6.2	52.6	-104.9	-14.1	-1.2	28.8
Bond Gold Mining Well -13	NC59		7.6	158.0	86.90	93.6	7.1	62.5	644.0	223.9	0.5	18.8	-97.3	-13.1	-7.0	5.1
REPEAT DATA																
Bond Gold Mining #13	200		7.3	144.5	79.50	85.5	7.0	63.5	621.5	225.1	0.6	16.5			-7.5	8.1
WT-17	64		7.1	8.9	0.85	49.0	2.6	6.4	17.5	106.2	2.0	39.0			-8.3	16.2
WT#3	65		7.6	11.2	1.00	49.0	3.9	6.0	18.3	113.6	2.3	56.2			-8.2	22.3
MISSING DATA																
ER-OV-03a3 (11/09/97)	9		8.3	13.3		120.5	5.7	44.9	81.2	151.1	2.1	55.1			-2.8	16.5
US Ecology MR-3	18		7.7							266.5					-6.5	323.0
15S/49E-13dda	102									0.0						
NC-EWDP-5S	154		8.3	17.0	3.50	149.0	11.0	39.0	146.0		1.0	3.7				
Spring Meadows Well #8	170			22.0	10.90	110.0	14.9	21.9	73.9	242.6	2.1	31.0				
Spring Meadows Well #10	173			2.8	2.90	250.0	14.9	25.8	105.1	405.1	3.2	67.0				
UE-1a (09/01/1992)	192		7.4	48.5	23.90	50.5	8.7	26.3		330.1		19.3			-8.6	60.5
UE-1b (9/1/92)	193		7.4	37.4	13.70	31.3	10.7	5.9		150.9		80.9			-4.5	16.0

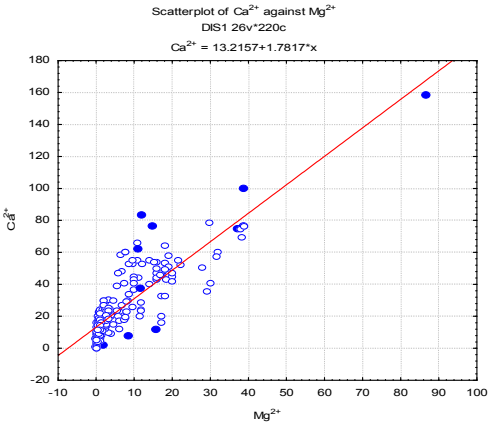
Scatterplot of Ca2+ against Mg2+
DIS1 26v*220c
Ca2+ = 13.2157+1.7817*x
Ca2+
Mg2+

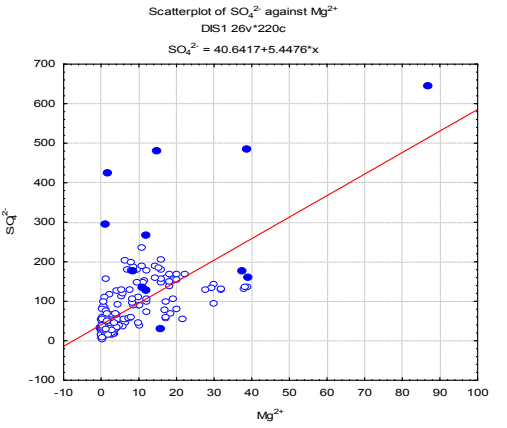
Scatterplot of SO4 2- against Mg2+
DIS1 26v*220c
SO4 2- = 40.6417+5.4476*x
SO4 2-
Mg2+

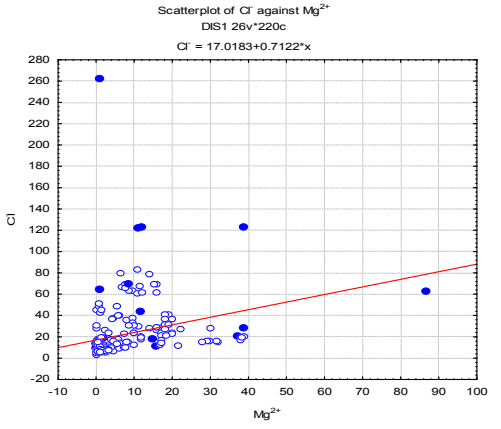
Scatterplot of Cl- against Mg2+
DIS1 26v*220c
Cl- = 17.0183+0.7122*x
Cl
Mg2+

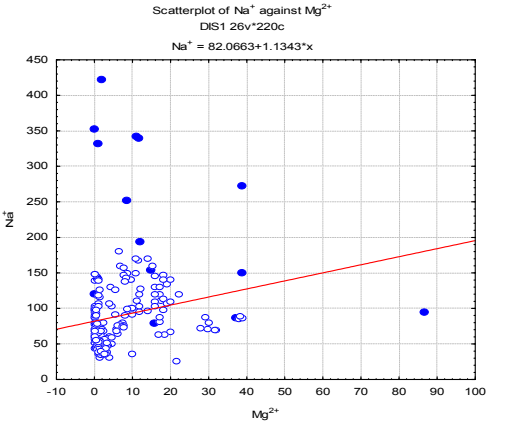
Scatterplot of Na+ against Mg2+
DIS1 26v*220c
Na+ = 82.0663+1.1343*x
Na+
Mg2+

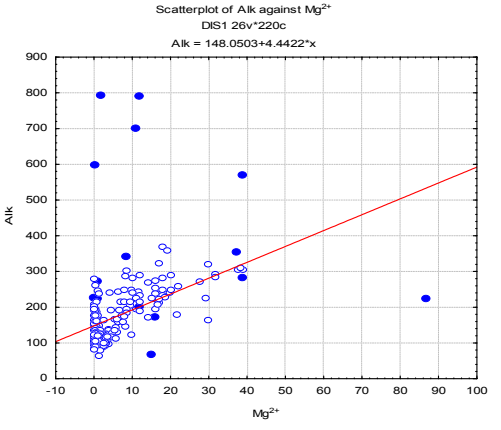
Scatterplot of Alk against Mg2+
DIS1 26v*220c
Alk = 148.0503+4.4422*x
Alk
Mg2+

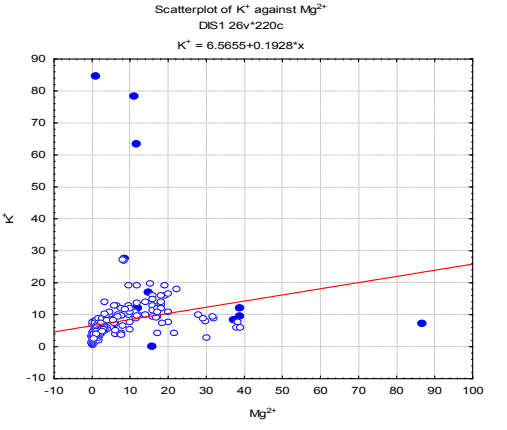
Scatterplot of K+ against Mg2+
DIS1 26v*220c
K+ = 6.5655+0.1928*x
K+
Mg2+

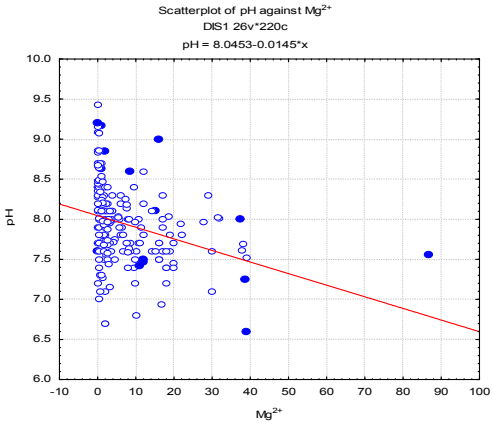
Scatterplot of pH against Mg2+
DIS1 26v*220c
pH = 8.0453-0.0145*x
pH
Mg2+

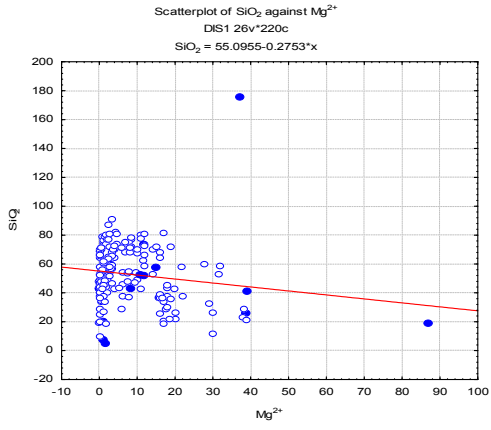
Scatterplot of SiO2 against Mg2+
DIS1 26v*220c
SiO2 = 55.0955-0.2753*x
SiO2
Mg2+

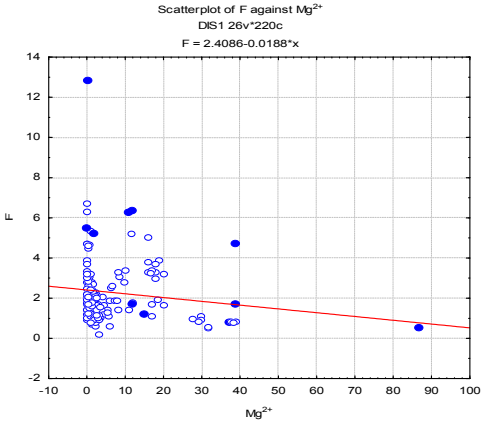
Scatterplot of F against Mg2+
DIS1 26v*220c
F = 2.4086-0.0188*x
F
Mg2+

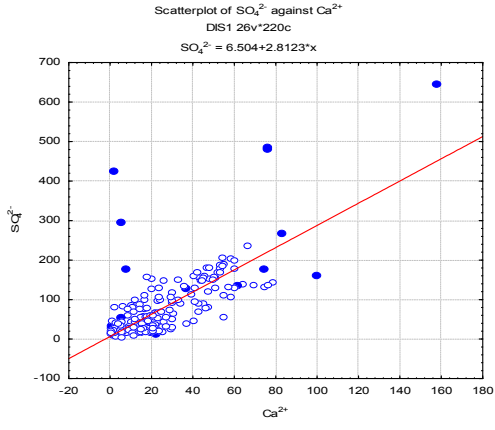
Scatterplot of SO4 2- against Ca2+
DIS1 26v*220c
SO4 2- = 6.504+2.8123*x
SO4 2-
Ca2+

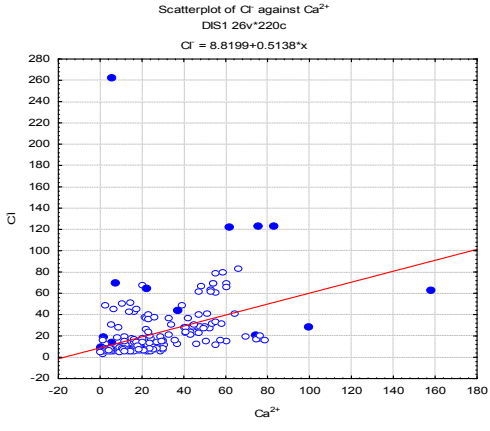
Scatterplot of Cl- against Ca2+
DIS1 26v*220c
Cl- = 8.8199+0.5138*x
Cl
Ca2+

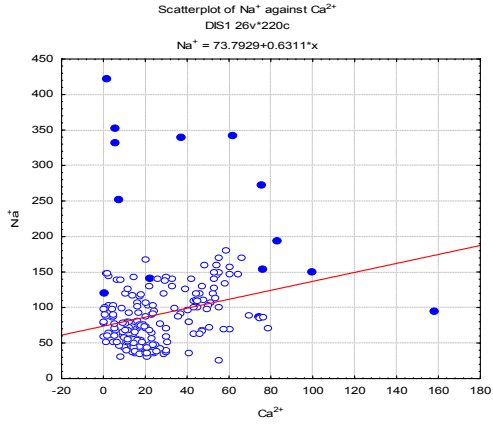
Scatterplot of Na+ against Ca2+
DIS1 26v*220c
Na+ = 73.7929+0.6311*x
Na+
Ca2+

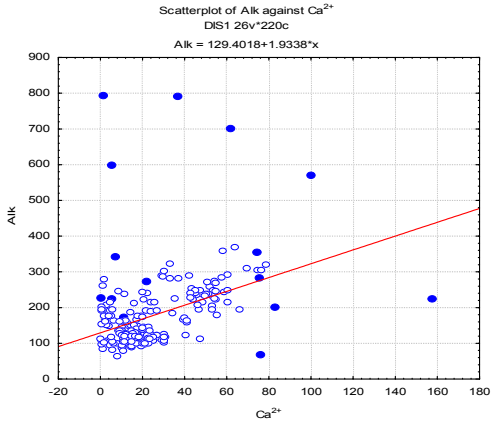
Scatterplot of Alk against Ca2+
DIS1 26v*220c
Alk = 129.4018+1.9338*x
Alk
Ca2+

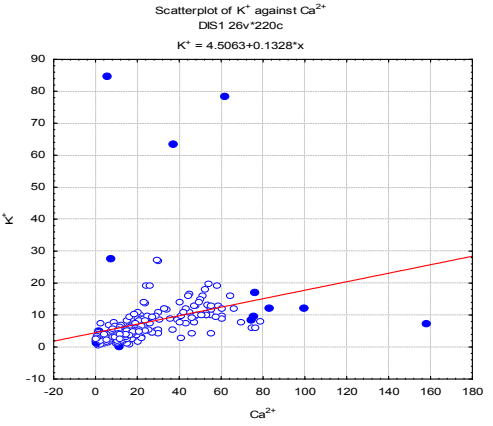
Scatterplot of K+ against Ca2+
DIS1 26v*220c
K+ = 4.5063+0.1328*x
K+
Ca2+

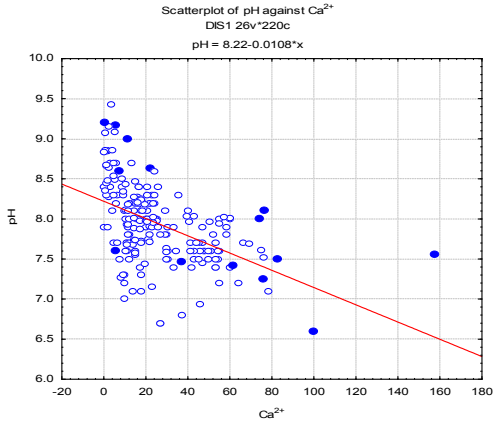
Scatterplot of pH against Ca2+
DIS1 26v*220c
pH = 8.22-0.0108*x
pH
Ca2+

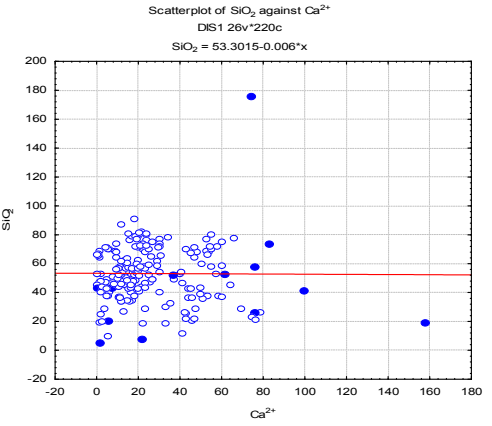
Scatterplot of SiO2 against Ca2+
DIS1 26v*220c
SiO2 = 53.3015-0.006*x
SiO2
Ca2+

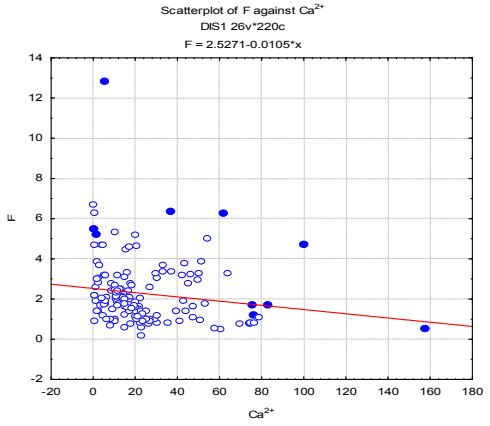
Scatterplot of F against Ca2+
DIS1 26v*220c
F = 2.5271-0.0105*x
F
Ca2+

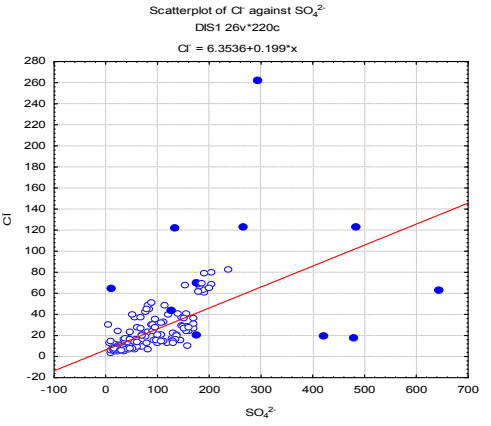
Scatterplot of Cl- against SO4 2-
DIS1 26v*220c
Cl- = 6.3536+0.199*x
Cl
SO4 2-

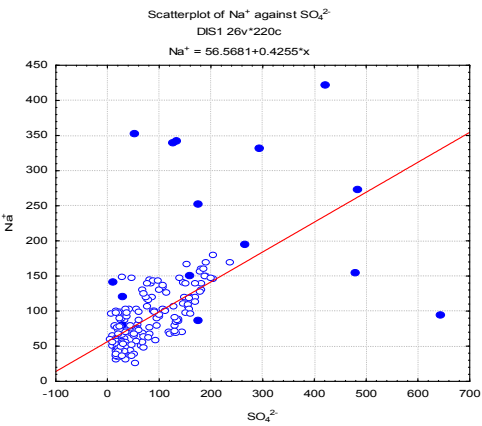
Scatterplot of Na+ against SO4 2-
DIS1 26v*220c
Na+ = 56.5681+0.4255*x
Na+
SO4 2-

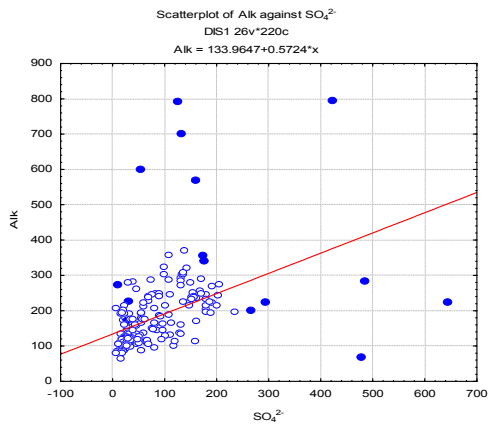
Scatterplot of Alk against SO4 2-
DIS1 26v*220c
Alk = 133.9647+0.5724*x
Alk
SO4 2-

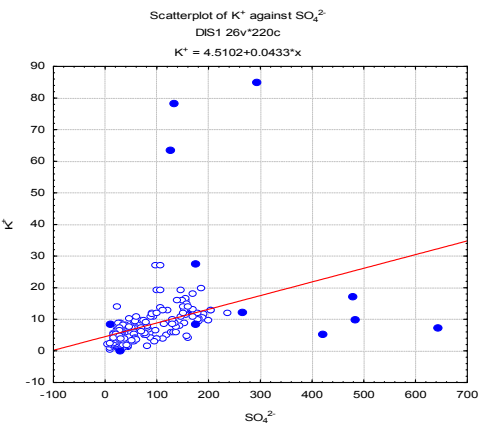
Scatterplot of K+ against SO4 2-
DIS1 26v*220c
K+ = 4.5102+0.0433*x
K+
SO4 2-

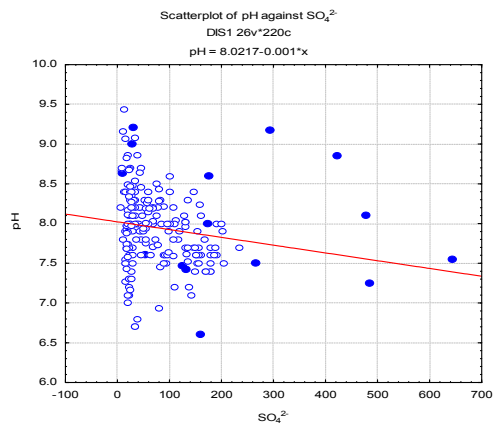
Scatterplot of pH against SO4 2-
DIS1 26v*220c
pH = 8.0217-0.001*x
pH
SO4 2-

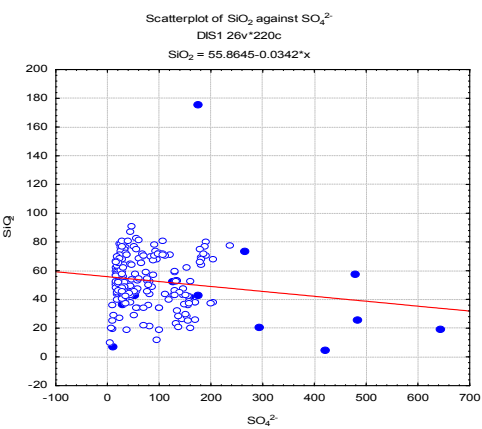
Scatterplot of SiO2 against SO4 2-
DIS1 26v*220c
SiO2 = 55.8645-0.0342*x
SiO2
SO4 2-

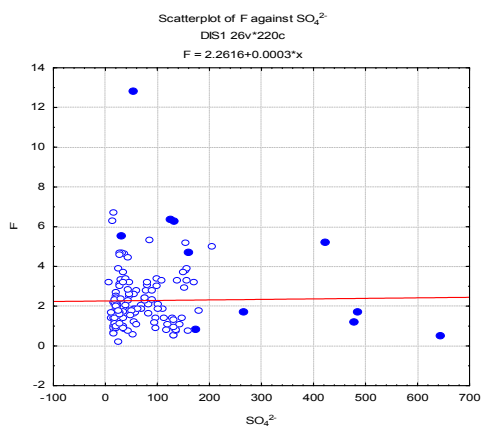
Scatterplot of F against SO4 2-
DIS1 26v*220c
F = 2.2616+0.0003*x
F
SO4 2-

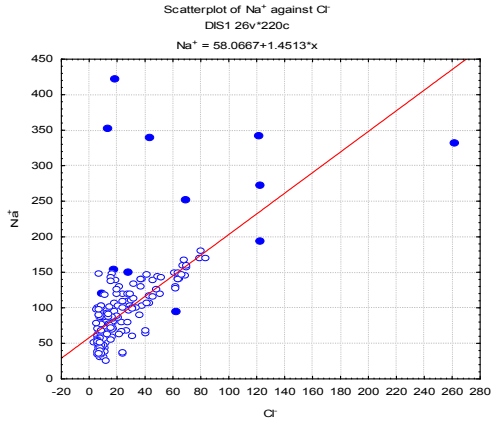
Scatterplot of Na+ against Cl-
DIS1 26v*220c
Na+ = 58.0667+1.4513*x
Na+
Cl-

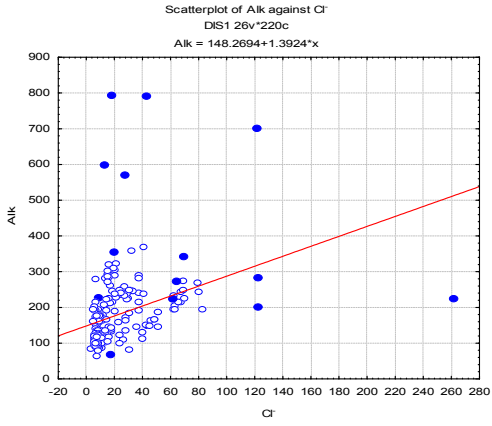
Scatterplot of Alk against Cl-
DIS1 26v*220c
Alk = 148.2694+1.3924*x
Alk
Cl-

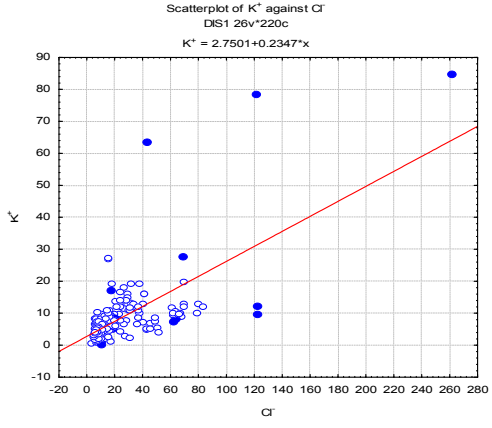
Scatterplot of K+ against Cl-
DIS1 26v*220c
K+ = 2.7501+0.2347*x
K+
Cl-

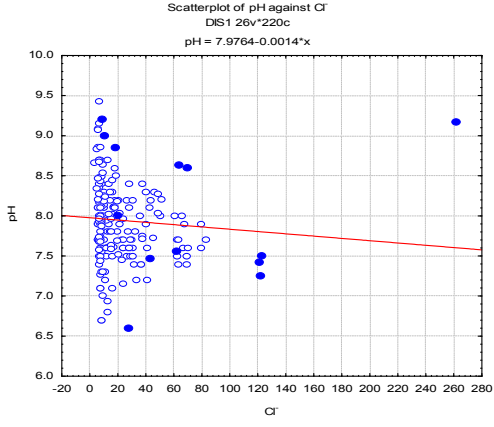
Scatterplot of pH against Cl-
DIS1 26v*220c
pH = 7.9764-0.0014*x
pH
Cl-

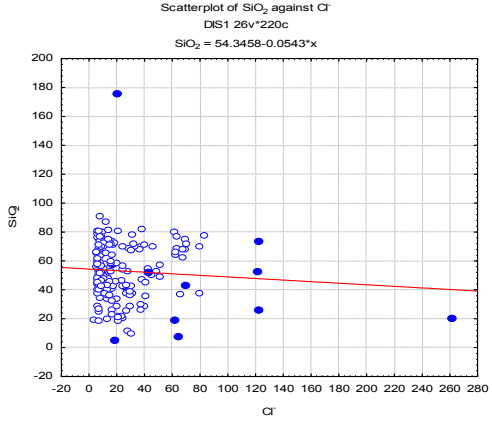
Scatterplot of SiO2 against Cl-
DIS1 26v*220c
SiO2 = 54.3458-0.0543*x
SiO2
Cl-

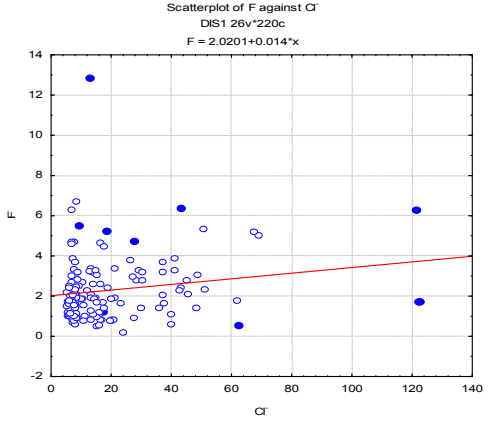
Scatterplot of F against Cl-
DIS1 26v*220c
F = 2.0201+0.014*x
F
Cl-

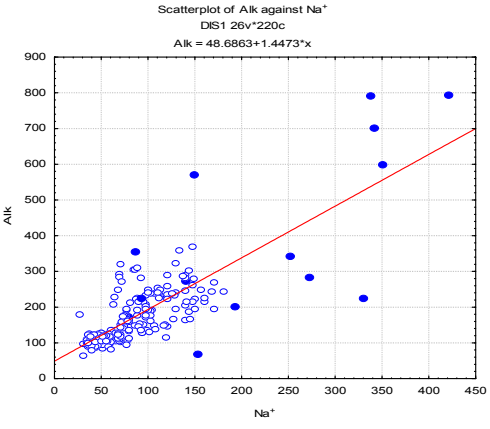
Scatterplot of Alk against Na+
DIS1 26v*220c
Alk = 48.6863+1.4473*x
Alk
Na+

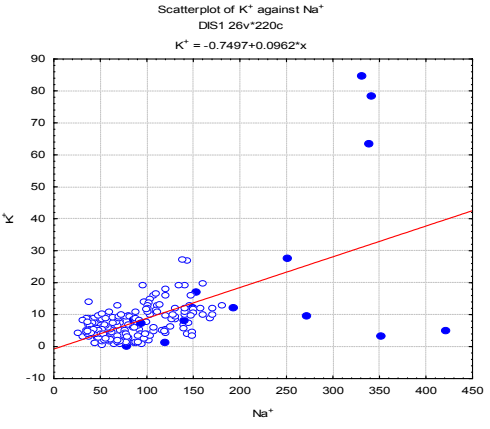
Scatterplot of K+ against Na+
DIS1 26v*220c
K+ = -0.7497+0.0962*x
K+
Na+

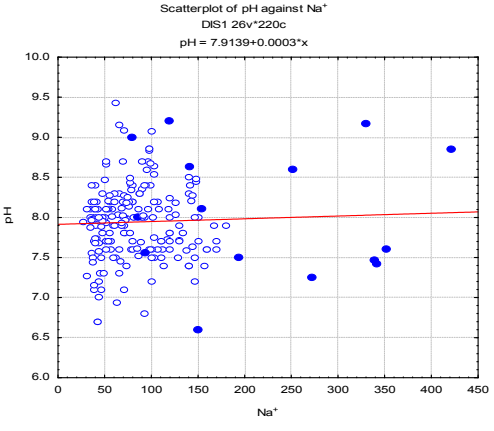
Scatterplot of pH against Na+
DIS1 26v*220c
pH = 7.9139+0.0003*x
pH
Na+

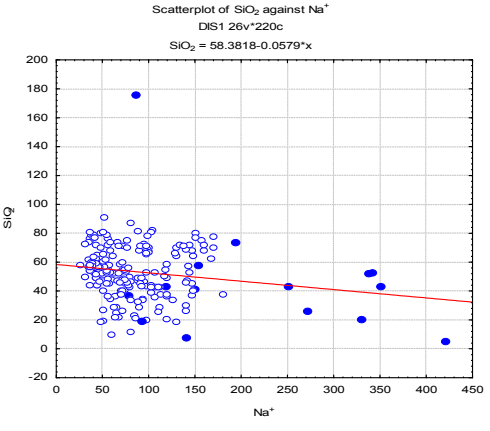
Scatterplot of SiO2 against Na+
DIS1 26v*220c
SiO2 = 58.3818-0.0579*x
SiO2
Na+

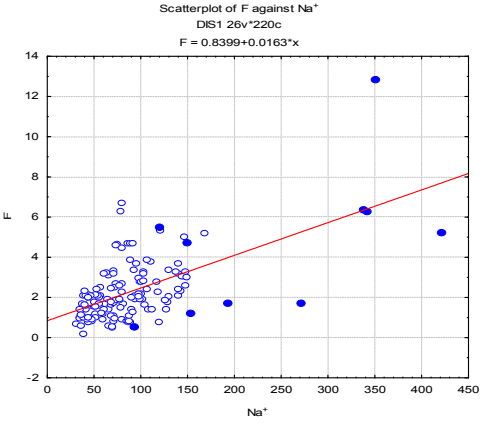
Scatterplot of F against Na+
DIS1 26v*220c
F = 0.8399+0.0163*x
F
Na+

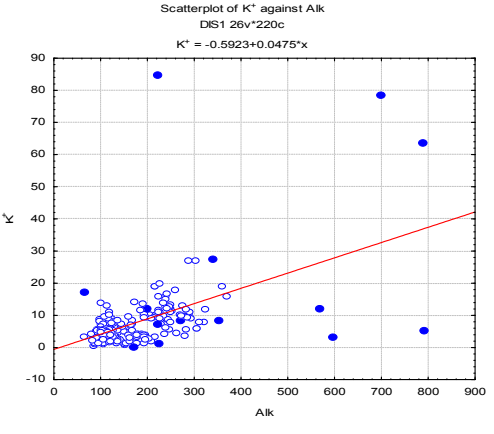
Scatterplot of K+ against Alk
DIS1 26v*220c
K+ = -0.5923+0.0475*x
K+
Alk

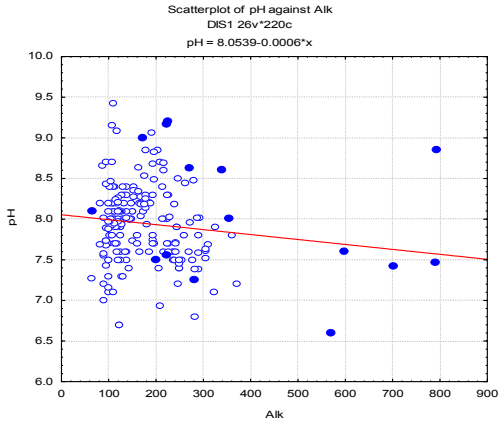
Scatterplot of pH against Alk
DIS1 26v*220c
pH = 8.0539-0.0006*x
pH
Alk

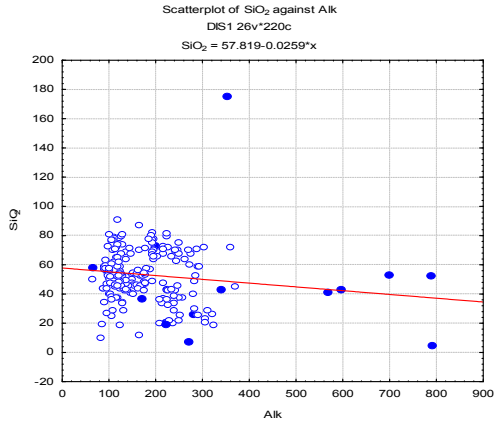
Scatterplot of SiO2 against Alk
DIS1 26v*220c
SiO2 = 57.819-0.0259*x
SiO2
Alk

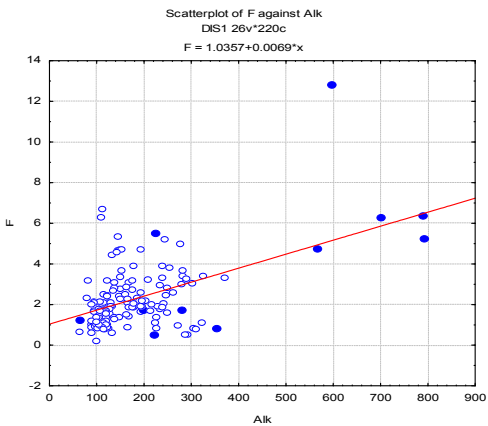
Scatterplot of F against Alk
DIS1 26v*220c
F = 1.0357+0.0069*x
F
Alk

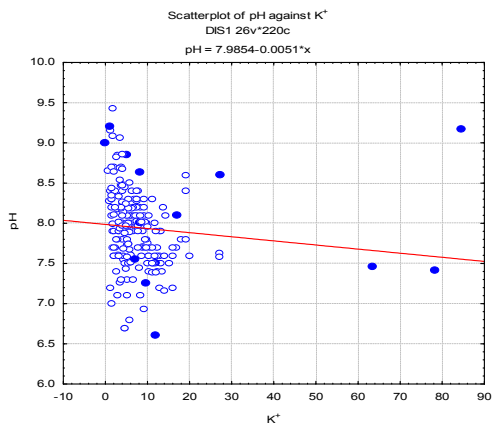
Scatterplot of pH against K+
DIS1 26v*220c
pH = 7.9854-0.0051*x
pH
K+

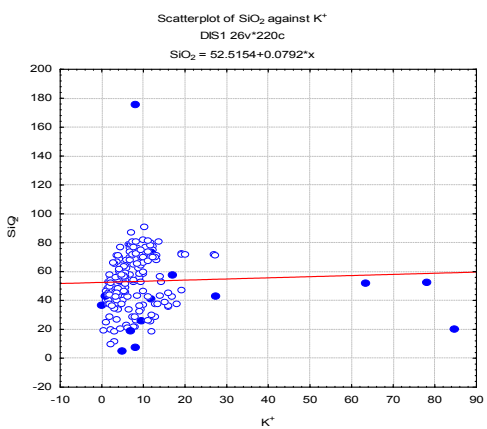
Scatterplot of SiO2 against K+
DIS1 26v*220c
SiO2 = 52.5154+0.0792*x
SiO2
K+

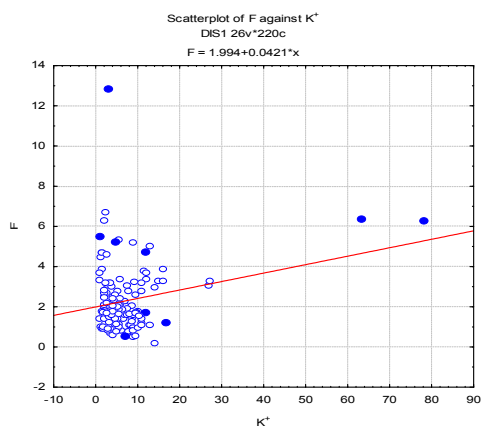
Scatterplot of F against K+
DIS1 26v*220c
F = 1.994+0.0421*x
F
K+

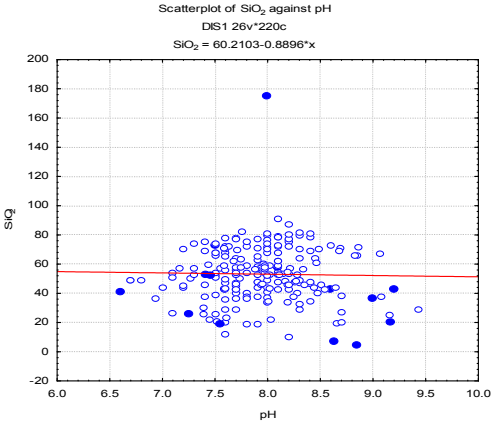
Scatterplot of SiO2 against pH
DIS1 26v*220c
SiO2 = 60.2103-0.8896*x
SiO2
pH

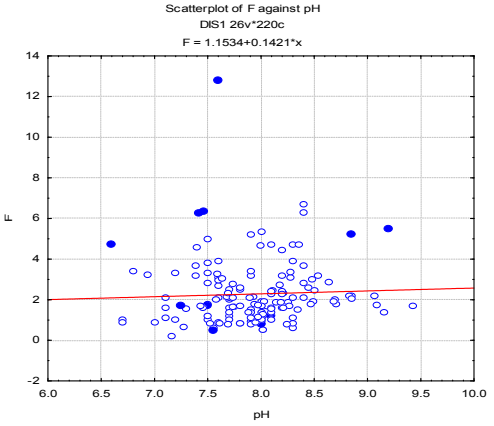
Scatterplot of F against pH
DIS1 26v*220c
F = 1.1534+0.1421*x
F
pH

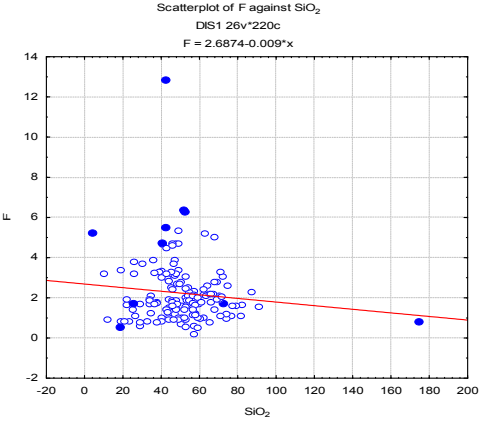
Scatterplot of F against SiO2
DIS1 26v*220c
F = 2.6874-0.009*x
F
SiO2

Summary: Mg2+

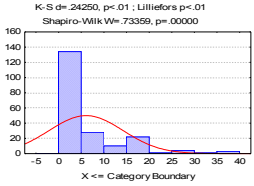

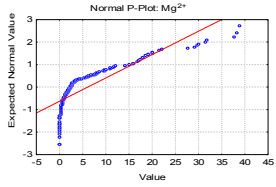

Summary Statistics:Mg2+
Valid N=205
% Valid obs.=100.000000
Mean= 6.069070
Median= 2.300000
Mode= 1.000000
Frequency of Mode= 8.000000
Sum=1244.159337
Minimum= 0.010000
Maximum= 38.950000
Lower Quartile= 0.660000
Upper Quartile= 8.500000
Variance= 66.944474
Std.Dev.= 8.181960
Coef.Var.=134.814071
Standard Error= 0.571453
Skewness= 1.920425
Std.Err. Skewness= 0.169846
Kurtosis= 3.600952
Std.Err. Kurtosis= 0.338102

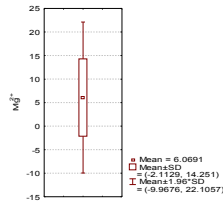

Summary: Ca2+

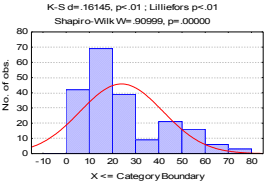

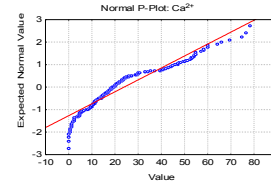

Summary Statistics:Ca2+
Valid N=205
% Valid obs.=100.000000
Mean= 23.912093
Median= 19.075000
Mode= 1.000000
Frequency of Mode= 6.000000
Sum=4901.979107
Minimum= 0.150000
Maximum= 78.500000
Lower Quartile= 11.300000
Upper Quartile= 33.000000
Variance=319.157557
Std.Dev.= 17.864961
Coef.Var.= 74.711073
Standard Error= 1.247744
Skewness= 0.938199
Std.Err. Skewness= 0.169846
Kurtosis= 0.143207
Std.Err. Kurtosis= 0.338102

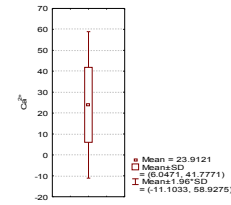

Summary: SO42-

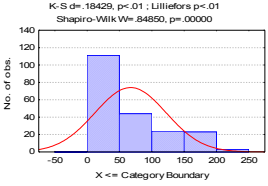

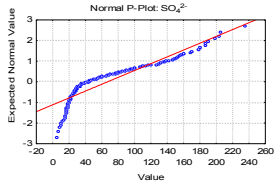

Summary Statistics:SO42-
Valid N=205
% Valid obs.=100.000000
Mean= 67.116709
Median= 43.000000
Mode= 1.000000
Frequency of Mode= 7.000000
Sum=13758.925286
Minimum= 5.000000
Maximum=235.300000
Lower Quartile= 23.225000
Upper Quartile= 99.900000
Variance=3050.564827
Std.Dev.= 55.231919
Coef.Var.= 82.292353
Standard Error= 3.857565
Skewness= 1.001872
Std.Err. Skewness= 0.169846
Kurtosis= -0.181533
Std.Err. Kurtosis= 0.338102

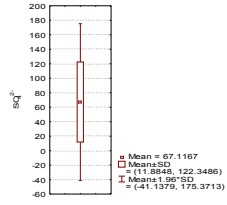

Summary: Cl-

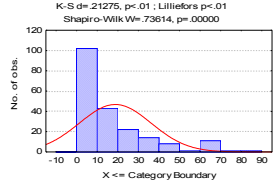

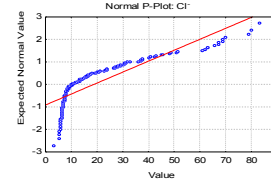

Summary Statistics:Cl-
Valid N=205
% Valid obs.=100.000000
Mean= 18.745843
Median= 10.300000
Mode= 1.000000
Frequency of Mode= 5.000000
Sum=3842.897738
Minimum= 3.200000
Maximum= 83.000000
Lower Quartile= 7.300000
Upper Quartile= 24.100000
Variance=305.892606
Std.Dev.= 17.489786
Coef.Var.= 93.299544
Standard Error= 1.221540
Skewness= 1.816102
Std.Err. Skewness= 0.169846
Kurtosis= 2.712458
Std.Err. Kurtosis= 0.338102

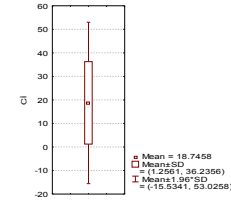

Summary: Na+

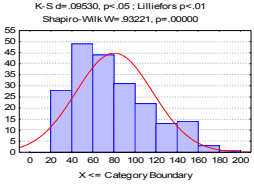

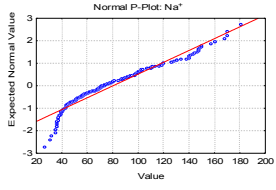

Summary Statistics:Na+
Valid N=205
% Valid obs.=100.000000
Mean= 80.274704
Median= 71.700000
Mode= 1.000000
Frequency of Mode= 5.000000
Sum=16456.314286
Minimum= 26.400000
Maximum=180.500000
Lower Quartile= 50.166667
Upper Quartile=102.500000
Variance=1332.293240
Std.Dev.= 36.500592
Coef.Var.= 45.469607
Standard Error= 2.549312
Skewness= 0.683120
Std.Err. Skewness= 0.169846
Kurtosis= -0.447484
Std.Err. Kurtosis= 0.338102

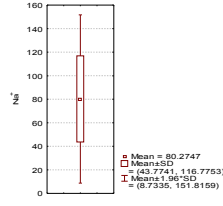

Summary: Alk

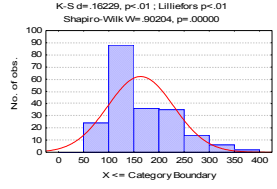

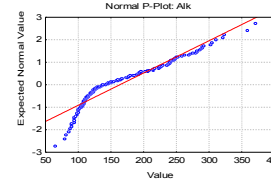

Summary Statistics:Alk
Valid N=205
% Valid obs.=100.000000
Mean=163.574645
Median=136.963537
Mode= 1.000000
Frequency of Mode= 4.000000
Sum=33532.802160
Minimum= 63.970993
Maximum=369.883563
Lower Quartile=110.062914
Upper Quartile=214.220813
Variance=4316.956375
Std.Dev.= 65.703549
Coef.Var.= 40.167319
Standard Error= 4.588935
Skewness= 0.867056
Std.Err. Skewness= 0.169846
Kurtosis= -0.147248
Std.Err. Kurtosis= 0.338102

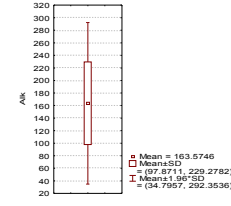

Summary: K+

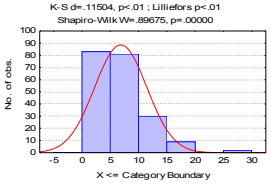

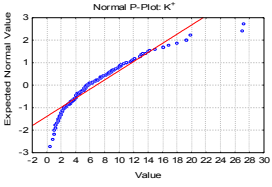

Summary Statistics:K+
Valid N=205
% Valid obs.=100.000000
Mean= 6.835913
Median= 5.558571
Mode= 1.000000
Frequency of Mode= 6.000000
Sum=1401.362202
Minimum= 0.510000
Maximum= 27.125000
Lower Quartile= 3.600000
Upper Quartile= 9.066667
Variance= 21.332796
Std.Dev.= 4.618744
Coef.Var.= 67.565867
Standard Error= 0.322587
Skewness= 1.416464
Std.Err. Skewness= 0.169846
Kurtosis= 2.964486
Std.Err. Kurtosis= 0.338102

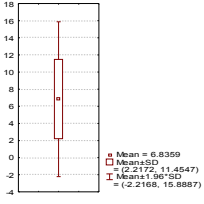

Summary: pH

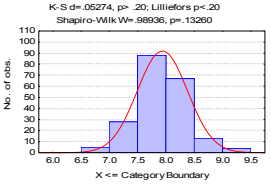

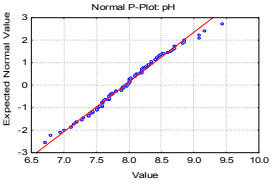

Summary Statistics:pH
Valid N=205
% Valid obs.=100.000000
Mean= 7.936459
Median= 7.970000
Mode= 1.000000
Frequency of Mode= 14.000000
Sum=1626.974044
Minimum= 6.700000
Maximum= 9.430000
Lower Quartile= 7.610000
Upper Quartile= 8.200000
Variance= 0.198289
Std.Dev.= 0.445297
Coef.Var.= 5.610778
Standard Error= 0.031101
Skewness= 0.113214
Std.Err. Skewness= 0.169846
Kurtosis= 0.702287
Std.Err. Kurtosis= 0.338102

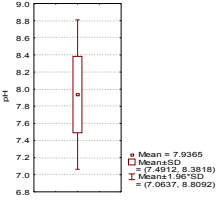

Summary: SiO2

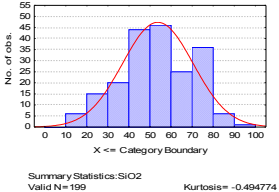

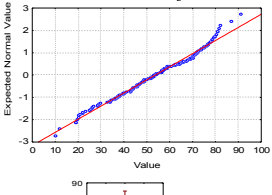

Summary Statistics:SiO2
Valid N=199
% Valid obs.= 97.073171
Mean= 53.679638
Median= 53.400000
Mode= 1.000000
Frequency of Mode= 4.000000
Sum=10682.7964
Minimum= 10.050000
Maximum= 91.200000
Lower Quartile= 43.200000
Upper Quartile= 68.000000
Variance=281.400297
Std.Dev.= 16.774990
Coef.Var.= 31.250192
Standard Error= 1.189148
Skewness= -.0.227610
Std.Err. Skewness= 0.172350
Kurtosis= -0.494774
Std.Err. Kurtosis= 0.343041

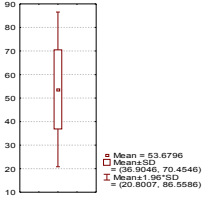

Summary: F

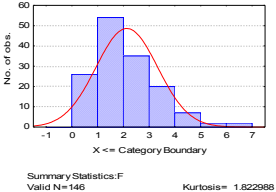

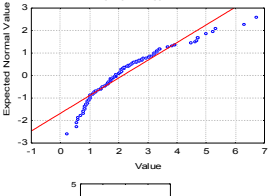

Summary Statistics:F
Valid N=146
% Valid obs.= 71.219512
Mean= 2.132556
Median= 1.887500
Mode= 1.000000
Frequency of Mode= 7.000000
Sum=311.353167
Minimum= 0.200000
Maximum= 6.700000
Lower Quartile= 1.216000
Upper Quartile= 2.716667
Variance= 1.436763
Std.Dev.= 1.198650
Coef.Var.= 56.207219
Standard Error= 0.099201
Skewness= 1.265512
Std.Err. Skewness= 0.200679
Kurtosis= 1.822988
Std.Err. Kurtosis= 0.398767